CONFIDENTIAL



NACA

# RESEARCH MEMORANDUM

## AN EXPERIMENTAL AND THEORETICAL INVESTIGATION AT HIGH SUBSONIC SPEEDS OF THE EFFECTS OF HORIZONTAL-TAIL HEIGHT ON THE AERODYNAMIC CHARACTERISTICS IN SIDESLIP OF AN UNSWEPT, UNTAPERED TAIL ASSEMBLY

By Harleth G. Wiley and Donald R. Riley

Langley Aeronautical Laboratory
Langley Field, Va.



NATIONAL ADVISORY COMMITTEE
FOR AERONAUTICS

WASHINGTON

December 2, 1953

CONFIDENTIAL

NATIONAL ADVISORY COMMITTEE FOR AERONAUTICS

RESEARCH MEMORANDUM

# AN EXPERIMENTAL AND THEORETICAL INVESTIGATION AT HIGH SUBSONIC SPEEDS OF THE EFFECTS OF HORIZONTAL-TAIL HEIGHT ON THE AERODYNAMIC CHARACTERISTICS IN SIDESLIP OF AN UNSWEPT, UNTAPERED TAIL ASSEMBLY

By Harleth G. Wiley and Donald R. Riley

## SUMMARY

An investigation was made in the Langley high-speed 7- by 10-foot tunnel of the effects of horizontal-tail height at high subsonic speeds and $0^{\circ}$ angle of attack on the aerodynamic characteristics of a tail assembly in sideslip. The horizontal and vertical surfaces were of unswept, untapered plan form and were of aspect ratio 4.5 and 2.16, respectively.

Results indicated that above a Mach number of 0.7, abrupt changes in lift coefficient occurred with increase in Mach number for all horizontal-tail positions. The lowest values of minimum drag coefficient throughout the Mach number range were obtained for the low horizontal-tail position with the fuselage acting as a fairing in the intersection of the horizontal and vertical surfaces. Pitching-moment coefficient increased positively with horizontal-tail height and with Mach number for all configurations except that with the horizontal tail at 26 percent vertical-surface span. The variation of lateral-force coefficient with sideslip increased with Mach number up to a Mach number of 0.7. The highest variations of lateral-force coefficient with sideslip were obtained for the low and high horizontal-tail locations (0 and 100 percent vertical-surface span, respectively) with somewhat lower and generally equal values obtained for the intermediate tail positions (26 and 59 percent vertical-surface span). The lowest variation of rolling-moment coefficient with sideslip up to a Mach number of 0.70 was obtained for the low horizontal-tail position. Nonlinear Mach number effects apparent at the low Reynolds numbers of these tests were minimized with the horizontal tail in the low position. Generally good agreement was obtained between theory and the experimental results of this paper.

## INTRODUCTION

Increase of operational flight speeds into the high subsonic and transonic ranges has emphasized the necessity of quantitative determination of the aerodynamic characteristics of the tail as they affect the stability of the airplane and the loadings on the tail at these flight speeds. The National Advisory Committee for Aeronautics has therefore undertaken a comprehensive research program designed to furnish a complementary theoretical and experimental insight into the nature and magnitude of the stability contributions and loadings of the tail as they are affected by the various design parameters and maneuver attitudes. As part of this program, experiments were made in the Langley high-speed 7- by 10-foot tunnel to determine the effects of high subsonic speeds of vertical location of an unswept, untapered horizontal tail on the aerodynamic characteristics in sideslip of an unswept, untapered tail assembly. (These tests are similar to, and complement, the low-speed tests of ref. 1.) Configurations investigated included the fuselage alone, fuselage plus vertical tail, fuselage plus horizontal tail, and the fuselage plus vertical tail with the horizontal tail located at 0, 26, 59, and 100 percent vertical-surface span.

Tests were made at $0^\circ$ angle of attack through a sideslip range of $-2^\circ$ to $20^\circ$ and over a Mach number range of 0.5 to 0.94. Reynolds number for the tests, based on the mean aerodynamic chord of the vertical tail, varied from 1,500,000 to 2,000,000 for tests at the higher Mach numbers. Where applicable, experimental results are compared to theoretical calculations.

## COEFFICIENTS AND SYMBOLS

The data presented herein are in the form of standard NACA coefficients of forces and moments referred to the stability system of axes with the origin coinciding with the intersection of the fuselage center line and the quarter-chord line of the vertical tail (fig. 1). The coefficients and symbols are defined as follows:

| | |
|---|---|
| X | longitudinal force |
| Y | lateral force |
| L | rolling moment about x-axis |
| M | pitching moment about y-axis |

| | |
|---|---|
| $N$ | yawing moment about z-axis |
| $C_L$ | lift coefficient, $\frac{\text{Lift}}{qS_v}$ |
| $C_X$ | longitudinal-force coefficient, $\frac{X}{qS_v}$ |
| $C_{D_{min}}$ | minimum drag coefficient ($C_{D_{min}} = -C_X$ at $0^\circ$ angle of attack and sideslip) |
| $C_Y$ | lateral-force coefficient, $\frac{Y}{qS_v}$ |
| $C_l$ | rolling-moment coefficient, $\frac{L}{qS_v b_v}$ |
| $C_m$ | pitching-moment coefficient, $\frac{M}{qS_v \bar{c}_v}$ |
| $C_n$ | yawing-moment coefficient, $\frac{N}{qS_v b_v}$ |
| $S$ | tail area, sq ft |
| $b$ | tail span, ft |
| $\bar{c}_v$ | mean aerodynamic chord of vertical tail, ft |
| $h$ | horizontal-tail height (measured from fuselage center line), ft |
| $h/b_v$ | ratio of horizontal-tail height to span of the vertical tail |
| $A$ | aspect ratio, $b^2/S$ |
| $V$ | free-stream air velocity, fps |
| $\rho$ | mass density of air, slugs/cu ft |
| $q$ | free-stream dynamic pressure, $1/2\rho V^2$, lb/sq ft |
| $M$ | Mach number |

$\alpha$ angle of attack, deg

$\beta$ angle of sideslip, deg

$C_{Y_\beta} = \frac{\partial C_Y}{\partial \beta}$

$C_{l_\beta} = \frac{\partial C_l}{\partial \beta}$

$C_{n_\beta} = \frac{\partial C_n}{\partial \beta}$

(All slopes were taken at $\alpha = 0^\circ$ through the linear range near $\beta = 0^\circ$)

Subscripts:

h horizontal tail

v vertical tail

## MODEL AND APPARATUS

Sketches and dimensions of the models used in this investigation are presented in figure 2 and table I. The horizontal and vertical tails, of NACA 64A010 airfoil section and untapered, unswept plan forms of equal chord, were made of steel and were originally equipped with full-span, 0.20c trailing-edge control surfaces. For these tests, steel trailing edges were welded in place to form solid surfaces. For maximum strength, separate models were built for each configuration, with the horizontal tail mounted at 0, 26, 59, and 100 percent vertical-surface span. Aspect ratio of the vertical tails was 2.16 and aspect ratio of the horizontal tails, while nominally designed for 4.5, actually was 4.81 for the 0-percent-vertical-span location, and 4.52 for the 26-, 59-, and 100-percent-vertical-span locations.

The tail models were directly mounted on a six-component electrical strain-gage balance attached to the sting support system in the tunnel with the horizontal surfaces in a vertical plane. The balance was housed in a stub fuselage of circular cross section and a fineness ratio of 10.9 in the original configuration. The original fuselage consisted of a mahogany nosepiece, the ordinates of which are given in figure 2, and a constant-diameter, sheet-aluminum afterbody. For several tests to determine the effects of fuselage nose shape, a modified nosepiece, hemispherical in shape, was used (fig. 2).

## TESTS AND CORRECTIONS

Most of the tests were made in the Langley high-speed 7- by 10-foot tunnel through a corrected Mach number range of 0.50 to 0.94. Brief supplementary tests were made in the Langley stability tunnel at a Mach number of about 0.2. Reynolds number, based on the mean aerodynamic chord of the vertical tail, was approximately $0.6 \times 10^6$ for the tests at $M = 0.2$, and varied from about $1.5 \times 10^6$ to $2.0 \times 10^6$ at Mach numbers of 0.50 to 0.94 (see fig. 3). The models were tested at $0^\circ$ angle of attack through a range of sideslip angles of $-2^\circ$ to about $20^\circ$.

Blockage corrections, computed by the method of reference 2, were derived as an incremental correction to Mach number. Corrected Mach number, because of differences of model configurations, varied somewhat between models.

Jet-boundary corrections, because of the relatively small area of the "lifting" vertical surface, were negligible and were therefore not applied. Drag data are presented with no base pressure corrections applied to account for the difference in pressure at the base of the model and that of static free stream.

The angle of sideslip was corrected for deflection of the sting support system under load. Similar corrections to angle of attack were negligible and were not applied.

Deflection of the horizontal and vertical surfaces, when statically loaded to anticipated aerodynamic load limits, was found to be negligible, and no corrections were applied.

Welding of the steel trailing edges at the 0.80-chord line of the horizontal and vertical tails caused a possible airfoil camber change equivalent to a maximum trailing-edge deflection of about $\pm 1^\circ$. No corrections were made for these model inaccuracies.

## RESULTS AND DISCUSSION

### Experimental Longitudinal Characteristics

Lift coefficient.- The variation of lift coefficient $C_L$ with angle of sideslip $\beta$ at Mach numbers from 0.50 to 0.94 for all configurations tested is presented in figure 4. A summary of the variation of $C_L$ with Mach number at $0^\circ$ angle of attack and $0^\circ$ and $12^\circ$ angle of sideslip is presented in figure 5. The pronounced variation in absolute value and

sign of $C_L$ for the various tail configurations at Mach numbers less than 0.7, even at 0° angle of attack at which these tests were made, can be attributed partly to model physical inaccuracies such as possible airfoil camber changes caused by welding of the trailing edges, and partly to the mutual flow interactions between the fuselage and the horizontal surfaces at their various locations. Primary emphasis, however, should be placed on the abrupt changes in value of $C_L$ with Mach number above Mach numbers of about 0.7 for all configurations with complete horizontal and vertical tails (fig. 5). Such variations of $C_L$ of the horizontal tail may cause appreciable longitudinal trim changes with Mach number for a complete airplane configuration.

Longitudinal-force and minimum-drag coefficients.- The variation of longitudinal-force coefficient $C_X$ with $\beta$ is presented in figure 6 with a summary of the minimum-drag characteristics of the various model configurations presented in figure 7. ($C_{D_{min}} = -C_X$ at 0° angles of attack and sideslip.) Above $M = 0.7$, at which Mach number the "force break" occurred, $C_{D_{min}}$ increased with increase in Mach number for all configurations investigated (fig. 7(a)). The minimum drag coefficient $C_{D_{min}}$ (fig. 7(b)) was of minimum value for the model with the fuselage acting as a fairing in the intersection of the horizontal and vertical surfaces ($h/b_v = 0$), particularly above $M = 0.8$. Minimum drag for the horizontal tail located at 26, 59, and 100 percent vertical-surface span was generally of similar magnitude at all Mach numbers.

Pitching-moment coefficient.- The variation of pitching-moment coefficient $C_m$ with $\beta$ is presented in figure 8 and the variation of $C_m$ with Mach number at $\beta = 0°$ and 12° is presented in figure 9. At 0° and 12° angle of sideslip, the positive value of $C_m$ increased with increase in Mach number and horizontal-tail height for all horizontal-tail positions except $h/b_v = 0.26$ (fig. 9). Mutual flow interactions between the fuselage and the low intermediate horizontal-tail position, $h/b_v = 0.26$, and possible model physical inaccuracies shifted the direction of $C_L$ (see fig. 5) and probably account for the reversal in sign of $C_m$. (It should be pointed out that the fuselage physical characteristics may well be of importance in affecting the magnitude of values of all of the aerodynamic characteristics of the empennage.)

## Experimental Lateral Stability and Loading Characteristics

The yawing-moment, lateral-force, and rolling-moment coefficients $C_n$, $C_Y$, and $C_l$, respectively, are generally considered to be aerodynamic parameters. It is of interest to note, however, that for detached

empennage tests of the type presented in this paper, the parameters $C_n$, $C_Y$, and $C_l$ may also be usefully considered as coefficients of torsion, side force, and bending, respectively, of the vertical tail. In this paper, therefore, these coefficients will be discussed in the twofold role.

Yawing-moment coefficient.- The variation of yawing-moment coefficient $C_n$ with $\beta$ is presented in figure 10. Higher variations of $C_n$ with $\beta$ were generally exhibited for configurations with horizontal surfaces at the intermediate positions ($h/b_v = 0.26$ and 0.59), than at the end positions with $h/b_v = 0$ and 1.00, respectively.

Lateral-force coefficient.- Presented in figure 11 is the variation of lateral-force coefficient $C_Y$ with $\beta$ for all configurations investigated. An asymmetrical nonlinearity in the variation of $C_Y$ with $\beta$ near $0^\circ$ angle of sideslip (figs. 11(e), 11(f), and 11(g), respectively) occurred at $M = 0.80$ and 0.86 for tail configurations with simple, unfaired intersections between the horizontal and vertical surfaces ($h/b_v = 0.26$, 0.59, and 1.00). This nonlinearity may probably be attributed to the critically unstable flow condition present on relatively thick airfoil sections at the low Reynolds numbers of these tests, which may be prematurely aggravated at Mach numbers of 0.80 to 0.92 by the presence of the unfaired intersection. (A flow breakdown similar to that apparently present in these tests at or near $0^\circ$ angles of attack and sideslip may well account for the recurrent reports of transient and unpredictable stability, loading, and control-force difficulties experienced on some service aircraft at relatively low subsonic speeds.) As is evident in figure 11(d), such effects are minimized on an empennage with a faired intersection such as the tail configuration with the horizontal surface mounted on the fuselage ($h/b_v = 0$).

A pronounced "break" in the variation of $C_Y$ with $\beta$ occurred at about $8^\circ$ angle of sideslip up to a Mach number of 0.86 for all configurations equipped with the vertical surface (fig. 11). In order to isolate the effects of fuselage nose shape on the nonlinearity at $\beta = 8^\circ$, tests were made with a modified fuselage nose at a Mach number of 0.2. Substitution of a hemispherical nose in place of the elliptical nose of the original test configuration (fig. 2) had no appreciable effect on the variation of $C_Y$ with $\beta$ at $M = 0.2$ (fig. 11(c)). The nonlinearity at $\beta = 8^\circ$ is apparently, therefore, also a characteristic of the airfoil section which may be aggravated by the interference effects of the fuselage at the low Reynolds numbers of these tests.

At constant values of $\beta$, the highest values of $C_Y$ were consistently obtained for the high horizontal-tail position ($h/b_v = 1.00$) as

shown in figure 11. Somewhat lower values of $C_Y$ of the same general order of magnitude resulted for the low and intermediate tail positions ($h/b_v$ = 0, 0.26, and 0.59).

Presented in figure 12 is a summary of the variation of $C_{Y_\beta}$ with Mach number and with horizontal-tail position. Below a Mach number of about 0.7, the Mach number at which the "force break" occurred for the airfoils, $C_{Y_\beta}$ increased slightly with increase in Mach number for all configurations (fig. 12(a)). At Mach numbers of 0.80 and 0.86, the previously mentioned Mach number and viscous effects present at low angles of sideslip for the configurations with $h/b_v$ = 0.26 and 0.59 became manifest as a sharp reduction in the value of $C_{Y_\beta}$ with a similar but lesser effect for $h/b_v$ = 1.00. (It should be noted, however, that the reduction in value of $C_{Y_\beta}$ at these Mach numbers is not indicative of a reduction in the absolute value of $C_Y$ at the higher sideslip angles.) At the higher Mach numbers, above M = 0.92 for most configurations, $C_{Y_\beta}$ increased rapidly with increase in Mach number. Location of the horizontal tail in the intermediate positions ($h/b_v$ = 0.26 and 0.59) resulted in consistently lower values of $C_{Y_\beta}$ (fig. 12(b)), than did location at the outer tips of the vertical tail ($h/b_v$ = 0 and 1.00) or for the vertical-tail-alone configuration.

Rolling-moment coefficient.- The variation of rolling-moment coefficient $C_l$ with $\beta$ is presented in figure 13 for all tail configurations and Mach numbers investigated. The viscosity and compressibility effects apparent in the curves of $C_Y$ against $\beta$ (fig. 11), are also evident in the variation of $C_l$, which is, of course, a function of the lateral force on the vertical tail. (Scatter of the repeated data points at M = 0.92 and 0.94 for the configuration with the horizontal surface located at 59 percent vertical-surface span, (fig. 13(f)) is an indication of the unsteady data readings obtained and caused by the critical loading conditions present at these Mach numbers.)

Presented in figure 14 are the experimental variations of $C_{l_\beta}$ with Mach number and with horizontal-tail position. A general trend of a slight increase in magnitude of $C_{l_\beta}$ with Mach number up to the "force break" Mach number occurred for all configurations (fig. 14(a)). Above M = 0.7, a pronounced decrease in $C_{l_\beta}$ is evident with a reversal in trend and increase in $C_{l_\beta}$ from M = 0.92 to 0.94. At the low Mach numbers of 0.5 to 0.7, the parameter $C_{l_\beta}$ increased with increase

in horizontal-tail height (fig. 14(b)), the value of $C_{l_\beta}$ at $h/b_v = 1.0$ being about 3 times that at $h/b_v = 0$.

Between Mach numbers of 0.80 and 0.92, a marked decrease in values of $C_{l_\beta}$ occurred for the intermediate tail positions ($h/b_v = 0.26$ and 0.59) which is a result of the nonlinear viscous and Mach number effects on the variation of $C_l$ with $\beta$ near $\beta = 0^\circ$. At the highest Mach number tested, $M = 0.94$, these effects were minimized and the variation of $C_{l_\beta}$ with horizontal-tail height was more linear, assuming a trend somewhat similar to that at low Mach numbers. From the standpoint of loads on the vertical tail, the low horizontal-tail position ($h/b_v = 0$), with consistently lower values of $C_{l_\beta}$, again appears as the most satisfactory empennage arrangement.

## Comparison of Experimental and Theoretical Results

Calculations to determine the theoretical span loadings of four of the tail configurations investigated experimentally and presented in this paper were performed using a finite-step method of replacing the vertical and horizontal tail surfaces by a finite number of horseshoe vortices. A discussion of the method used (ref. 1) and its application to the various model configurations is contained in the appendix of this paper. Calculations were made for the fuselage and vertical tail alone and with horizontal surfaces mounted at 0, 60, and 100 percent vertical-surface span. Spanwise step loadings were calculated for each configuration at several Mach numbers by applying the Prandtl-Glauert transformation. Integrated results of the span loadings, expressed as $C_{Y_\beta}$ and $C_{l_\beta}$, are presented and compared in figure 15 with the experimental results of this paper.

Agreement between the experimental and theoretical values of $C_{Y_\beta}$ (fig. 15) up to the "force break" Mach number of about 0.7 is fair, with the theoretical values being somewhat smaller than those obtained from experiments. Above the "force break" Mach number, the combined viscous and compressibility effects apparent in the variation of $C_Y$ with $\beta$ (fig. 11) caused a sharp reduction in the experimental values of $C_{Y_\beta}$ with attendant divergence from the theoretical curve.

Good agreement is obtained, up to Mach number of 0.7, between the experimental and theoretical values of $C_{l_\beta}$ (fig. 15). Above $M = 0.7$, the nonlinear viscous and compressibility effects apparent in figures 11

and 13 again cause a sharp divergence between experiment and theory with the theoretical values being larger.

Generally good agreement between the experimental and theoretical values of $C_{Y_\beta}$ and $C_{l_\beta}$ (fig. 15) indicates that the calculated spanwise step loadings obtained by means of the finite-step method are fairly representative of the spanwise load distribution of the vertical and horizontal tails, at least up to the "force break" Mach number. At higher Mach numbers, however, the first-order approximations of theory do not take into account the nonlinear effects of viscosity and compressibility. (The slight displacement, even at Mach numbers of 0.2 to 0.7, between the theoretical curve and the experimental points for $C_{Y_\beta}$ is believed to be mainly the result of the simplified representation of the fuselage employed in the theoretical computations.) Of particular interest (fig. 15) is the large change in $C_{l_\beta}$ between the low and high tail configurations. Representative sketches of the load distributions calculated herein by means of the finite-step method and presented in figure 16 indicate the reasons for this change. For the low tail configuration, $h/b_v = 0$, the induced loading on the horizontal tail is such as to reduce the total moment, or $C_l$, of the combination. For the high tail configuration, $h/b_v = 1.00$, the reverse is true; that is, the moment of the induced loading on the horizontal tail increases the total moment, or $C_l$, about the fuselage center line. Although the loading and center-of-pressure location of the vertical tail influence the $C_{l_\beta}$ of the tail assembly, the dominating effect for a tail assembly having a horizontal tail of this size is the $C_{l_\beta}$ produced by the loading induced on the horizontal tail. (See ref. 1.) (It is of interest to note from figs. 11 and 13 that the ratio of $C_l$ to $C_Y$ at high sideslip angles is in general similar to the ratio at low values of $\beta$, thus implying that the calculated load distributions indicated in figure 16 are fairly representative of the loadings at the higher sideslip angles.)

## CONCLUSIONS

From an investigation at high subsonic speeds of the effects of horizontal-tail height on the aerodynamic characteristics in sideslip of an unswept, untapered empennage, at $0^\circ$ angle of attack the following conclusions can be made:

1. Above a Mach number of about 0.7, even at $0^\circ$ angle of attack, abrupt changes in lift coefficient occurred with increase in Mach number for all horizontal-tail positions.

2. The lowest values of minimum drag coefficient $C_{D_{min}}$ were obtained for the low tail configuration with the fuselage acting as a fairing between the horizontal and vertical surfaces. The value of $C_{D_{min}}$ was generally independent of horizontal-tail height at all Mach numbers for configurations with simple, unfaired intersections between the horizontal and vertical surfaces.

3. The positive value of pitching-moment coefficient $C_m$ increased with horizontal-tail height and with Mach number for all configurations except that with the horizontal tail at 26 percent vertical-surface span.

4. The variation of lateral-force coefficient with sideslip angle $C_{Y_\beta}$ increased slightly with increase in Mach number up to the "force break" Mach number of about 0.7 for all configurations. Viscous and compressibility effects, evidenced as a sharp reduction in the value of $C_{Y_\beta}$ at Mach numbers of 0.80 and 0.86, were minimized for the low horizontal-tail position with the fuselage acting as a fairing in the intersection of the horizontal and vertical surfaces. Location of the horizontal tail in the intermediate positions (26- and 59-percent vertical-span location) resulted in consistently lower values of $C_{Y_\beta}$ than did location at the outer tips of the vertical tail (0 and 100 percent span).

5. The variation of rolling-moment coefficient with angle of sideslip $C_{l_\beta}$ increased with Mach number up to the "force-break" Mach number. At constant Mach number $C_{l_\beta}$ increased with increase in horizontal-tail height.

6. Theoretical calculations of the parameters $C_{Y_\beta}$ and $C_{l_\beta}$ by the finite-step method reasonably agreed with the experimental values up to the "force-break" Mach number.

Langley Aeronautical Laboratory,
National Advisory Committee for Aeronautics,
Langley Field, Va., October 7, 1953.

## APPENDIX

## THEORETICAL COMPUTATIONS FOR THE TAIL ASSEMBLY

Basic considerations.- The finite-step method used herein to evaluate the subsonic span loadings on the vertical and horizontal tails for several of the tail-assembly configurations indicated in figure 2 is particularly well known from its application to the problem of determining the span loading on wings. Reference 3, for example, uses the method for determining span load distributions on several wings of unusual plan form and in addition presents a detailed mathematical derivation of the method as applied to wings. In connection with intersecting surfaces, reference 1 employs the finite-step method for calculating the sideslipping span load distributions for a somewhat geometrically similar tail-assembly model.

The finite-step method involves replacing the vertical and horizontal tail surfaces by a finite number of horseshoe vortices that are distributed in a spanwise direction across the tail surfaces with the bound portion located at the quarter-chord line. The velocity normal to the surface arising from the complete vortex system is then calculated at the three-quarter-chord line for the midspan location of each horseshoe vortex. At each of these control points, the requisite boundary condition of tangential flow is satisfied by equating the expression for the normal velocity resulting from the complete vortex system to the component of the free-stream velocity normal to the surface. For the vertical tail the free-stream component is $V\beta$ and for the horizontal tail it is $V\alpha$ which is zero since $\alpha$ was held at zero for the experimental tests. The expression for the normal velocity at a given control point contains the unknown circulations of all horseshoe vortices used to define the configuration and when the expressions for all the control points are solved simultaneously, values of the unknown circulations and hence the span loadings are obtained. For a more detailed discussion see references 1 and 3.

Application of method.- Calculations to determine the span loadings were performed for four of the tail configurations investigated experimentally. These configurations are the fuselage—vertical-tail combination alone, and with the horizontal tail at vertical locations of 0, 60, and 100 percent of the vertical-tail span. Since the vertical-tail span was considered in the experimental investigation to extend from the tip of the vertical tail to the fuselage center line, five equal-span horseshoe vortices were distributed across the vertical tail with the bound portion located at the quarter-chord line. Using this vortex span, which is approximately equal to the fuselage radius, resulted in the use of five horseshoe vortices on each panel of the horizontal tail

for the mid and high horizontal-tail locations (0.60 and 1.00h/$b_v$, respectively). For the horizontal tail in the low position, however, it was necessary to include a half-span vortex at each tip of the horizontal tail to approximate more closely the dimensions of the tail-assembly model. An approximation of the effect of the fuselage was also incorporated into the computations in the manner of reference 1, which simply considers fuselage depth as an extension to the vertical-tail span and fuselage width as an end plate. Since the original horseshoe vortices were about equal to the fuselage radius in span, this approximation required only three additional vortices: one to account for the remaining fuselage depth and two to account for the fuselage width. Sketches of the four horseshoe vortex configurations considered herein are presented in figure 17.

The solution of the expressions for the normal velocity at the control points to obtain the span loadings was obtained by use of an elimination procedure in conjunction with a relay-type computing machine. The actual number of simultaneous equations necessary to solve for the different configurations could be reduced since the loadings in sideslip on the two panels of the horizontal tail were equal in magnitude but of opposite sign. This condition is also applicable to the representation used for the fuselage width.

Effect of compressibility.- In order to indicate the effect of Mach number on the calculated results, the Prandtl-Glauert transformation which accounts for the effect of compressibility was applied to each of the four configurations of the tail assembly considered. In accordance with the rule (see ref. 4) each configuration was stretched in the chordwise direction in the amount of the ratio $\frac{1}{\sqrt{1 - M^2}}$. The configurations were then replaced by the corresponding horseshoe vortex representation of figure 17. Loadings were calculated for the vortex representations as if in incompressible flow and the results were considered to be carried on the undistorted tail configuration at the Mach number in question. Computations to determine the loadings were performed herein for each of the four horseshoe-vortex representations of figure 17 at Mach numbers of 0, 0.60, 0.80, and 0.90.

Effect of section lift-curve slope.- Satisfying the boundary conditions at the three-quarter-chord line for the finite-step method, as enumerated herein, indicates that the theoretical thin-airfoil-section lift-curve slope of $2\pi/57.3$ is assumed. Before a comparison between theoretical and experimental results can be effected, a correction accounting for the difference between the actual and theoretical values of section lift-curve slope must be applied to the calculated results. For the case where the actual section lift-curve slope $c_{l_\alpha}$ is about constant across the span and where only a small correction is needed,

it appears sufficient to reduce the calculated values by the ratio $57.3c_{l_\alpha}/2\pi$. For more exact computations, the position of the control point may be shifted relative to the three-quarter-chord line to account for variations in $c_{l_\alpha}$. (See refs. 2 and 4.)

For the tail-assembly model investigated experimentally, both the vertical and horizontal tails had NACA 64A010 airfoil sections. Airfoil-section data of reference 5 indicate that the section lift-curve slope for an NACA 64A010 airfoil section is about 4 percent less than theoretical. Accordingly, all the calculated values were reduced in proportion to the ratio $57.3c_{l_\alpha}/2\pi$, including the values obtained for the horseshoe-vortex representation of the fuselage.

Some comments on effect of fuselage.- Although several simplifying assumptions were made in the use of the finite-step method and in the manner of reducing the calculated values to results comparable with experiment, the use of the simplified representation of the fuselage is believed to have enough influence to account for a large portion of the difference existing between experimental and calculated results for $C_{Y_\beta}$ shown in figure 15. Good agreement was obtained between experimental and calculated results of reference 3 for $C_{Y_\beta}$ where the fuselage was represented in the same manner as was done herein; however, the fuselage of the present investigation is widely different from that of reference 3, particularly in one of the more important geometric parameters, the ratio of body diameter at the tail to vertical-tail span $(d/b_v)$. The fuselage of reference 3 had a $d/b_v$ value of 0.25 while the fuselage of the present investigation had a $d/b_v$ value of approximately 0.39. The accuracy of the results for $C_{Y_\beta}$, of course, would be expected to decrease as $d/b_v$ increases. On the basis of some preliminary comparisons of experimental and calculated results for $C_{Y_\beta}$ for a normal-length fuselage model with a normally located tail, the method of references 6 and 7 appears to provide reasonable accuracy for the estimation for the effect of the fuselage. The method of references 6 and 7 would probably be an improvement over the simple representation used herein in that it attempts, although not rigorously, to approximate the boundary conditions of the fuselage.

## REFERENCES

1. Riley, Donald R.: Effect of Horizontal-Tail Span and Vertical Location on the Aerodynamic Characteristics of an Unswept Tail Assembly in Sideslip. NACA TN 2907, 1953.

2. Herriot, John G.: Blockage Corrections for Three-Dimensional-Flow Closed-Throat Wind Tunnels, With Consideration of the Effect of Compressibility. NACA Rep. 995, 1950. (Supersedes NACA RM A7B28.)

3. Campbell, George S.: A Finite-Step Method for the Calculation of Span Loadings of Unusual Plan Forms. NACA RM L50L13, 1951.

4. DeYoung, John, and Harper, Charles W.: Theoretical Symmetric Span Loading at Subsonic Speeds for Wings Having Arbitrary Plan Form. NACA Rep. 921, 1948.

5. Loftin, Laurence K., Jr.: Theoretical and Experimental Data for a Number of NACA 6A-Series Airfoil Sections. NACA Rep. 903, 1948. (Supersedes NACA TN 1368.)

6. Robinson, Samuel W., Jr., and Zlotnick, Martin: A Method for Calculating the Aerodynamic Loading on Wing—Tip-Tank Combinations in Subsonic Flow. NACA RM L53B18, 1953.

7. Zlotnick, Martin, and Robinson, Samuel W., Jr.: A Simplified Mathematical Model for Calculating Aerodynamic Loading and Downwash for Midwing Wing-Fuselage Combinations With Wings of Arbitrary Plan Form. NACA RM L52J27a, 1953.

TABLE I.- ORDINATES OF FUSELAGE NOSE AND NACA 64A010 AIRFOIL SECTION

All ordinates in inches

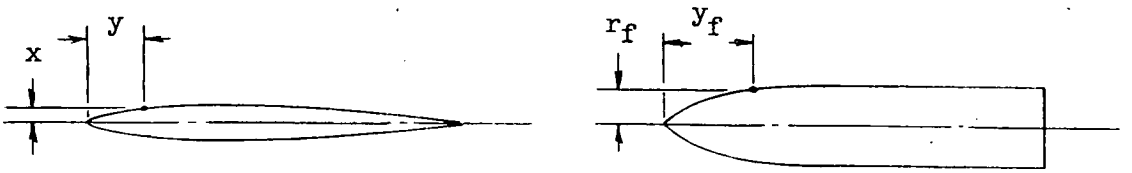


| Airfoil section ordinates | |
|---|---|
| x | y |
| 0 | 0 |
| .030 | .048 |
| .045 | .058 |
| .075 | .074 |
| .150 | .101 |
| .300 | .140 |
| .450 | .168 |
| .600 | .192 |
| .900 | .229 |
| 1.200 | .256 |
| 1.500 | .276 |
| 1.800 | .290 |
| 2.100 | .298 |
| 2.400 | .300 |
| 2.700 | .294 |
| 3.000 | .281 |
| 3.300 | .263 |
| 3.600 | .241 |
| 3.900 | .216 |
| 4.200 | .188 |
| 4.500 | .157 |
| 4.800 | .126 |
| 5.100 | .095 |
| 5.400 | .064 |
| 5.700 | .033 |
| 6.000 | .001 |
| L.E. radius = 0.041 in. | |
| T.E. radius = 0.001 in. | |

| Fuselage nose ordinates | |
|---|---|
| $x_f$ | $r_f$ |
| 0 | 0 |
| .06 | .16 |
| .20 | .32 |
| .41 | .49 |
| .81 | .73 |
| 1.28 | .95 |
| 1.95 | 1.19 |
| 3.05 | 1.49 |
| 4.16 | 1.73 |
| 5.44 | 1.95 |
| 6.73 | 2.12 |
| 7.93 | 2.23 |
| 9.10 | 2.32 |
| 10.23 | 2.37 |
| 11.38 | 2.42 |
| 12.74 | 2.46 |
| 14.15 | 2.48 |
| 15.50 | 2.49 |
| 16.86 | 2.50 |
| 24.00 | 2.50 |

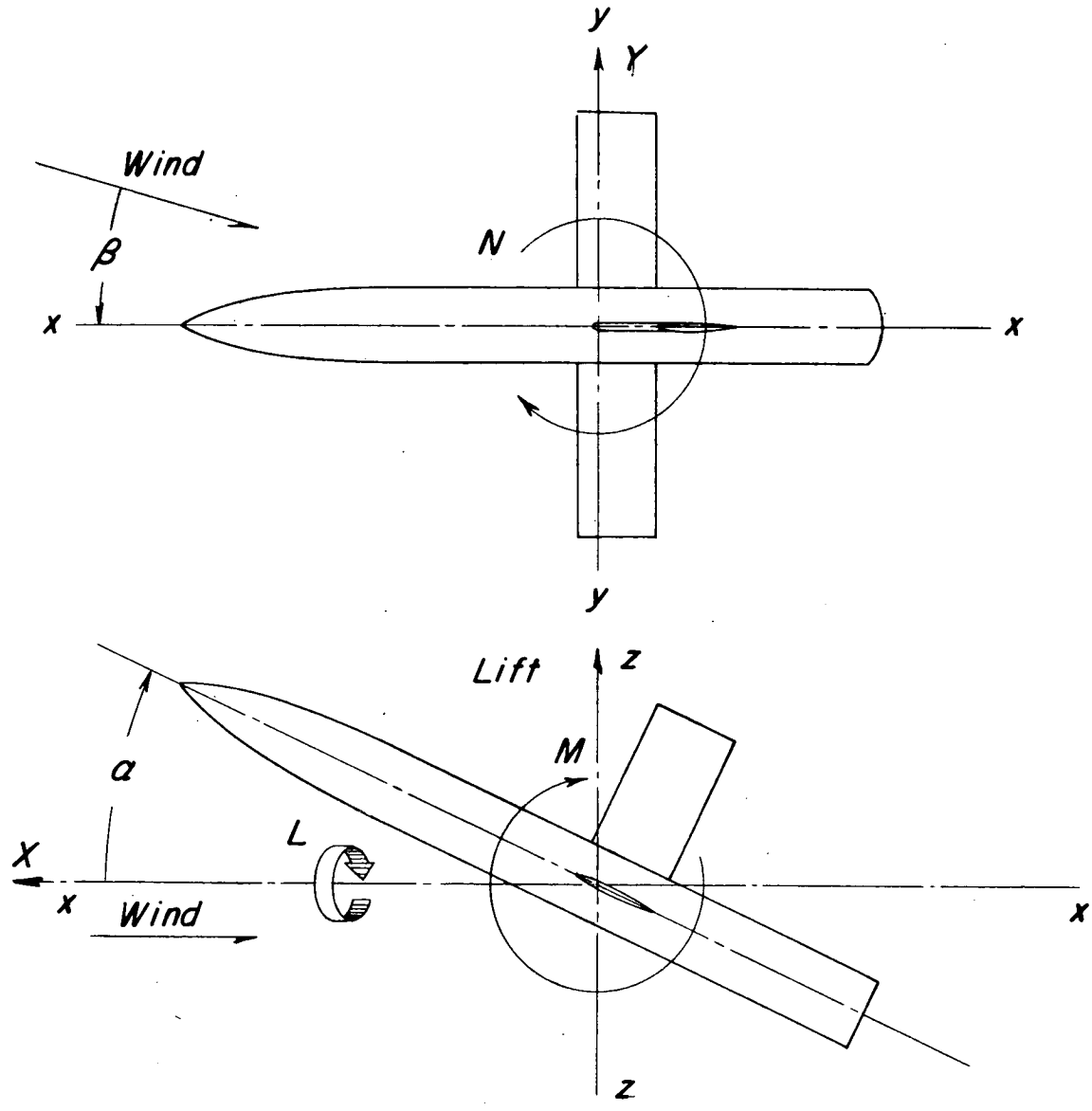


Figure 1.- System of stability axes. Positive directions of forces, moments, and angles are indicated by arrows.

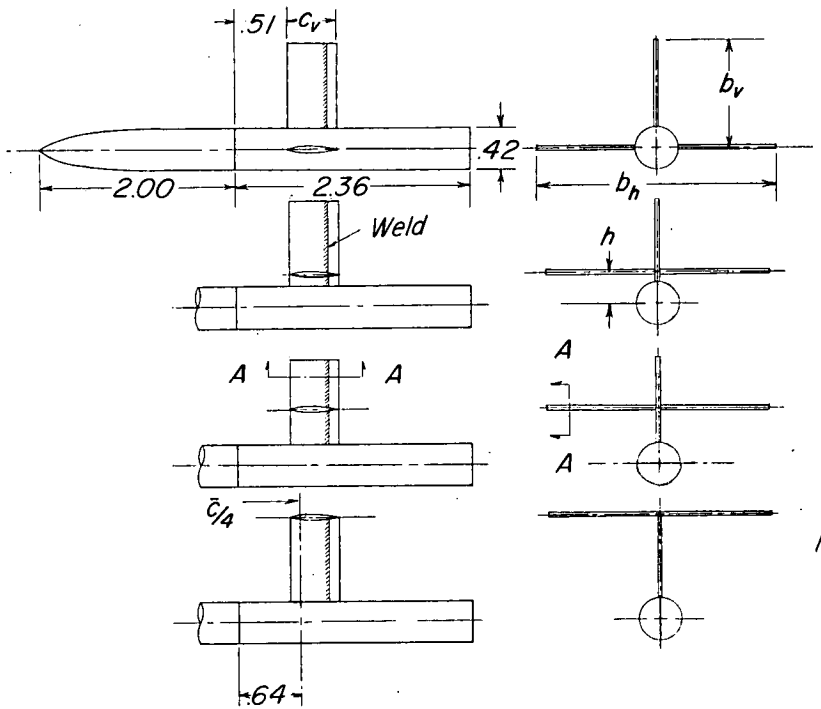


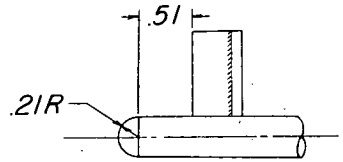


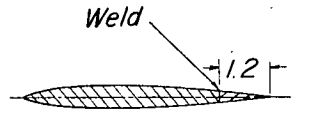


Note: Airfoil section and fuselage nose ordinates are given in table I.

Physical Characteristics of Various Tail Configurations

| Model | $b_v$ | $c_v$ | $S_v$ | $A_v$ | $b_h$ | $c_h$ | $S_h$ | $A_h$ | $h$ | $\frac{h}{b_v}$ |
|---|---|---|---|---|---|---|---|---|---|---|
| ○ | — | — | — | — | 2.406 | 0.5 | 1.203 | 4.81 | — | — |
| ⊢○⊣ | 1.078 | 0.5 | 0.539 | 2.16 | — | — | — | — | — | — |
| ⊢○⊣ | 1.078 | 0.5 | 0.539 | 2.16 | 2.406 | 0.5 | 1.203 | 4.81 | 0 | 0 |
| ⊢○⊣ | 1.078 | 0.5 | 0.539 | 2.16 | 2.270 | 0.5 | 1.135 | 4.52 | 0.280 | .26 |
| ⊢○⊣ | 1.078 | 0.5 | 0.539 | 2.16 | 2.270 | 0.5 | 1.135 | 4.52 | 0.640 | .59 |
| ⊢○⊣ | 1.078 | 0.5 | 0.539 | 2.16 | 2.270 | 0.5 | 1.135 | 4.52 | 1.078 | 1.00 |

Figure 2.- Sketches of the tail models as tested in the Langley high-speed 7- by 10-foot tunnel. (All dimensions in feet unless otherwise noted.)

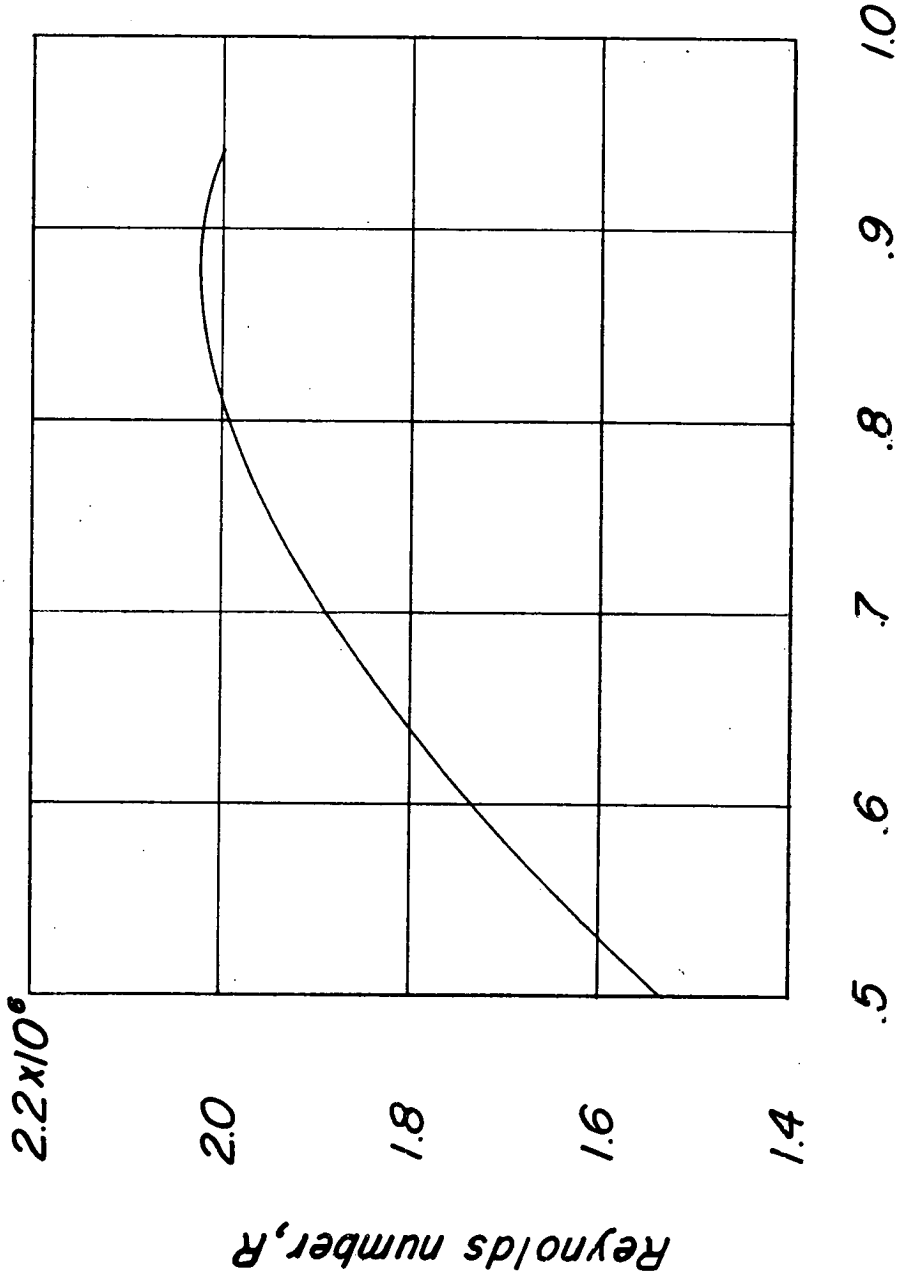


Figure 3.- Variation of test Reynolds number with Mach number. (Reynolds number based on the mean aerodynamic chord of the vertical surface.)

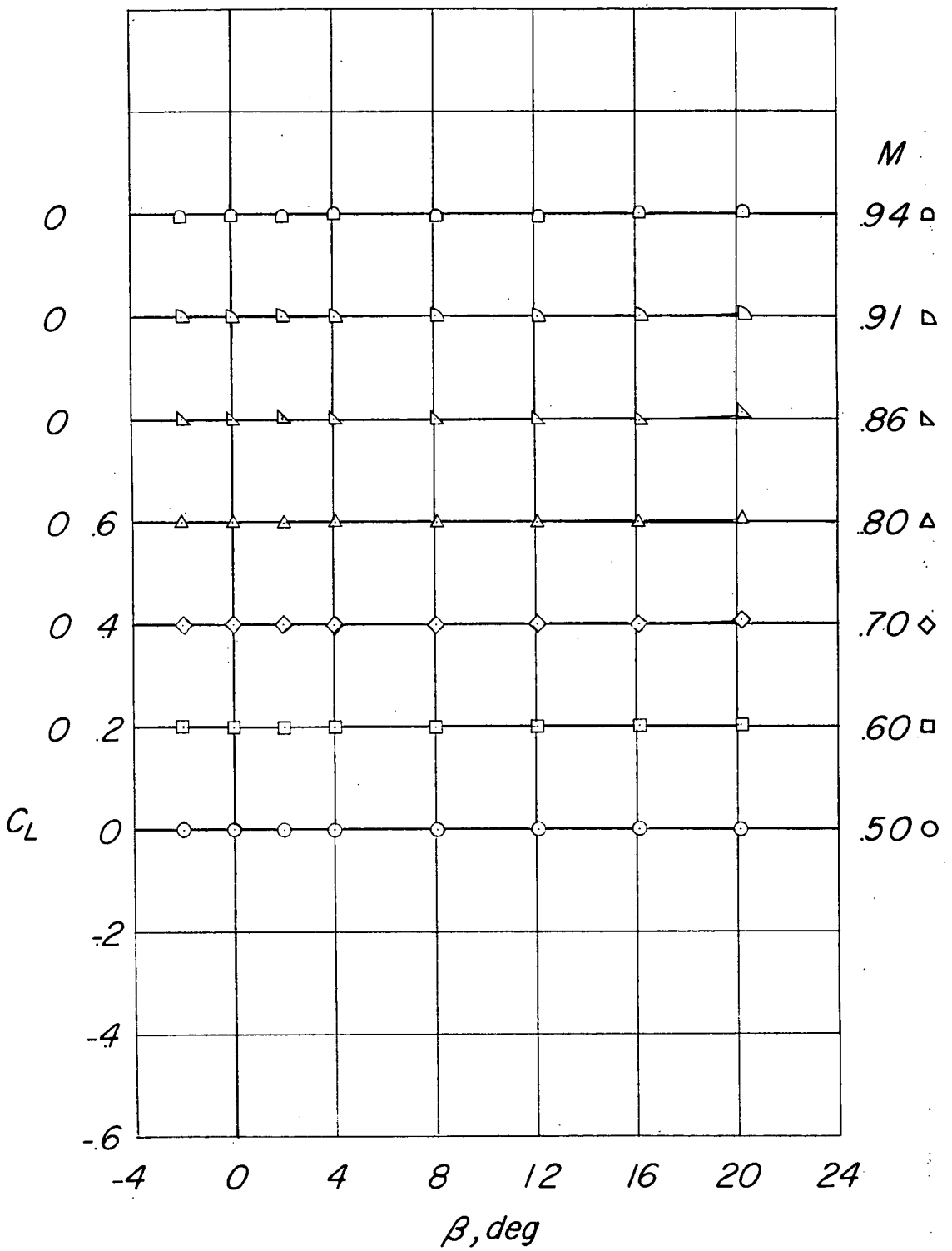


(a) Fuselage alone.

Figure 4.- Variation of $C_L$ with angle of sideslip. $\alpha = 0^\circ$.

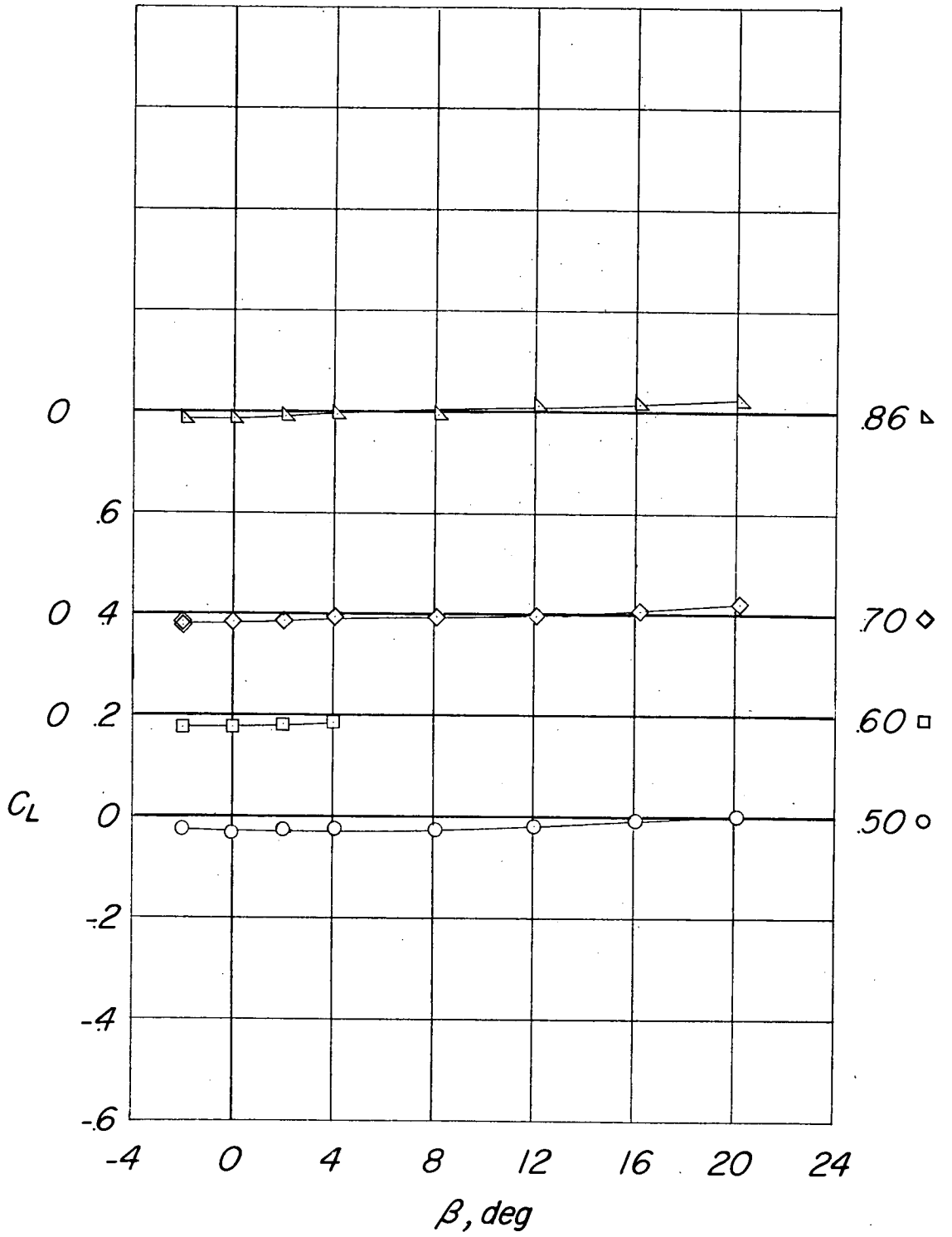


(b) Fuselage plus horizontal tail.

Figure 4.- Continued.

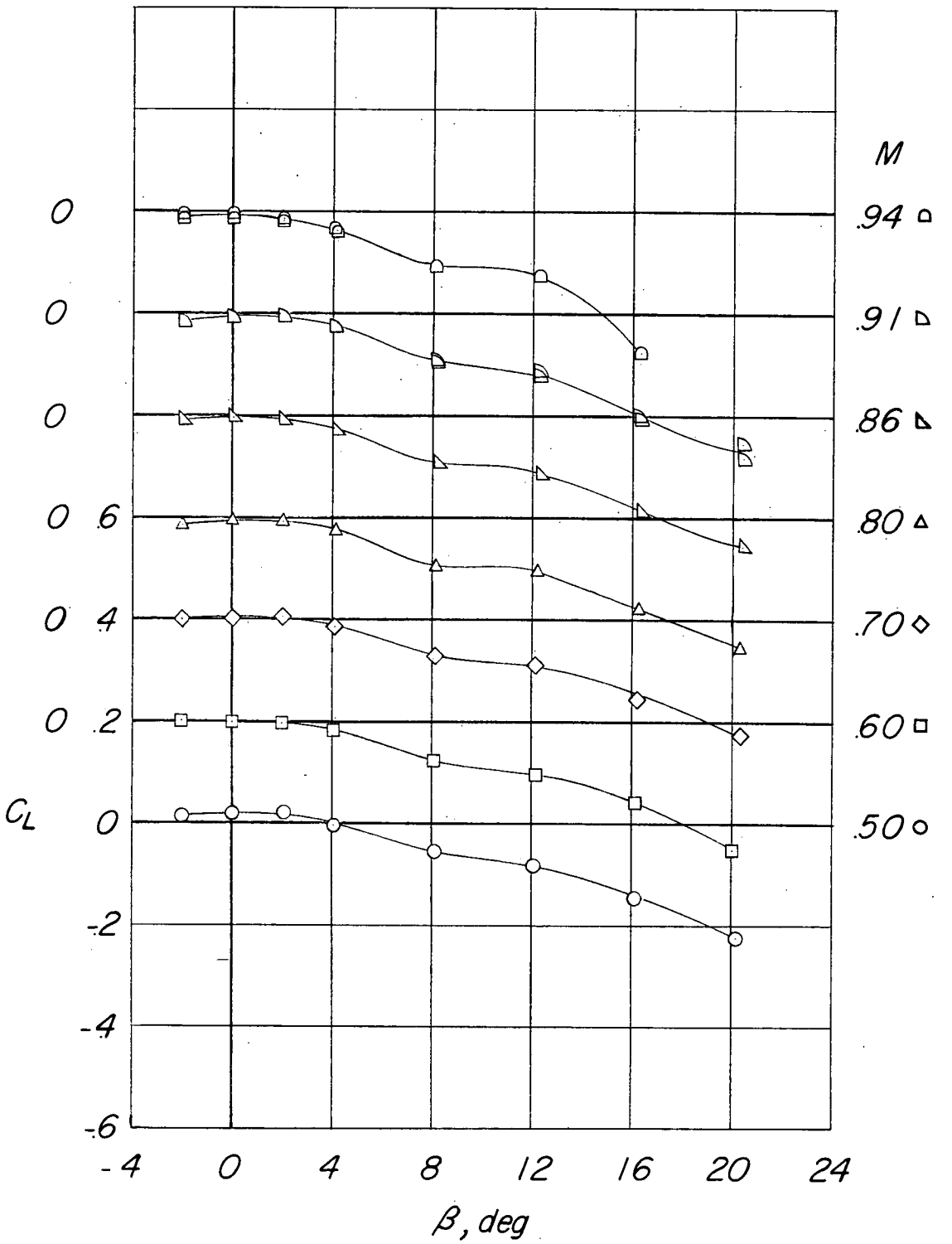


(c) Fuselage plus vertical tail.

Figure 4.- Continued.

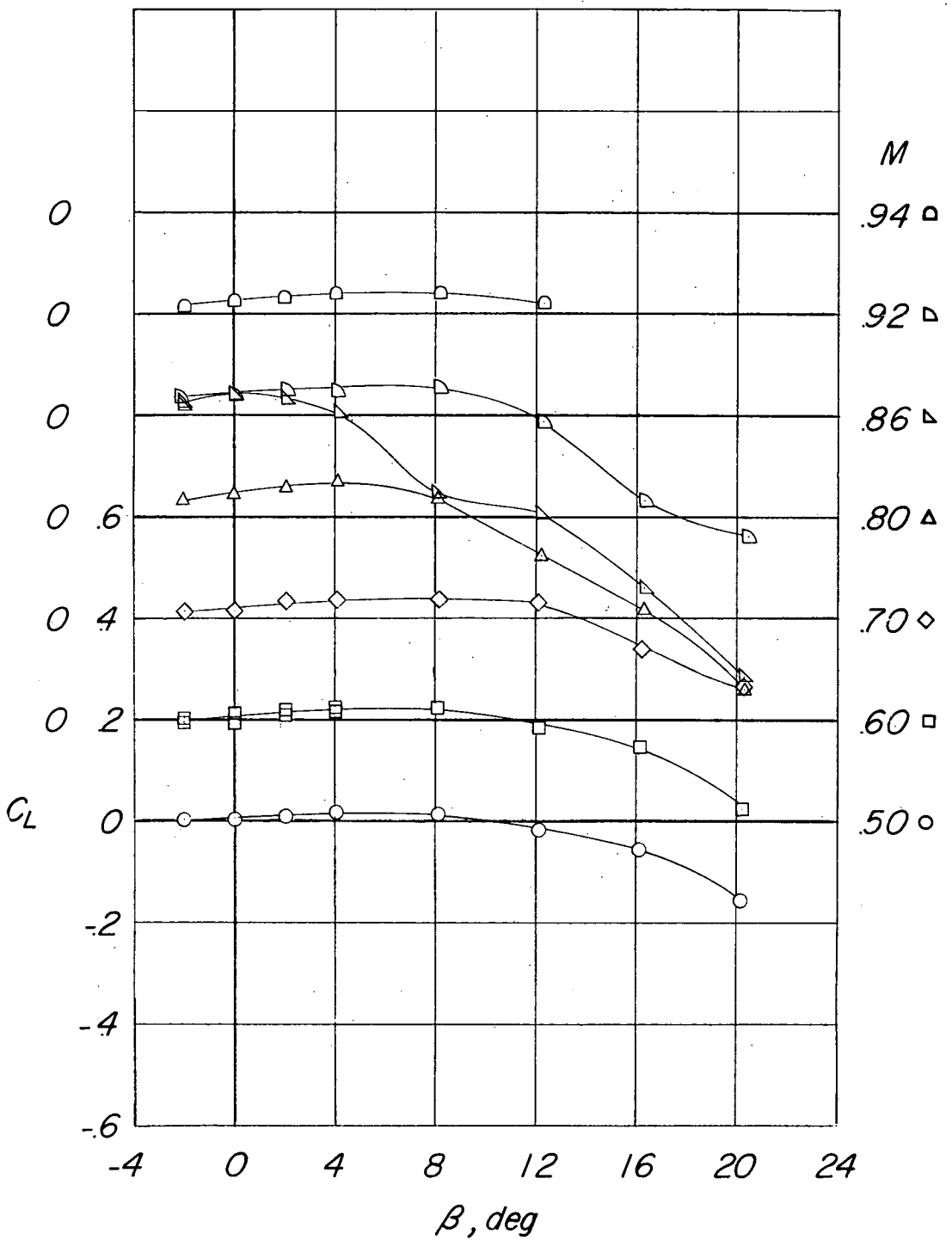


(d) Fuselage plus vertical tail plus horizontal tail. $\frac{h}{b_v} = 0$.

Figure 4.- Continued.

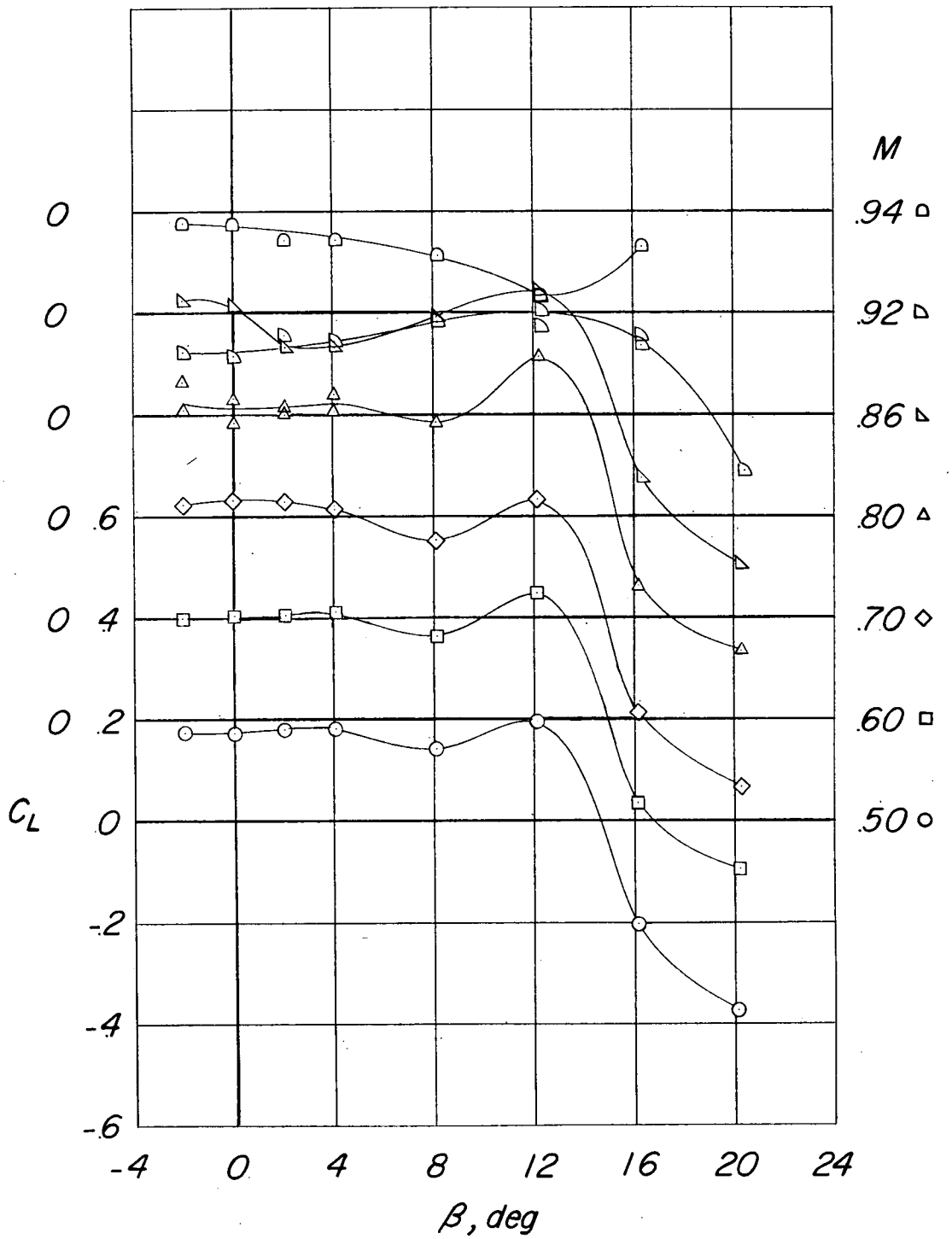


(e) Fuselage plus vertical tail plus horizontal tail. $\frac{h}{b_v} = 0.26$.

Figure 4.- Continued.

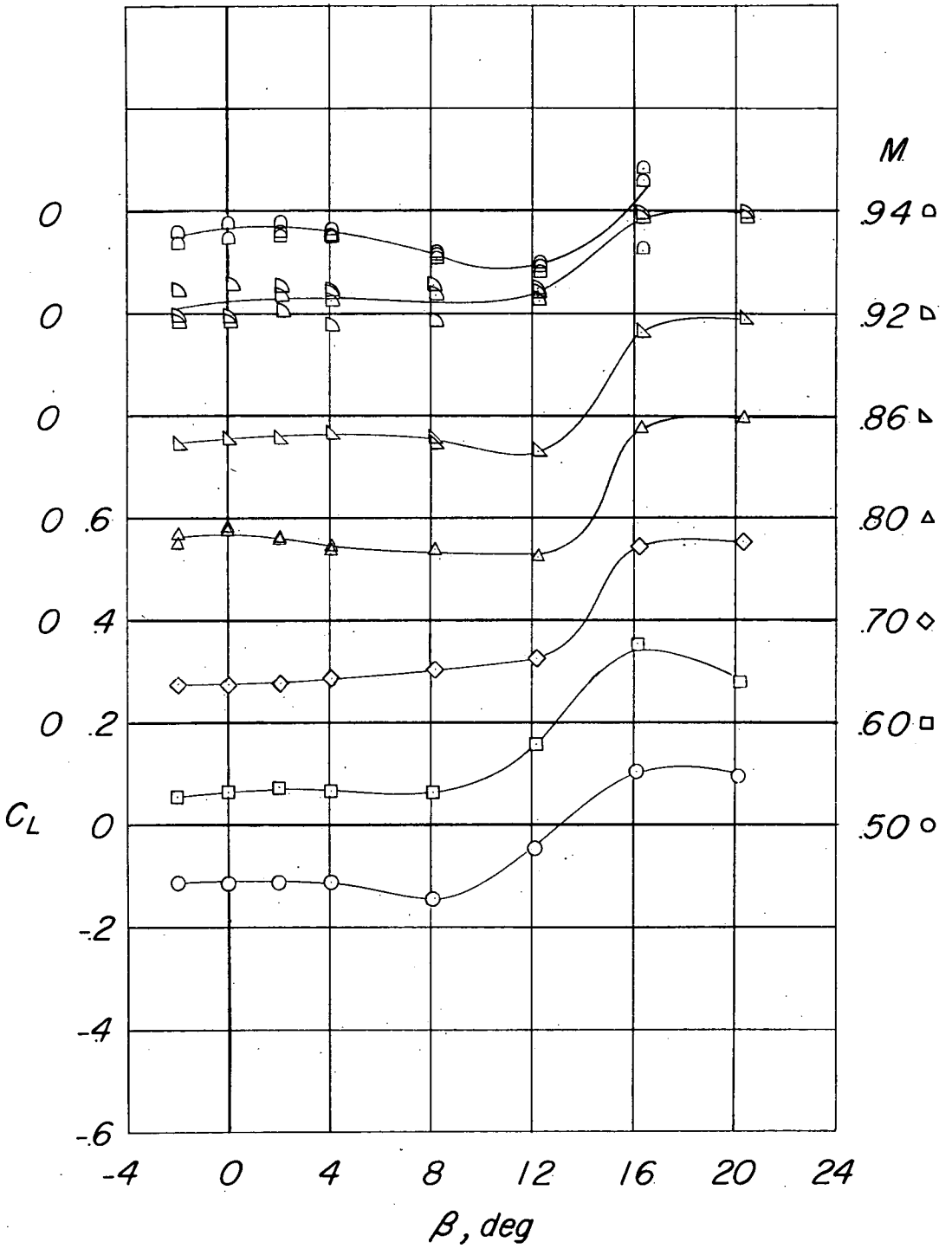


(f) Fuselage plus vertical tail plus horizontal tail. $\frac{h}{b_v} = 0.59$.

Figure 4.- Continued.

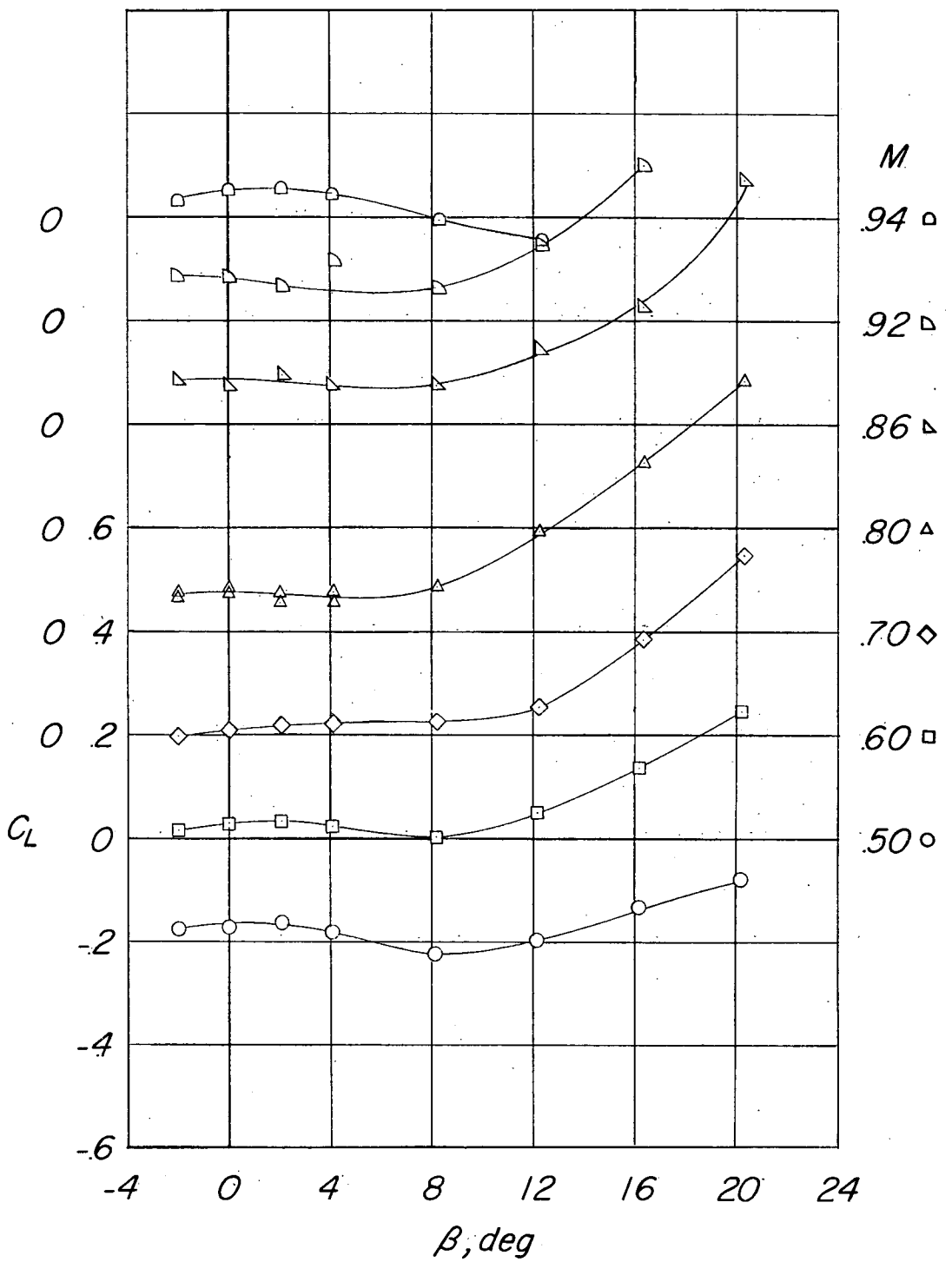


(g) Fuselage plus vertical tail plus horizontal tail. $\frac{h}{b_v} = 1.00$.

Figure 4.- Concluded.

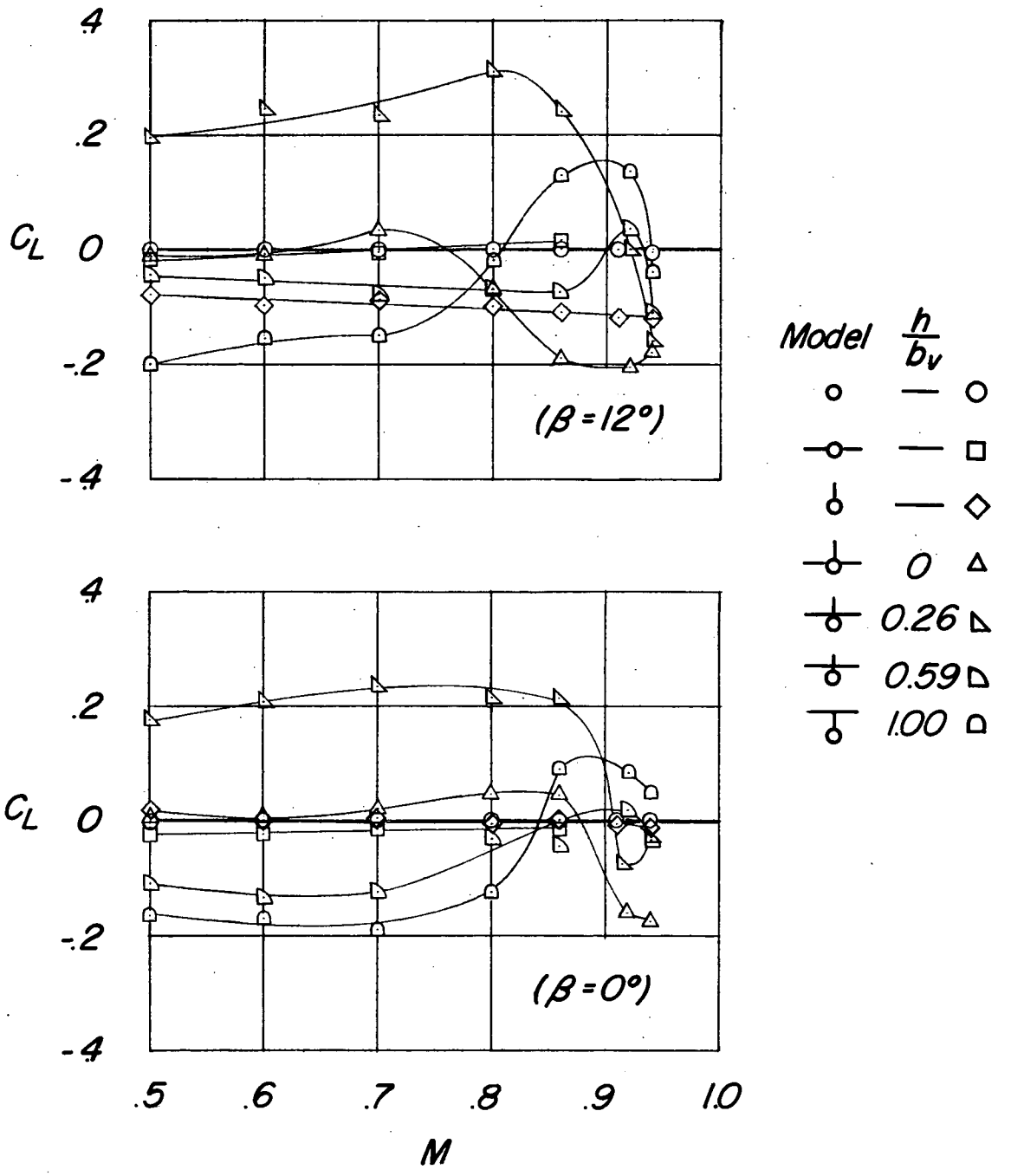


Figure 5.- Variation of lift coefficient with Mach number for various tail configurations. $\alpha = 0^{\circ}$.

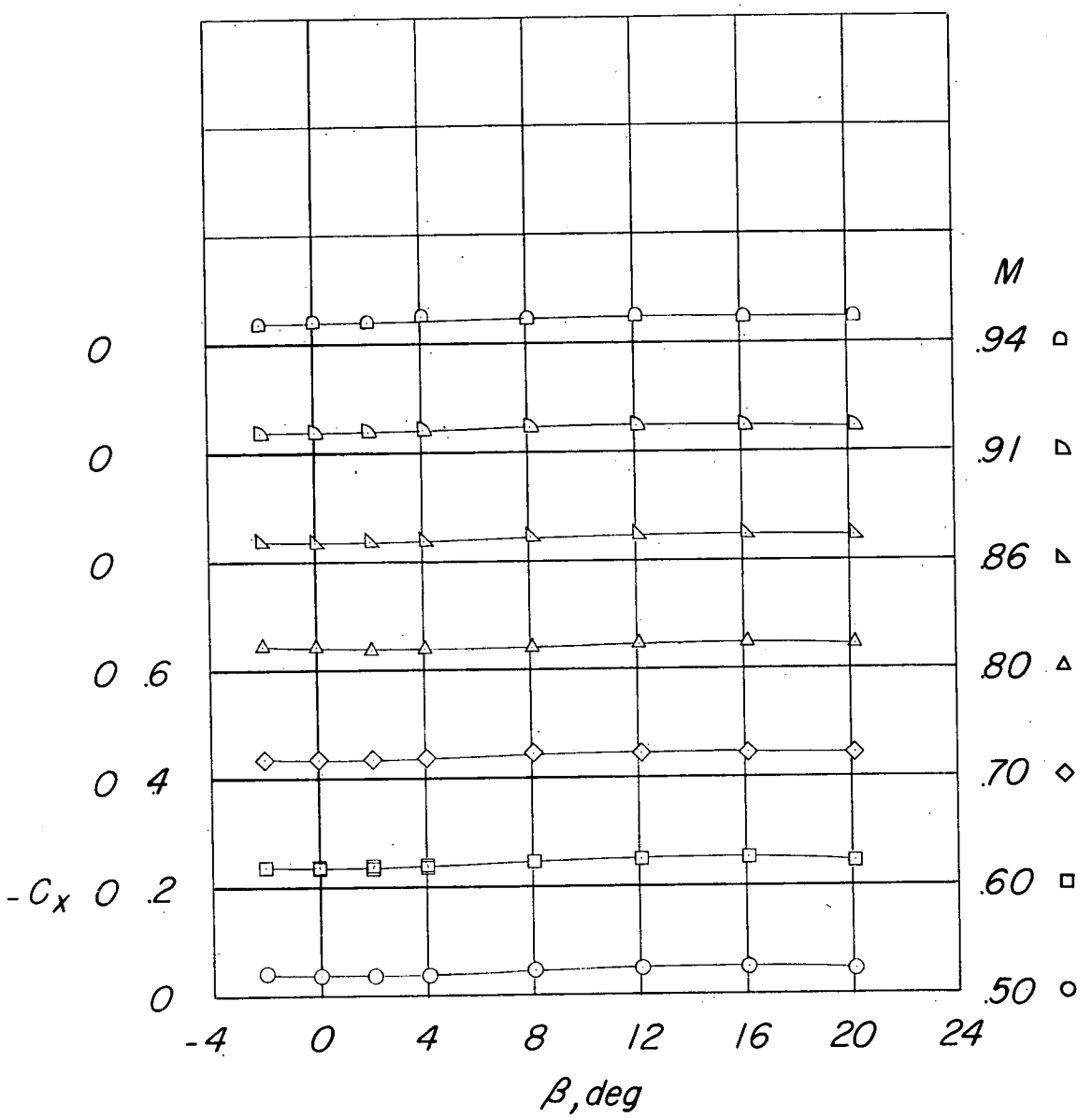


(a) Fuselage alone.

Figure 6.- Variation of $C_X$ with angle of sideslip. $\alpha = 0^\circ$.

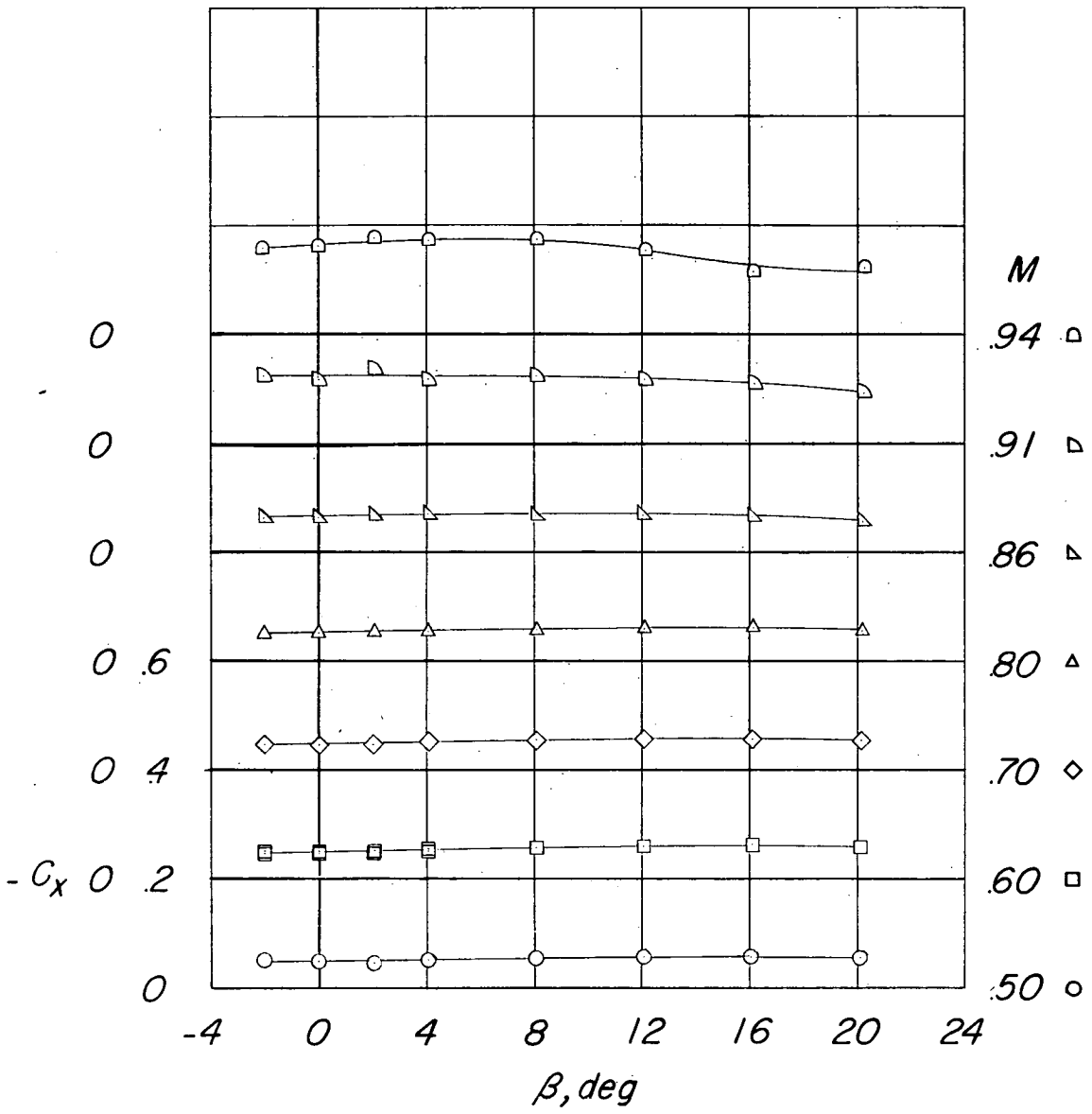


(b) Fuselage plus horizontal tail.

Figure 6.- Continued.

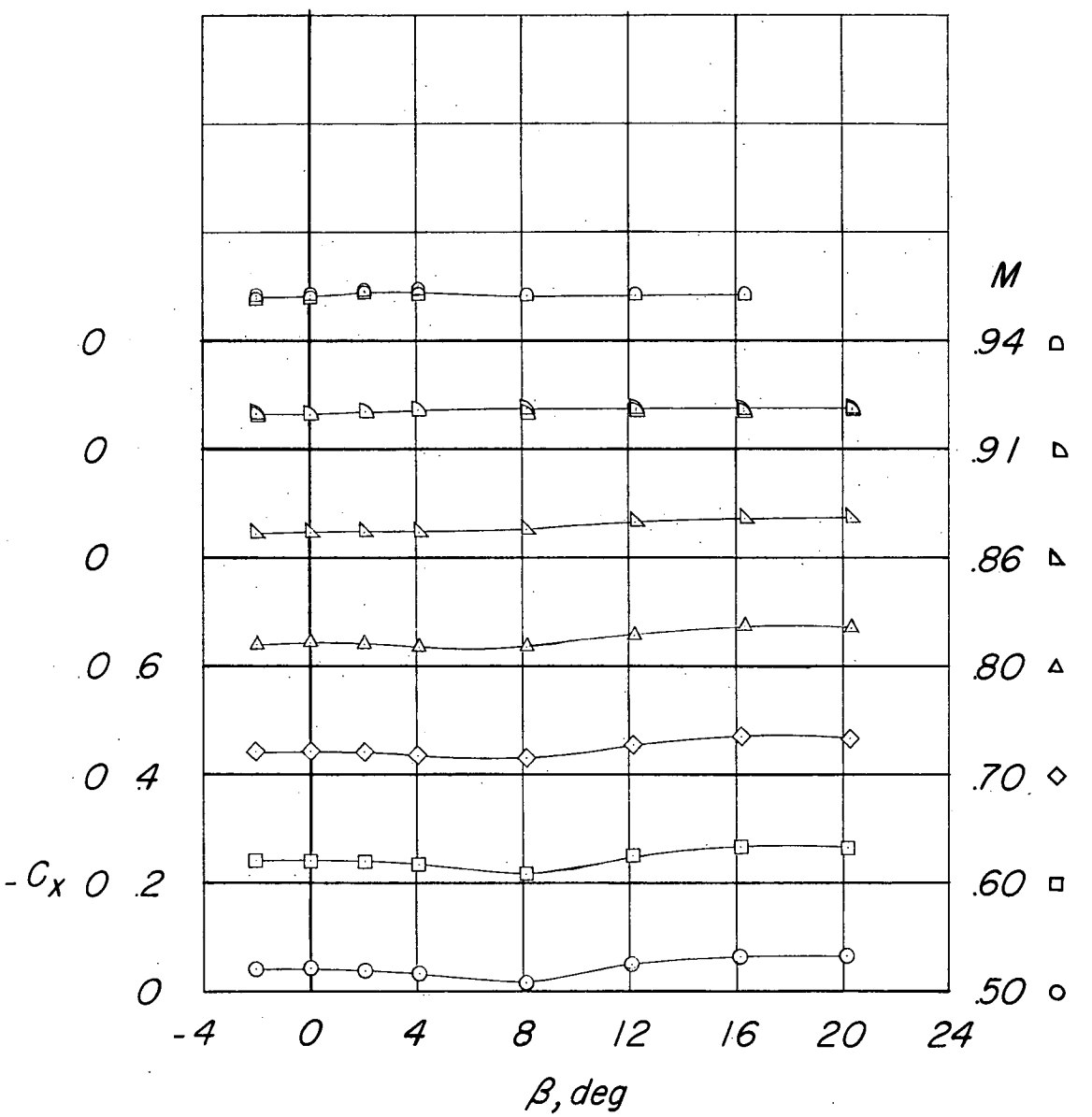


(c) Fuselage plus vertical tail.

Figure 6.- Continued.

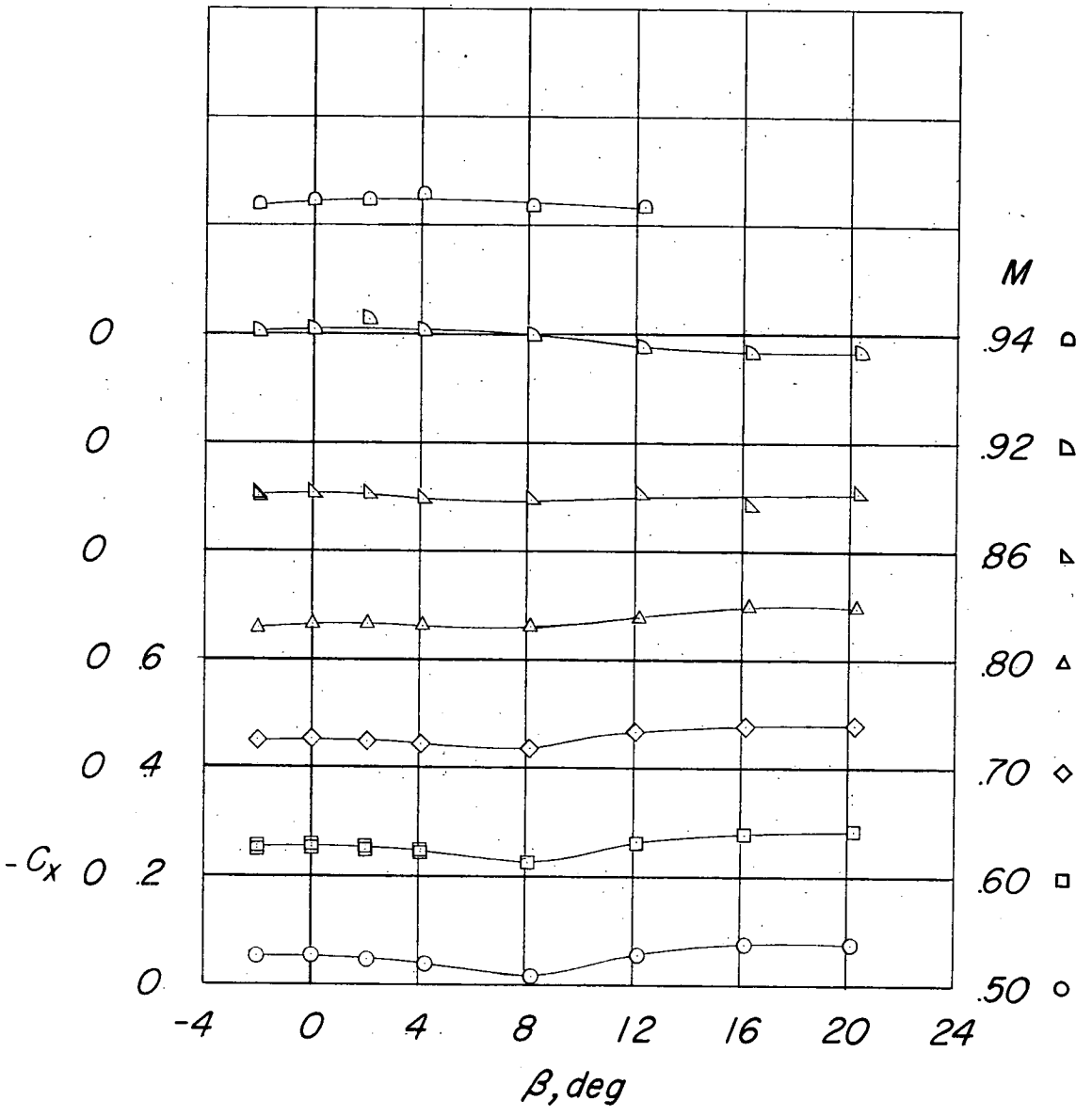


(d) Fuselage plus vertical tail plus horizontal tail. $\frac{h}{b_v} = 0.$

Figure 6.- Continued.

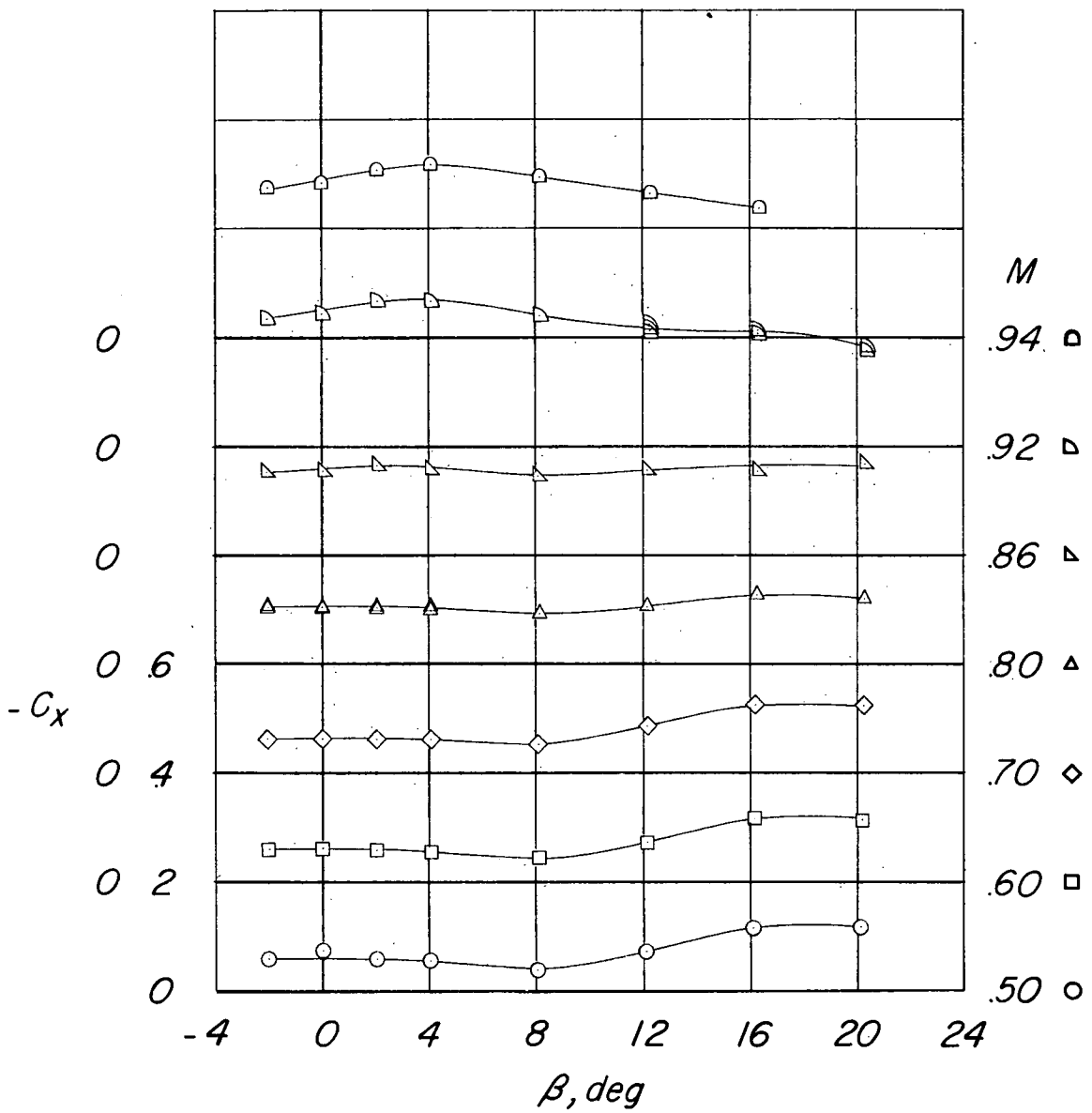


(e) Fuselage plus vertical tail plus horizontal tail. $\frac{h}{b_v} = 0.26$.

Figure 6.- Continued.

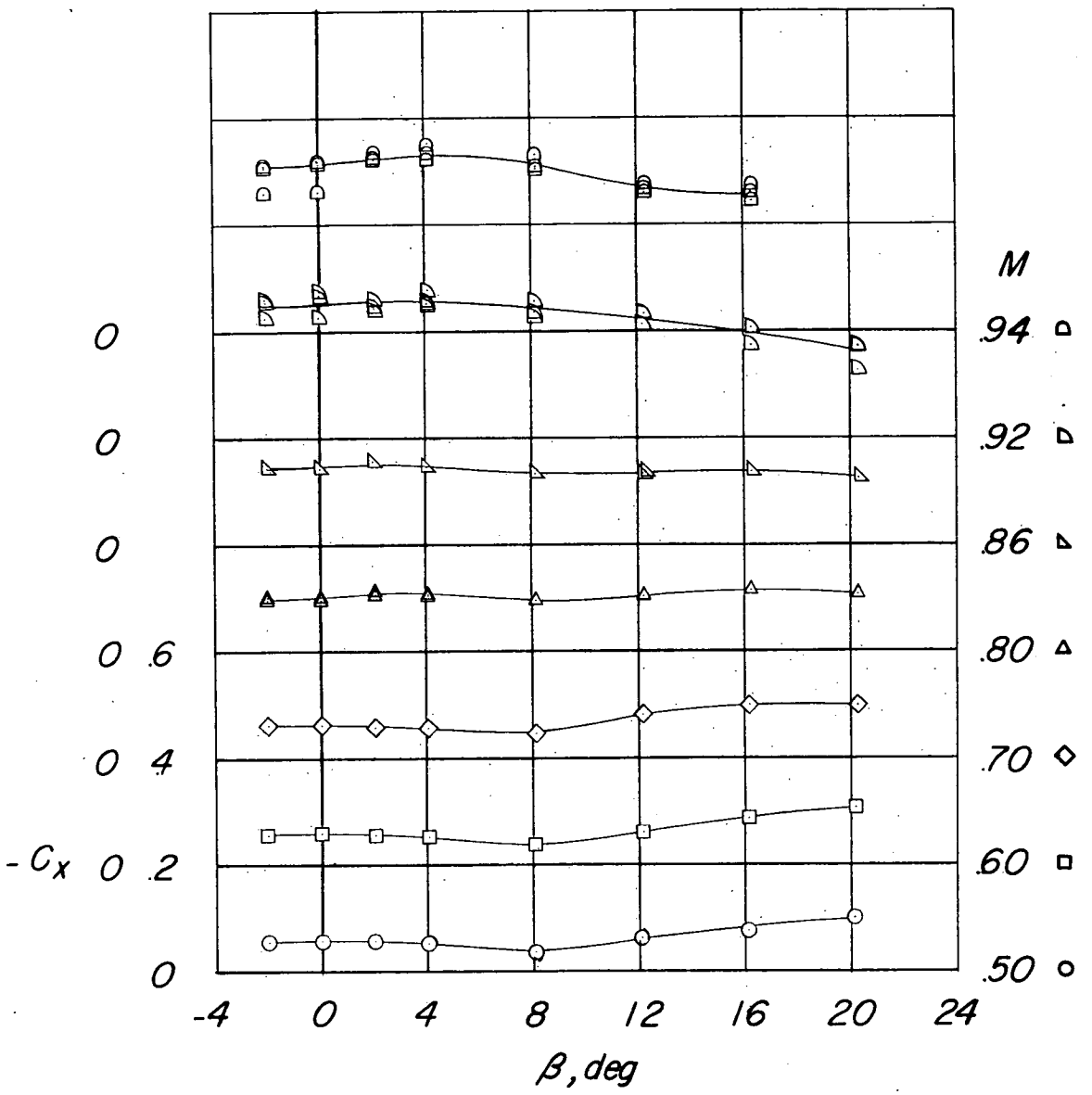


(f) Fuselage plus vertical tail plus horizontal tail. $\frac{h}{b_v} = 0.59$.

Figure 6.- Continued.

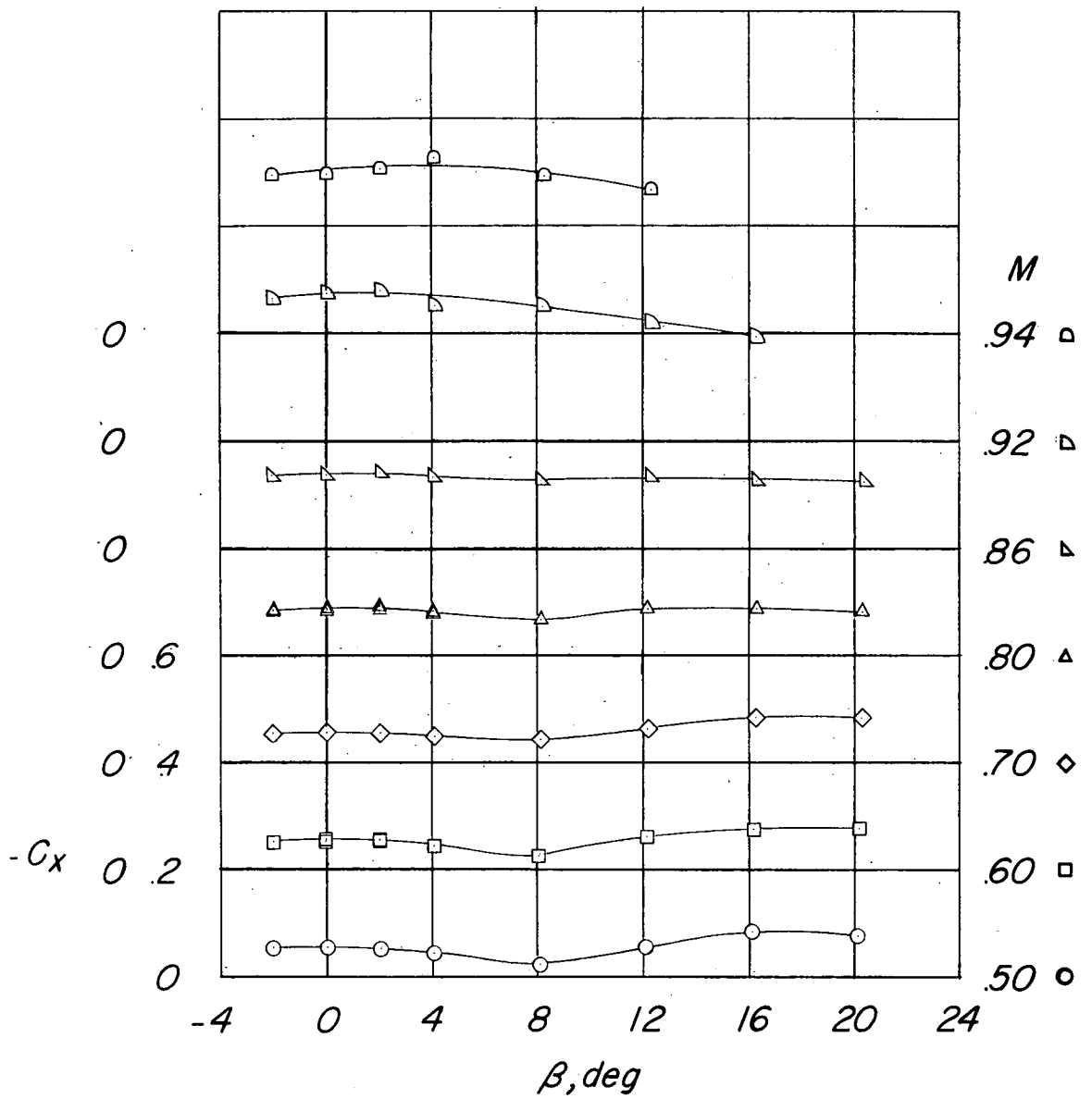


(g) Fuselage plus vertical tail plus horizontal tail. $\frac{h}{b_v} = 1.00$.

Figure 6.- Concluded.

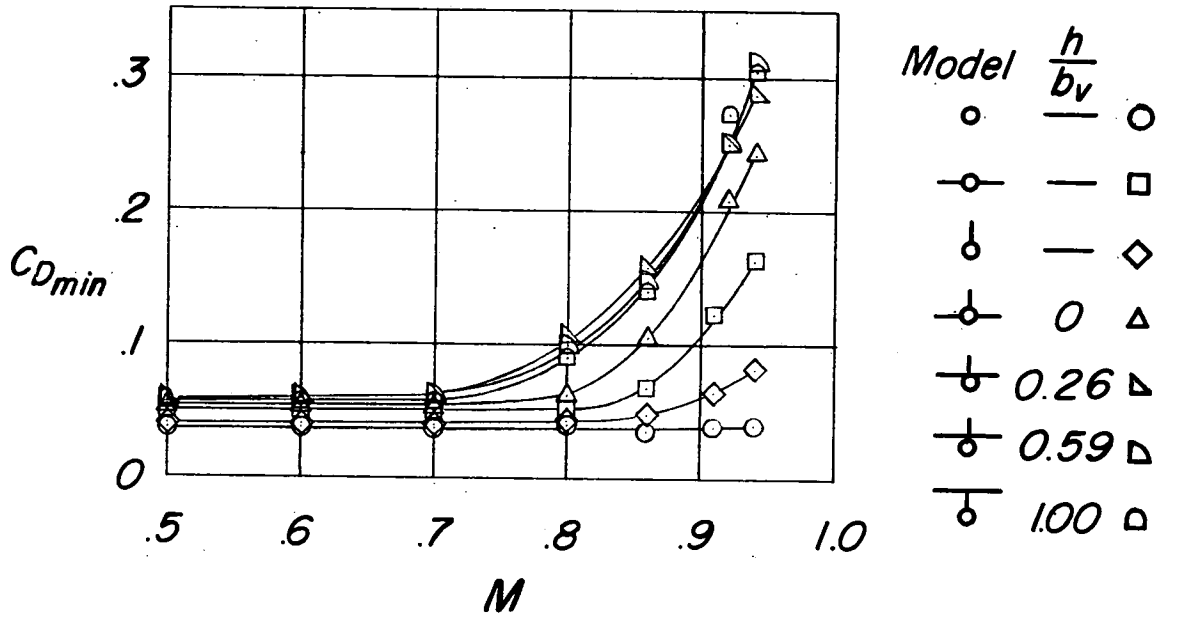


(a) Variation of $C_{D_{min}}$ with Mach number.

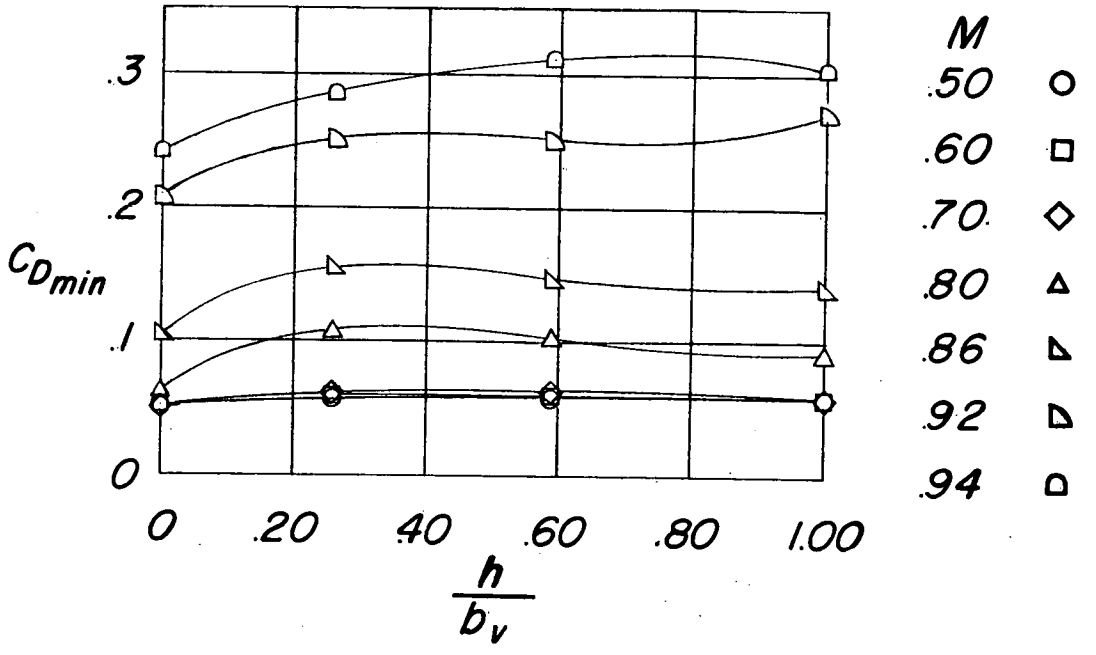


(b) Variation of $C_{D_{min}}$ with horizontal-tail position.

Figure 7.- Summary of drag characteristics for various tail configurations. $\alpha = 0^{\circ}$.

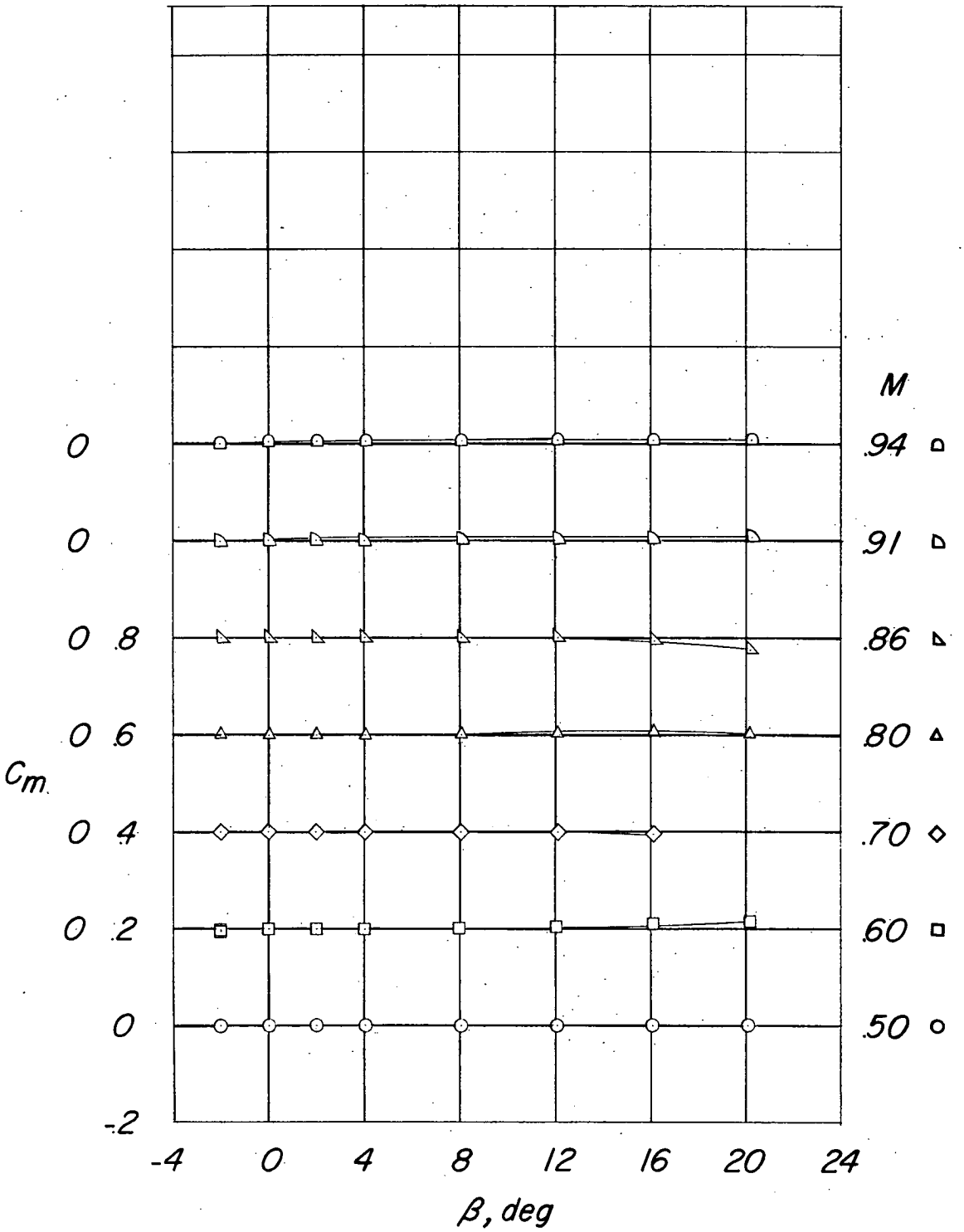


(a) Fuselage alone.

Figure 8.- Variation of $C_m$ with angle of sideslip. $\alpha = 0^\circ$.

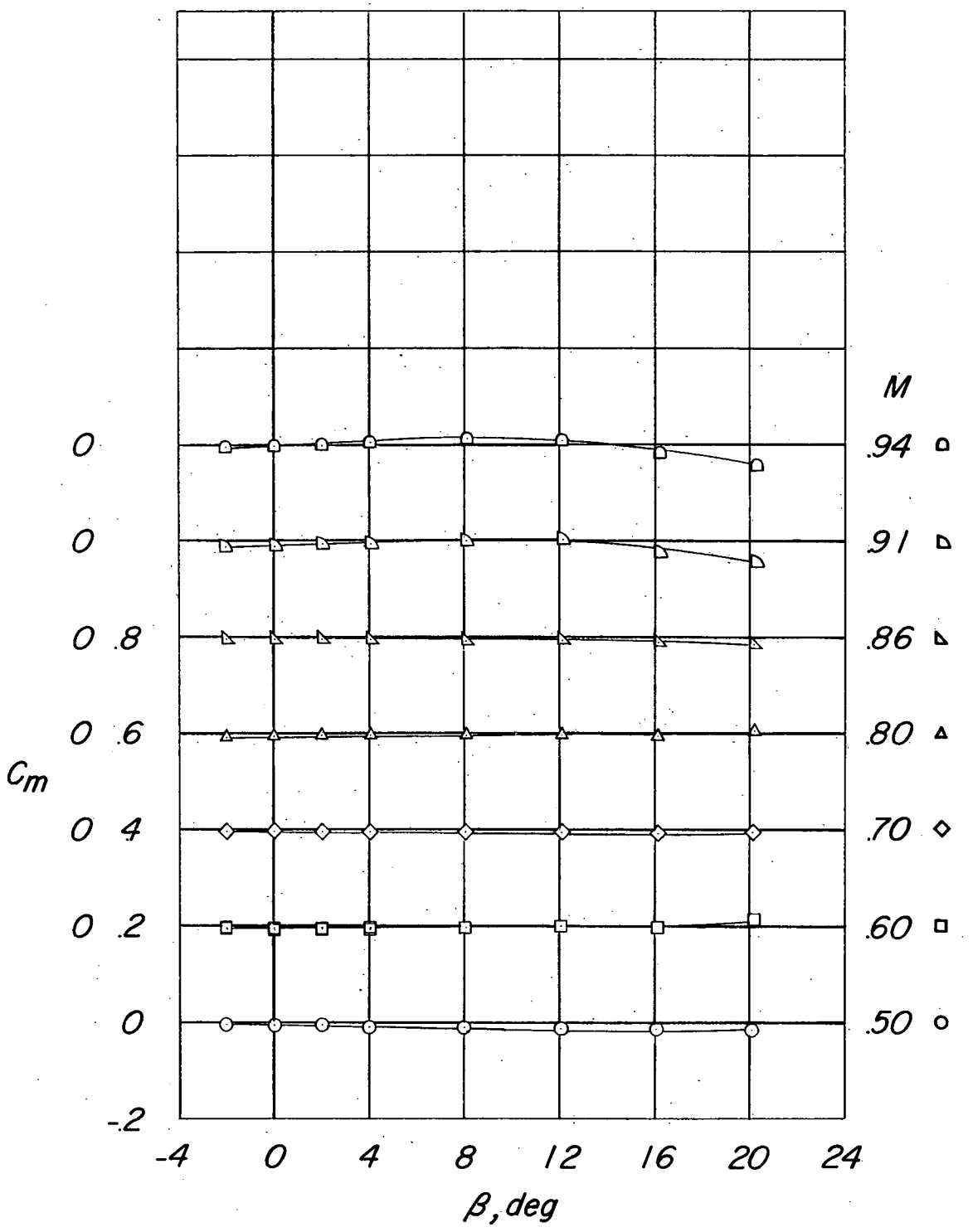


(b) Fuselage plus horizontal tail.

Figure 8.- Continued.

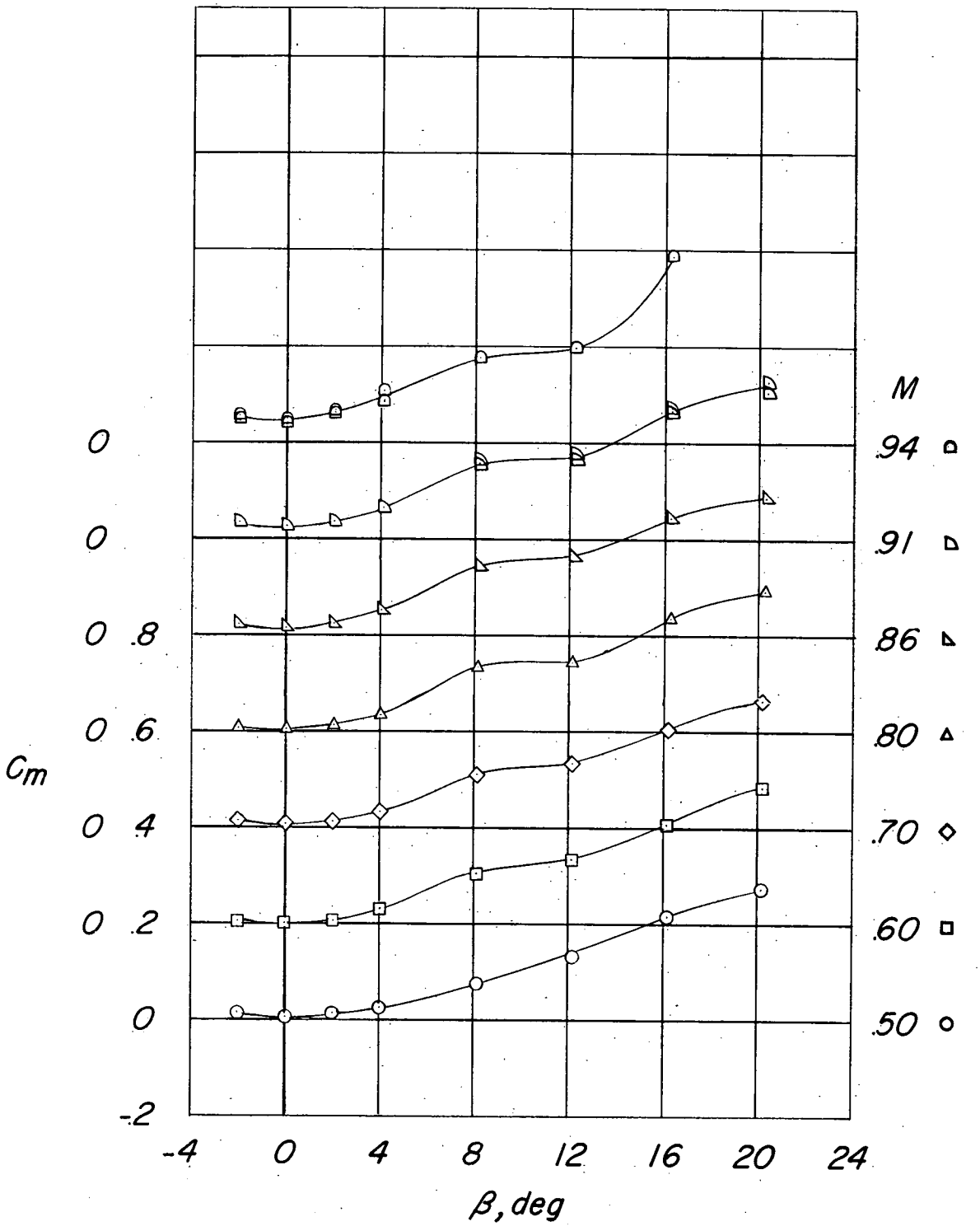


(c) Fuselage plus vertical tail.

Figure 8.- Continued.

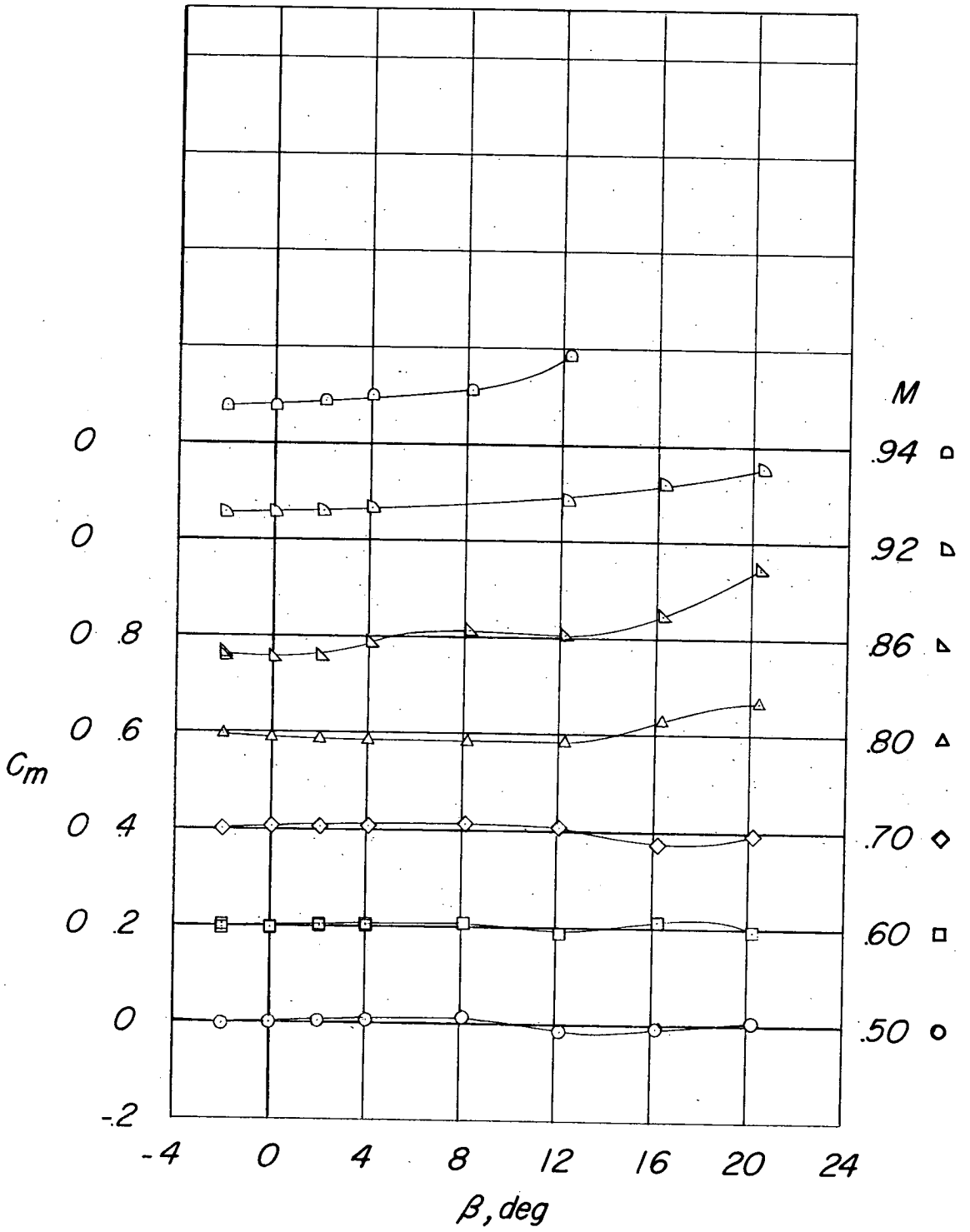


(d) Fuselage plus vertical tail plus horizontal tail. $\frac{h}{b_v} = 0$.

Figure 8.- Continued.

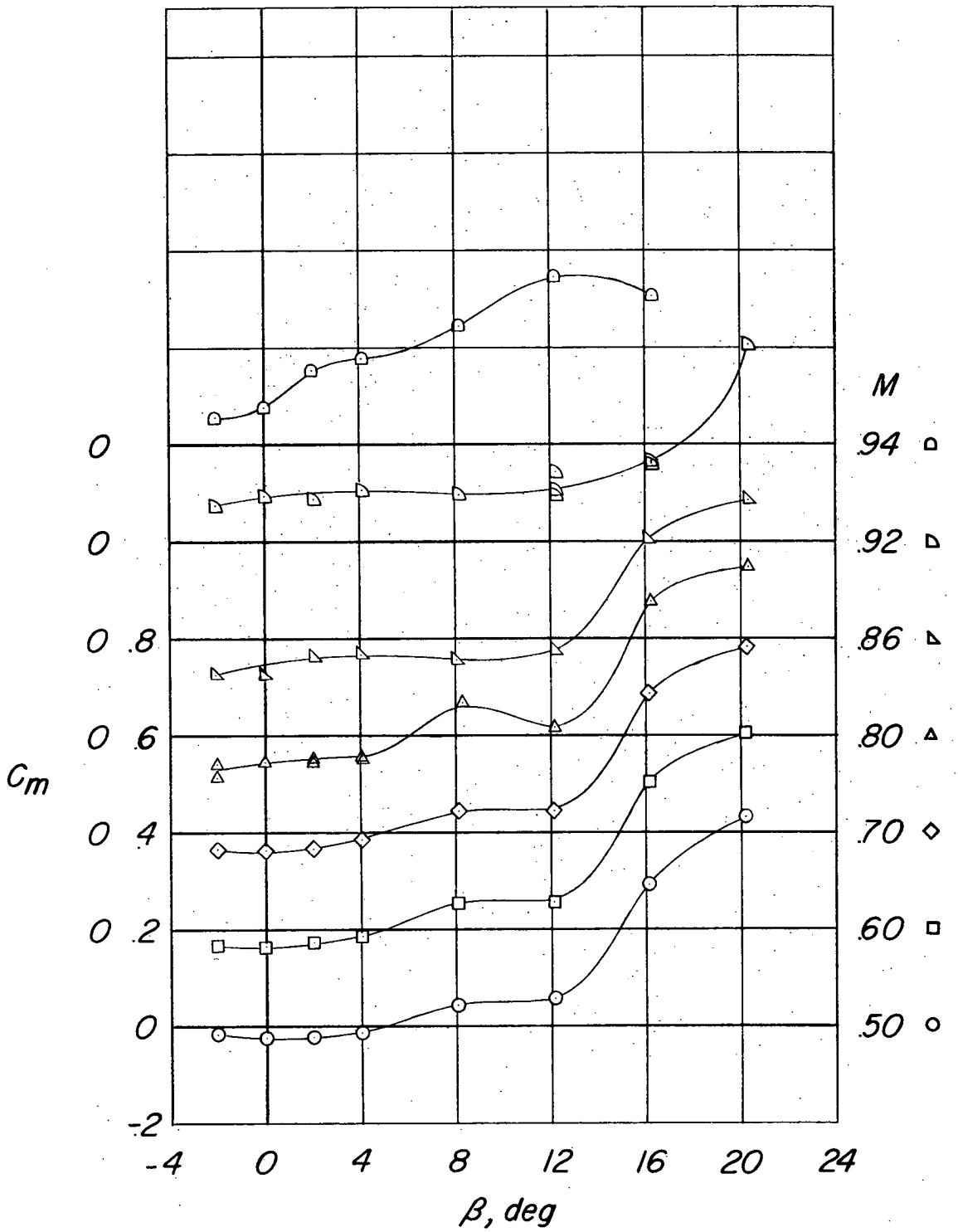


(e) Fuselage plus vertical tail plus horizontal tail. $\frac{h}{b_v} = 0.26$.

Figure 8.- Continued.

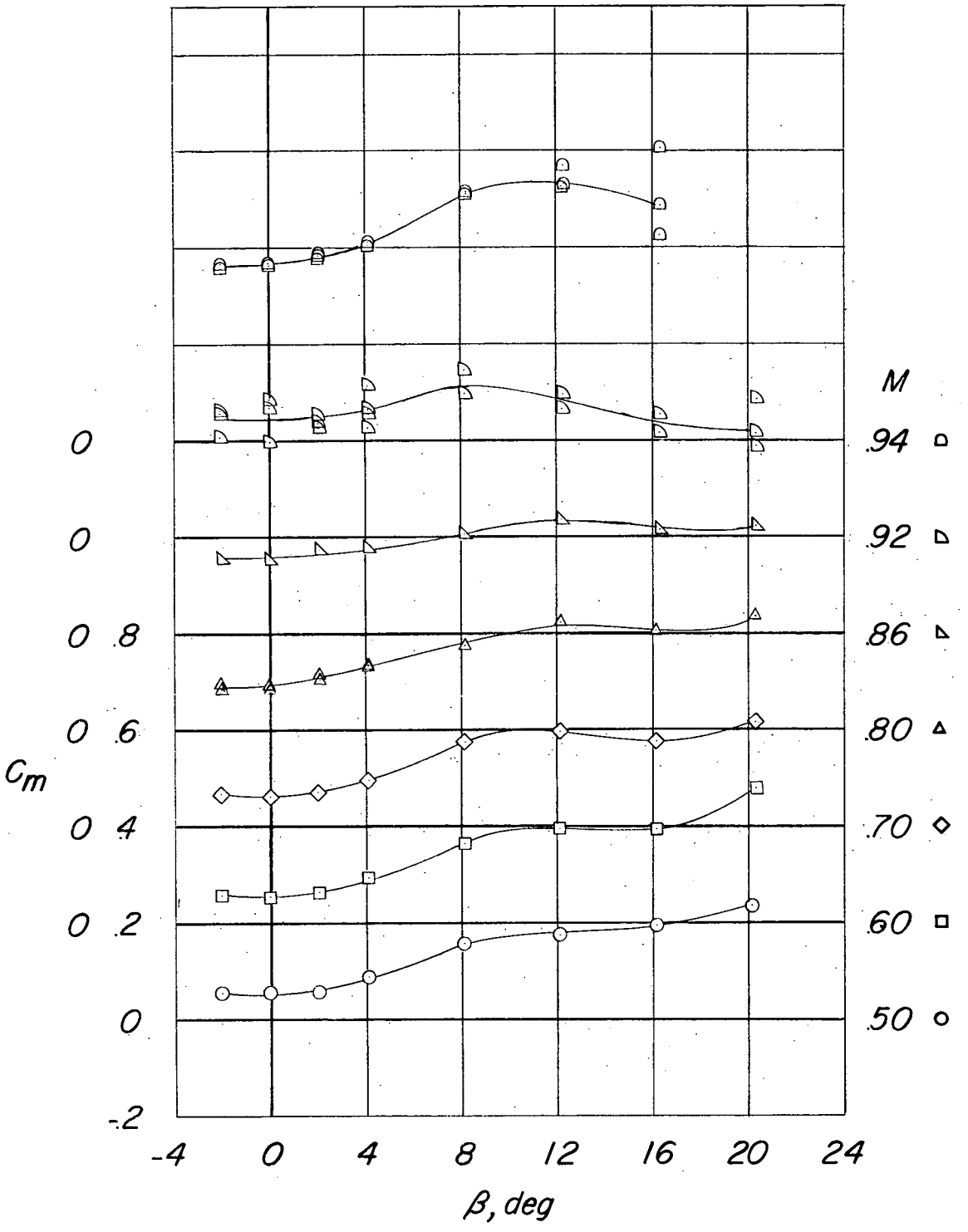


(f) Fuselage plus vertical tail plus horizontal tail. $\frac{h}{b_v} = 0.59$.

Figure 8.- Continued.

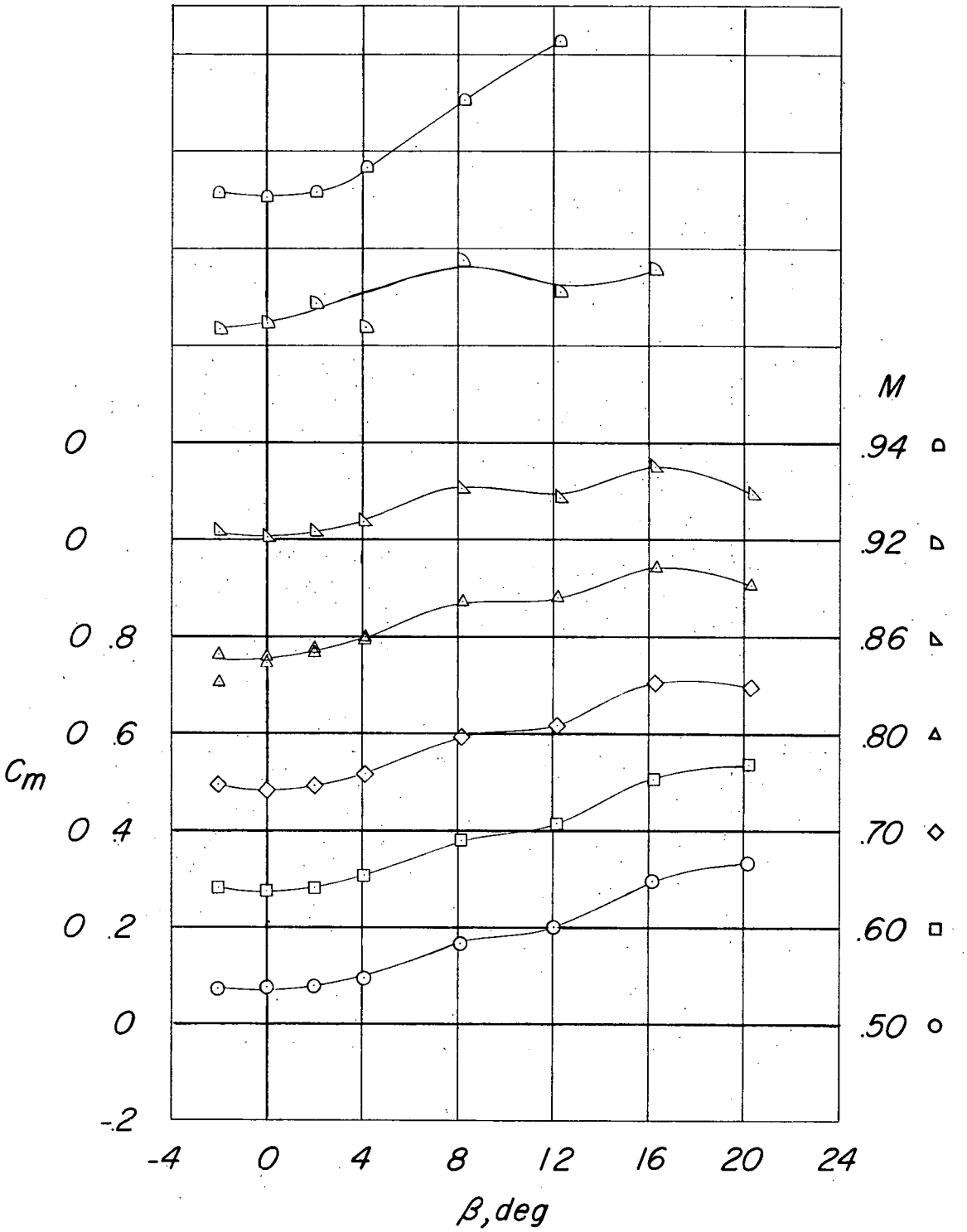


(g) Fuselage plus vertical tail plus horizontal tail. $\frac{h}{b_v} = 1.00$.

Figure 8.- Concluded.

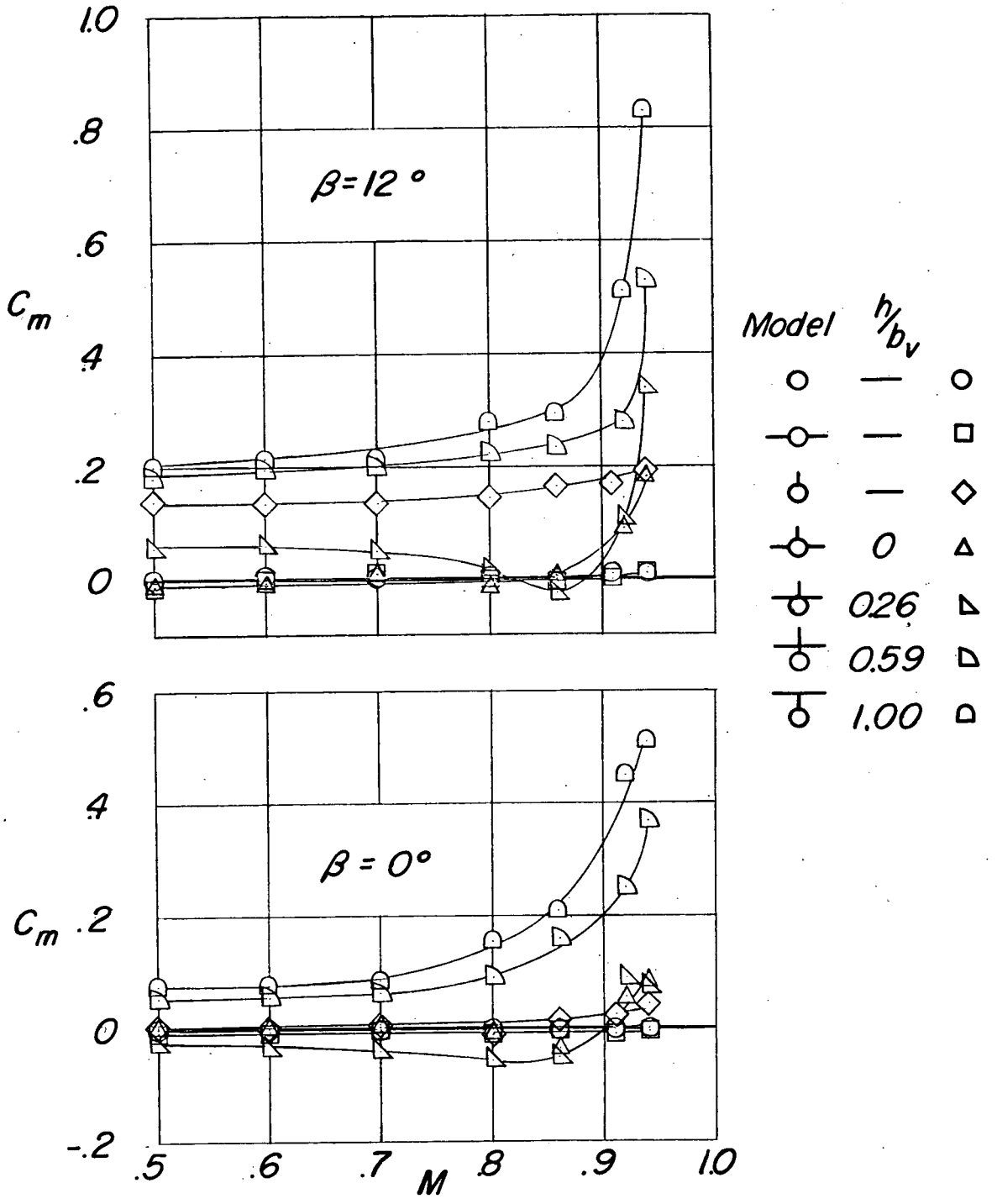


Figure 9.- Variation of pitching-moment characteristics with Mach number for various tail configurations. $\alpha = 0°$.

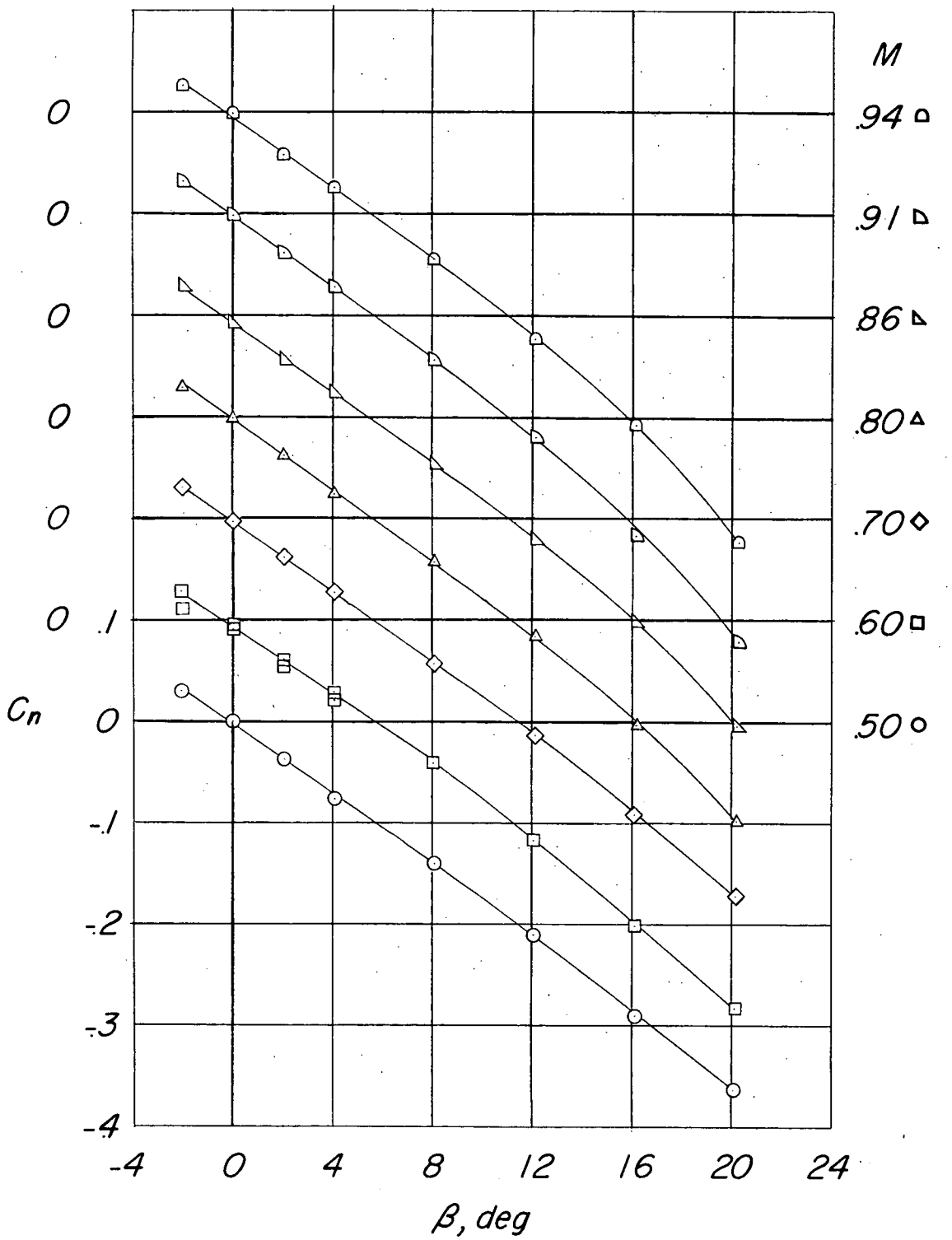


(a) Fuselage alone.

Figure 10.- Variation of $C_n$ with angle of sideslip. $\alpha = 0^\circ$.

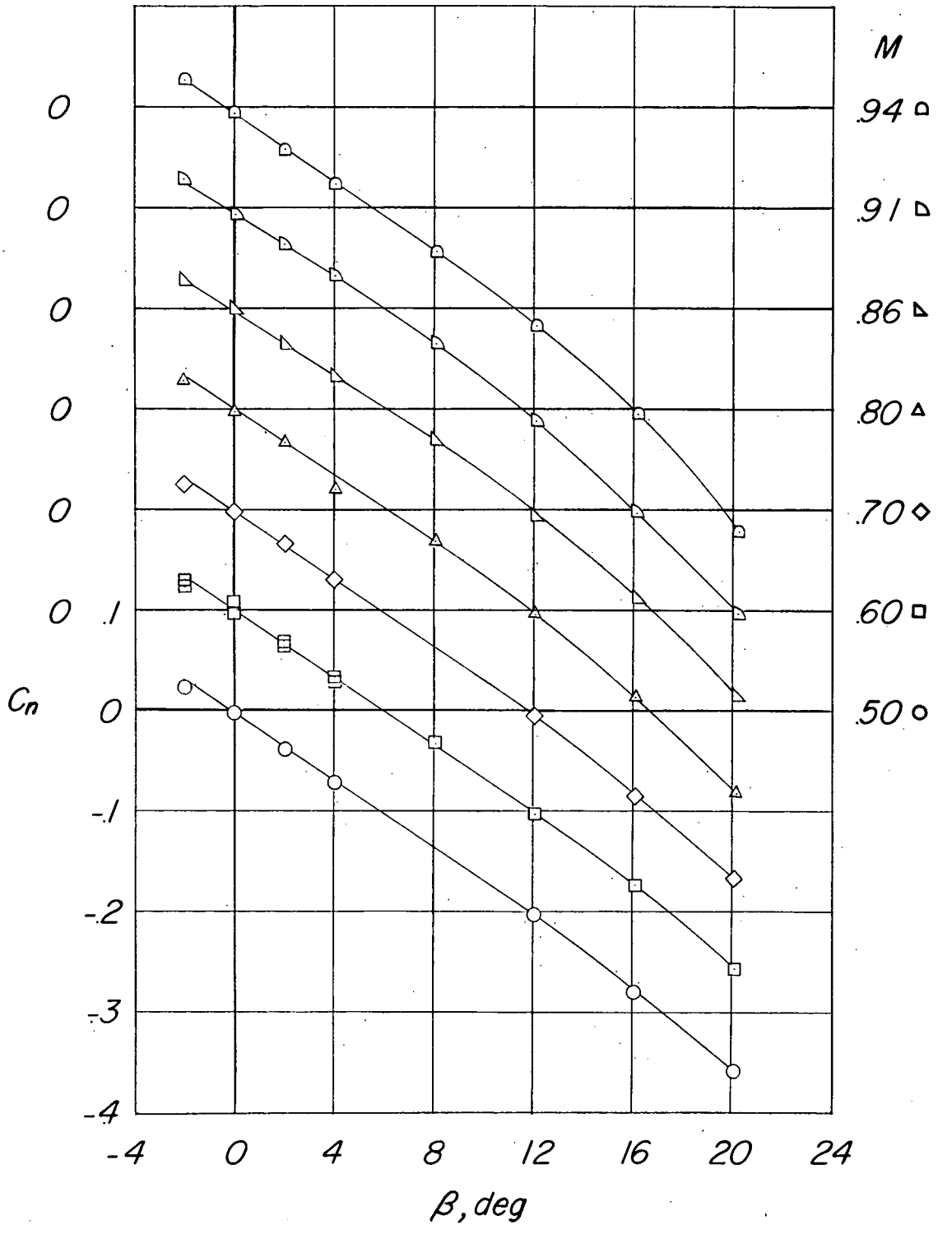


(b) Fuselage plus horizontal tail.

Figure 10.- Continued.

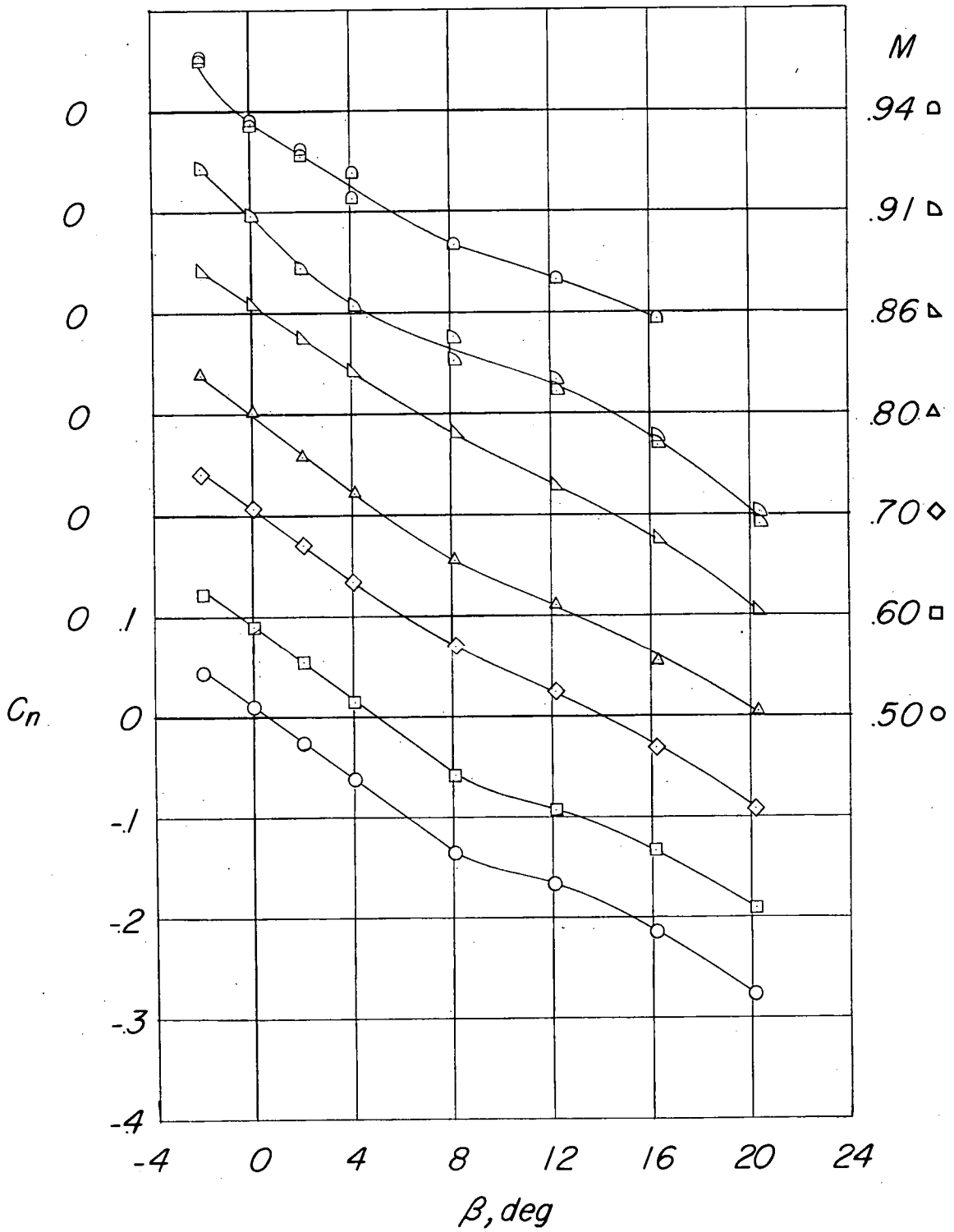


(c) Fuselage plus vertical tail.

Figure 10.- Continued.

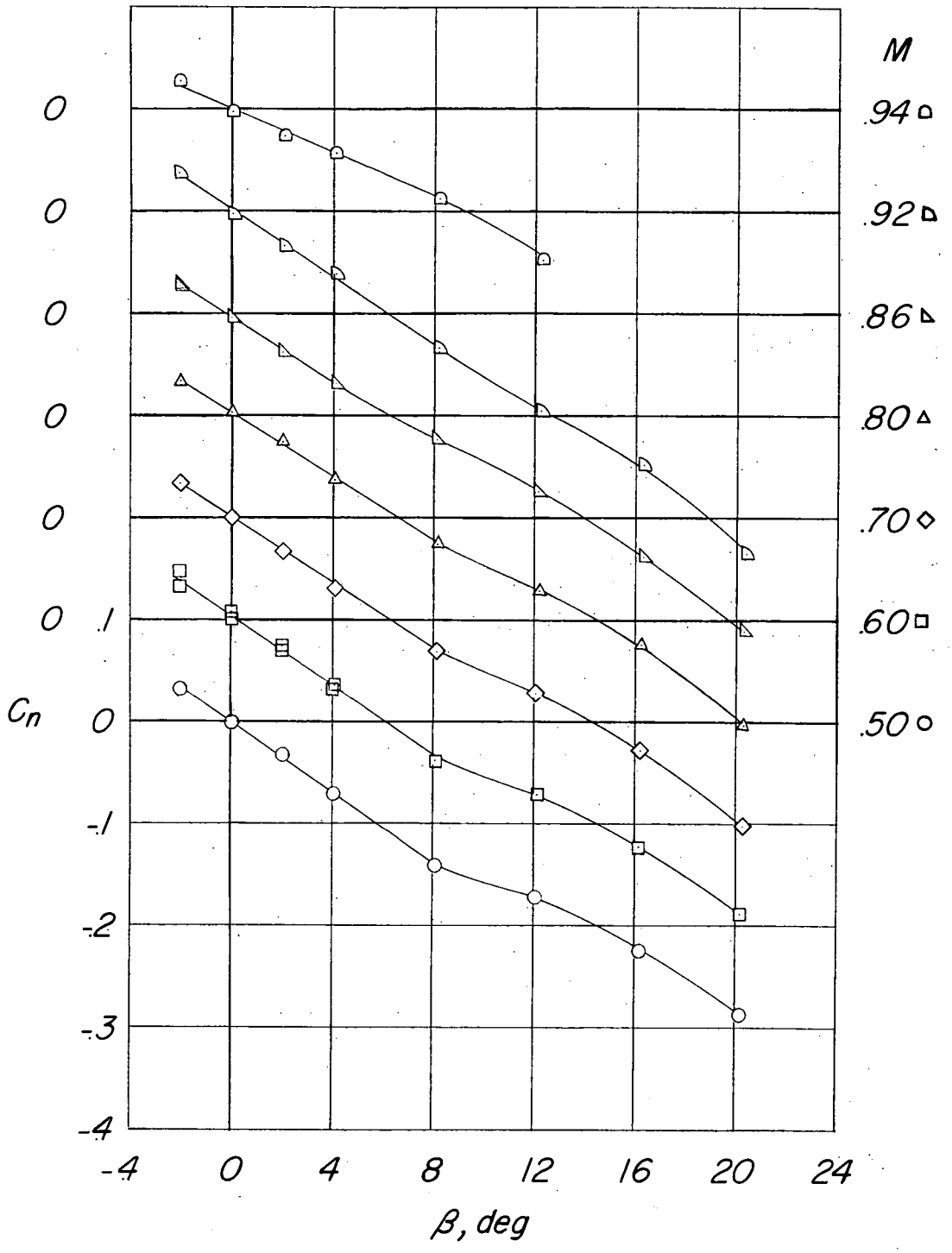


(d) Fuselage plus vertical tail plus horizontal tail. $\frac{h}{b_v} = 0$.

Figure 10.- Continued.

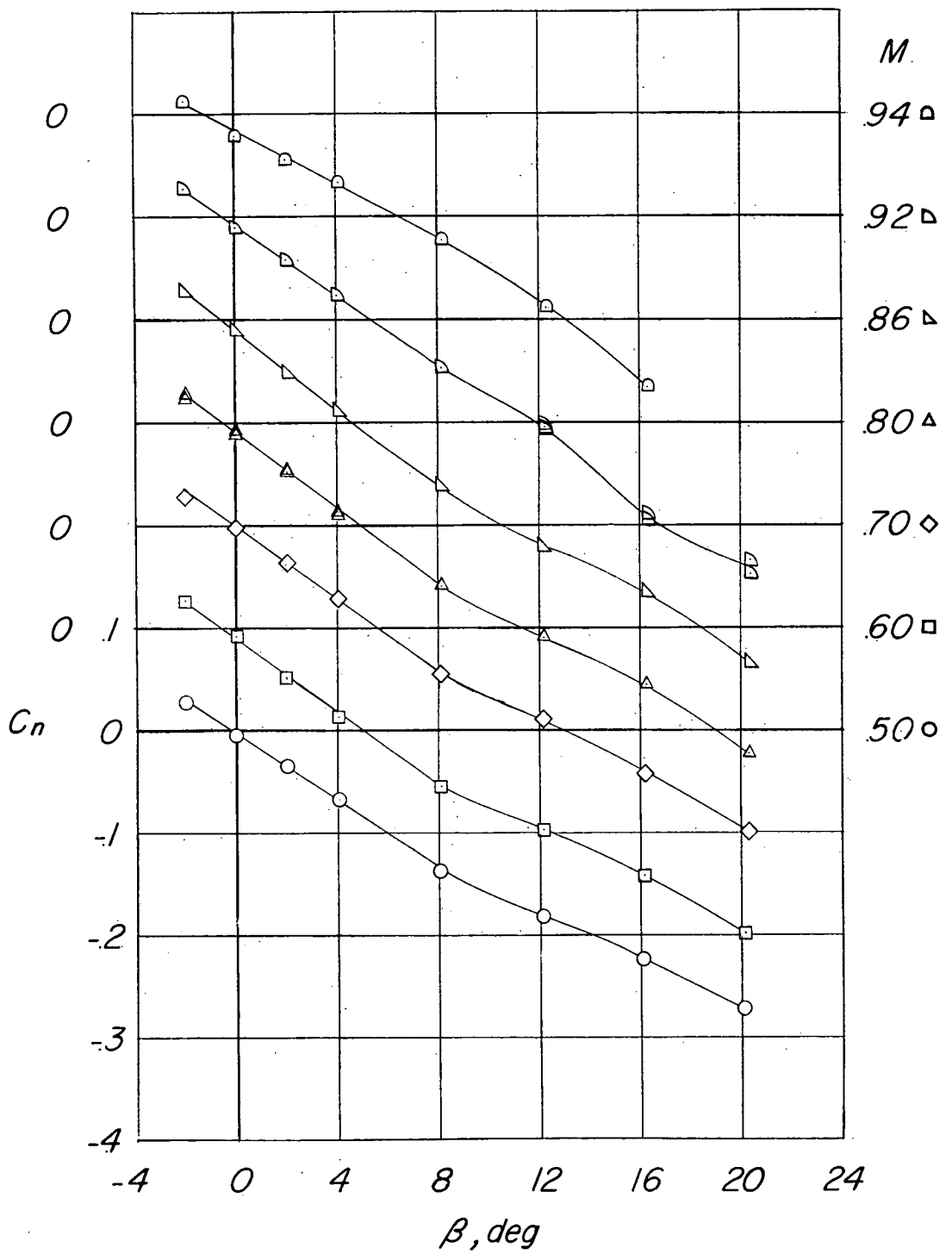


(e) Fuselage plus vertical tail plus horizontal tail. $\frac{h}{b_v} = 0.26$.

Figure 10.- Continued.

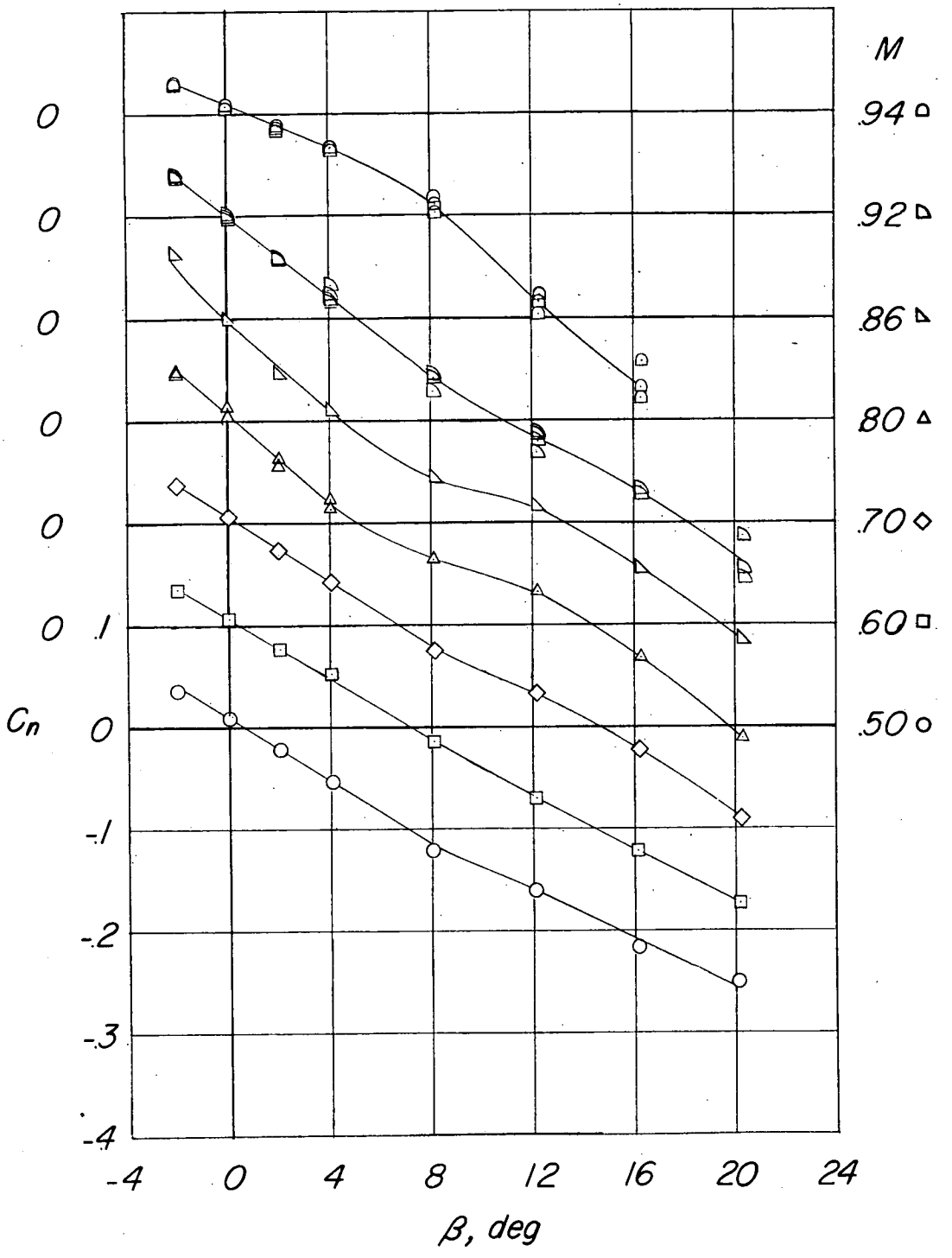


(f) Fuselage plus vertical tail plus horizontal tail. $\frac{h}{b_v} = 0.59$.

Figure 10.- Continued.

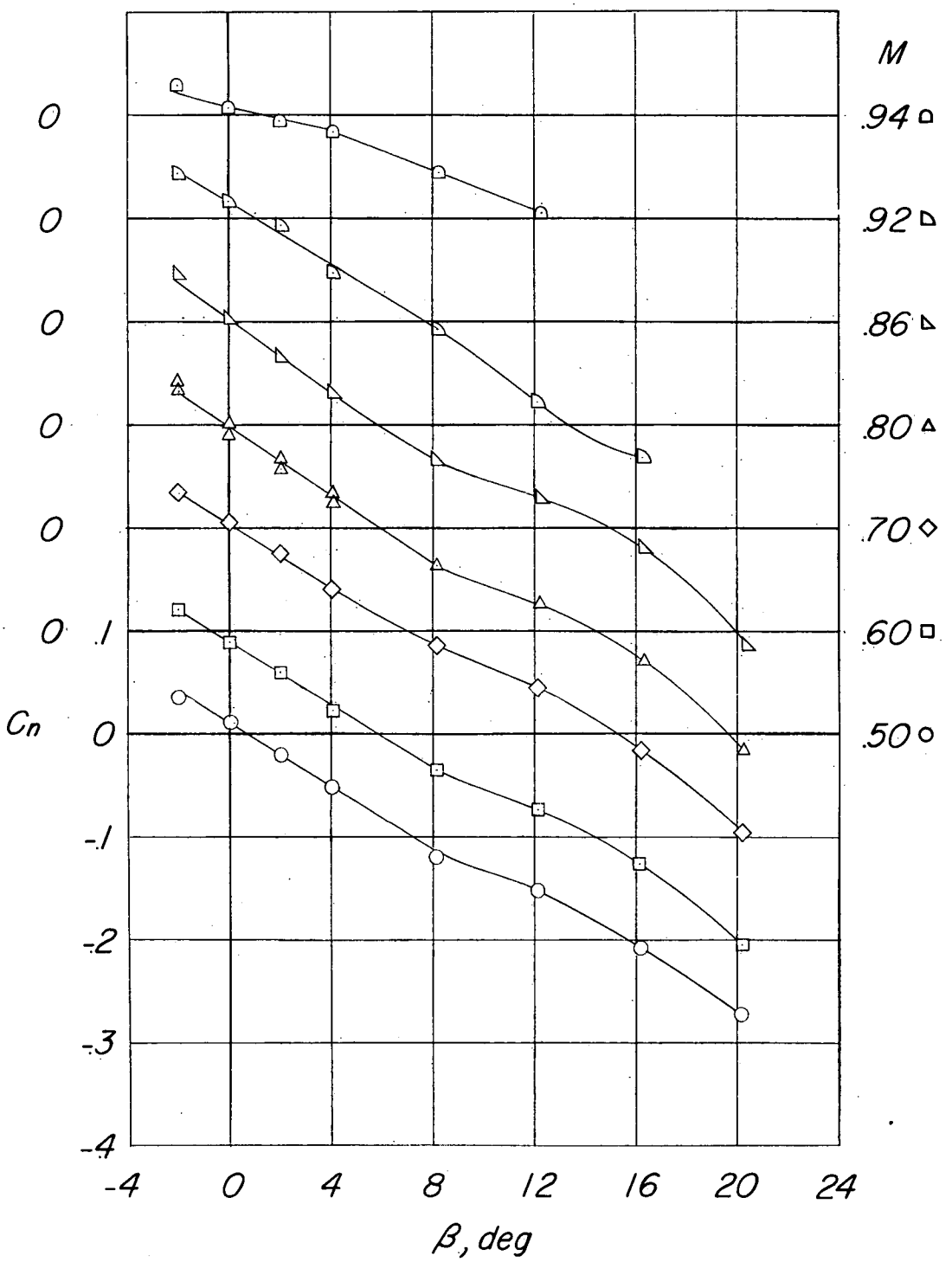


(g) Fuselage plus vertical tail plus horizontal tail. $\frac{h}{b_v} = 1.00$.

Figure 10.- Concluded.

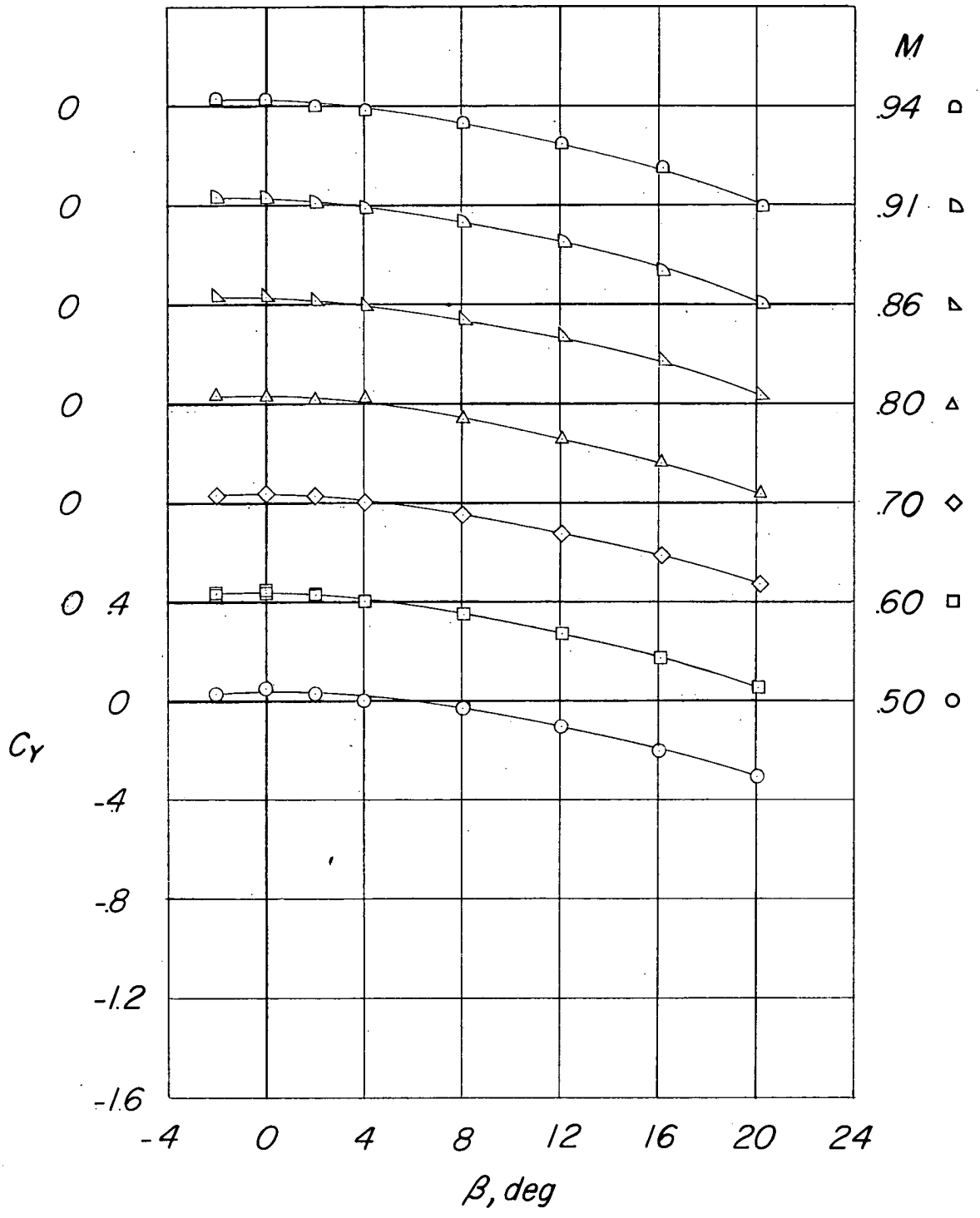


(a) Fuselage alone.

Figure 11.- Variation of $C_Y$ with angle of sideslip. $\alpha = 0^\circ$.

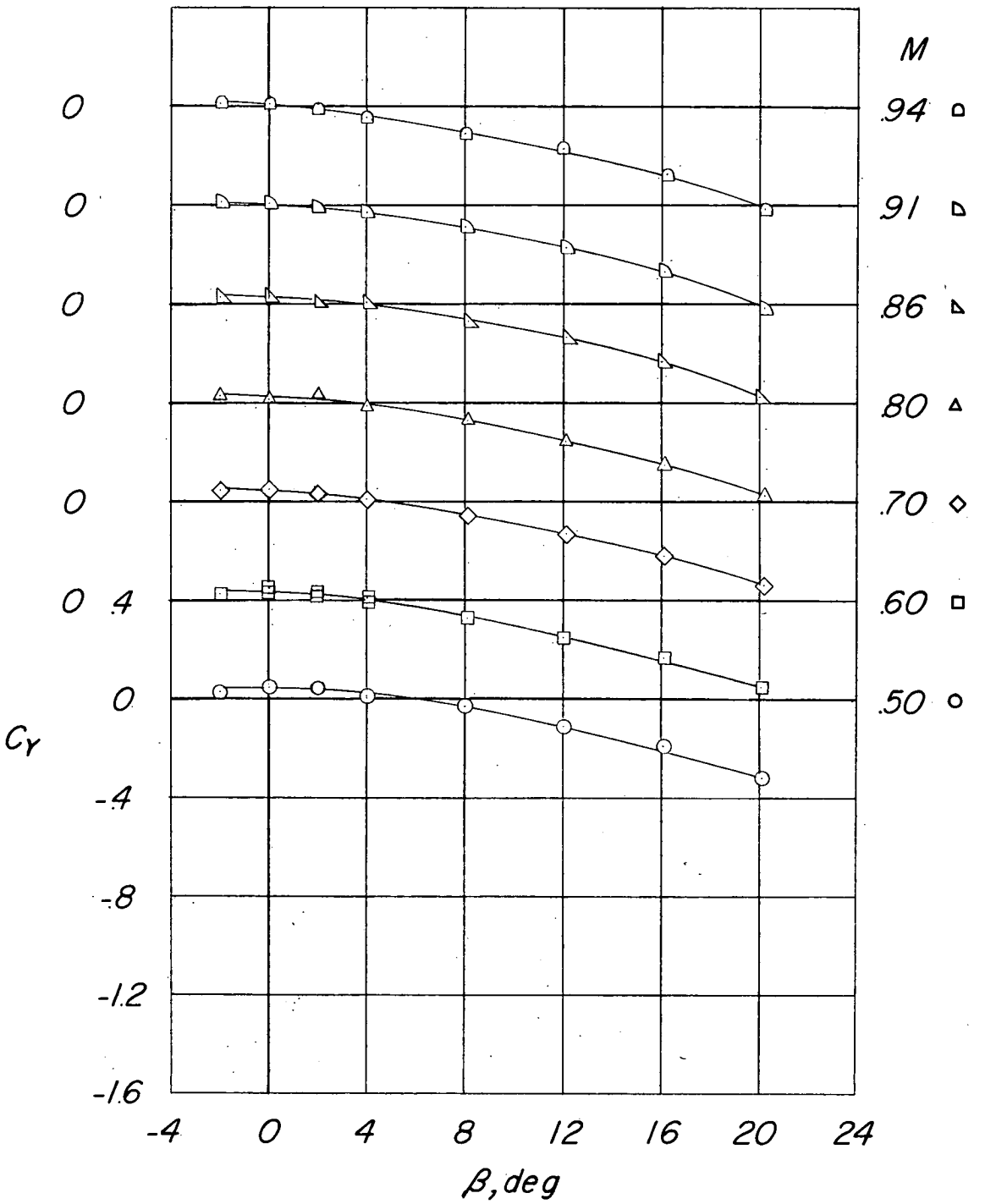


(b) Fuselage plus horizontal tail.

Figure 11.- Continued.

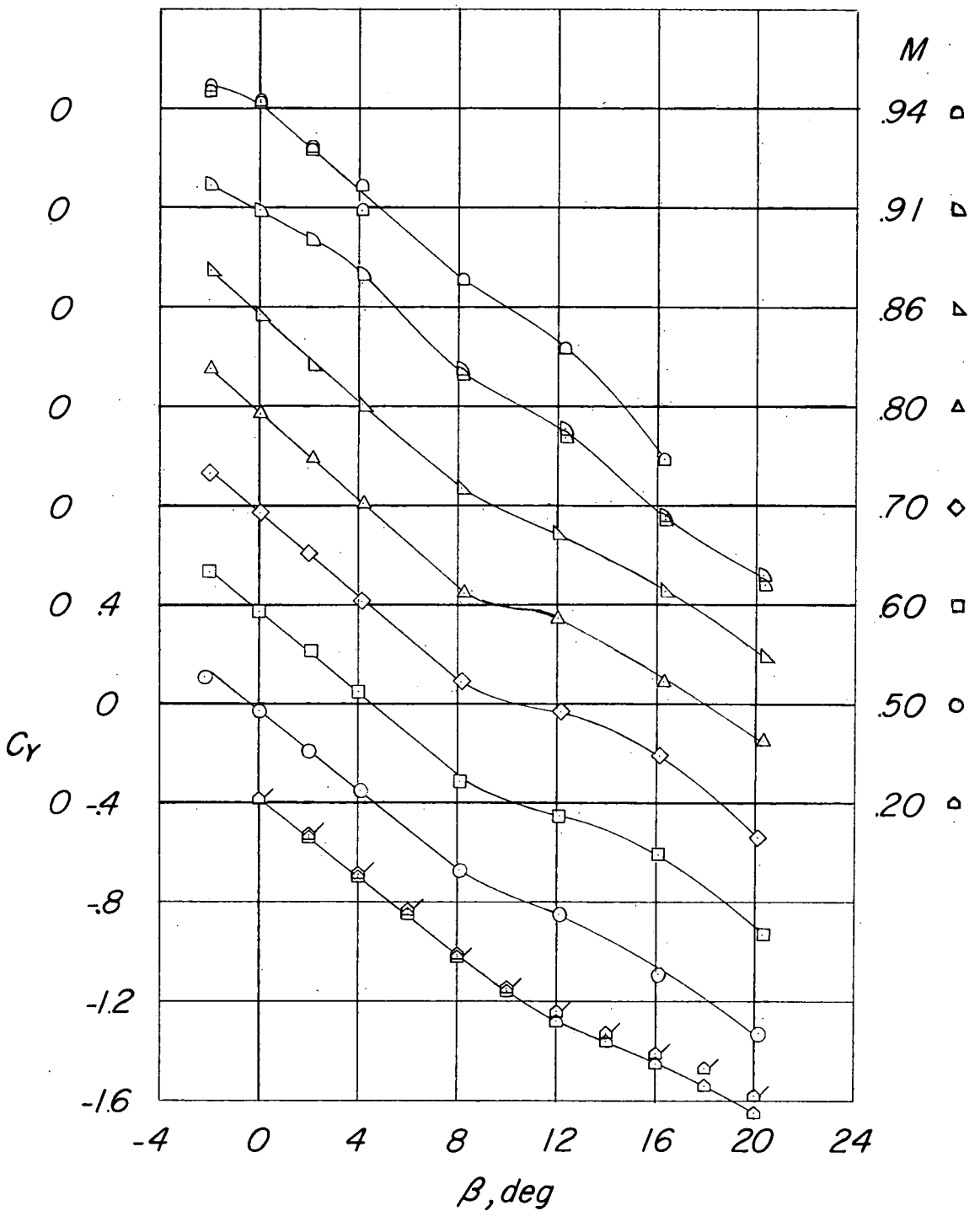


(c) Fuselage plus vertical tail. (Flagged symbols denote tests with modified fuselage nose.)

Figure 11.- Continued.

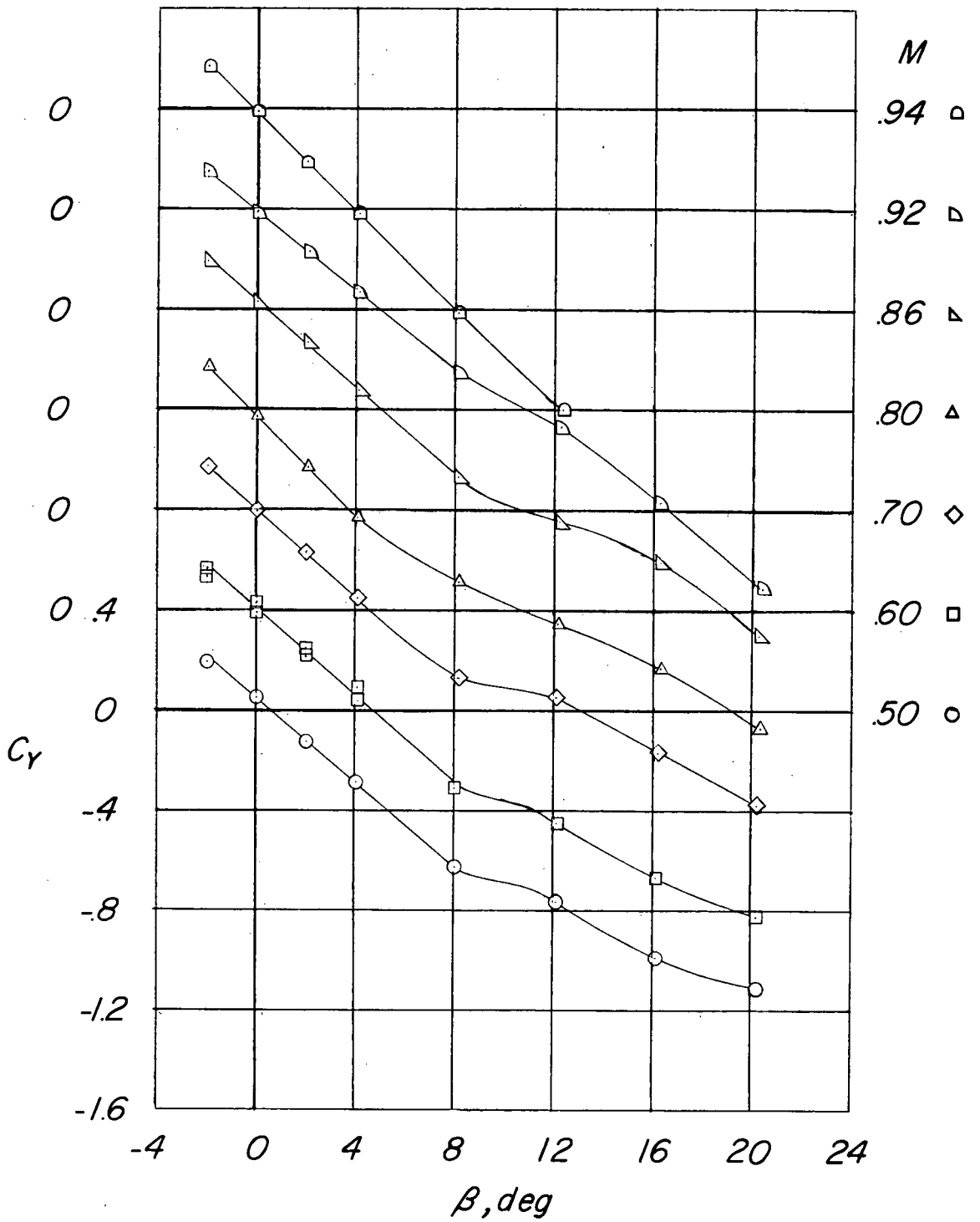


(d) Fuselage plus vertical tail plus horizontal tail. $\frac{h}{b_v} = 0$.

Figure 11.- Continued.

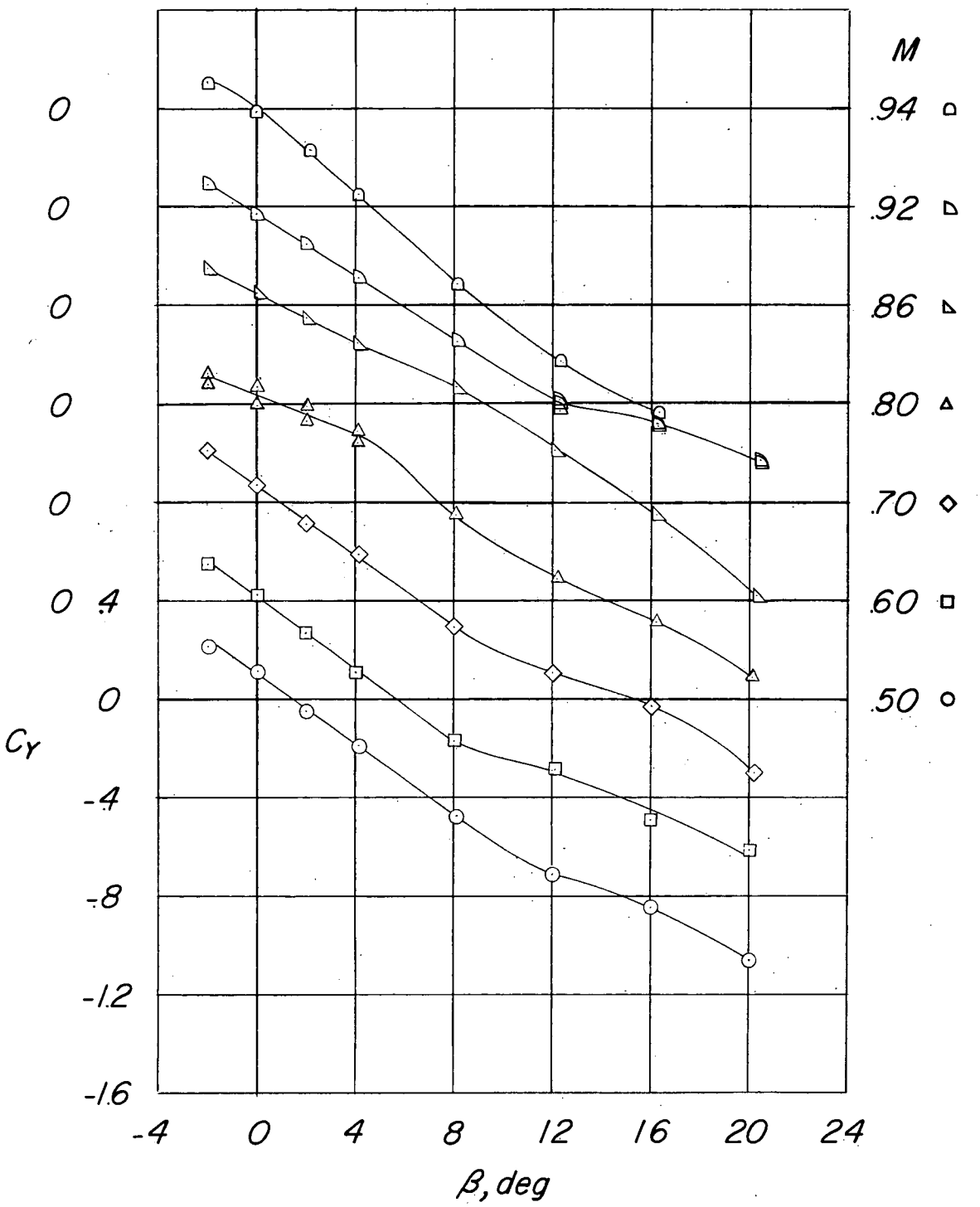


(e) Fuselage plus vertical tail plus horizontal tail. $\frac{h}{b_v} = 0.26$.

Figure 11.- Continued.

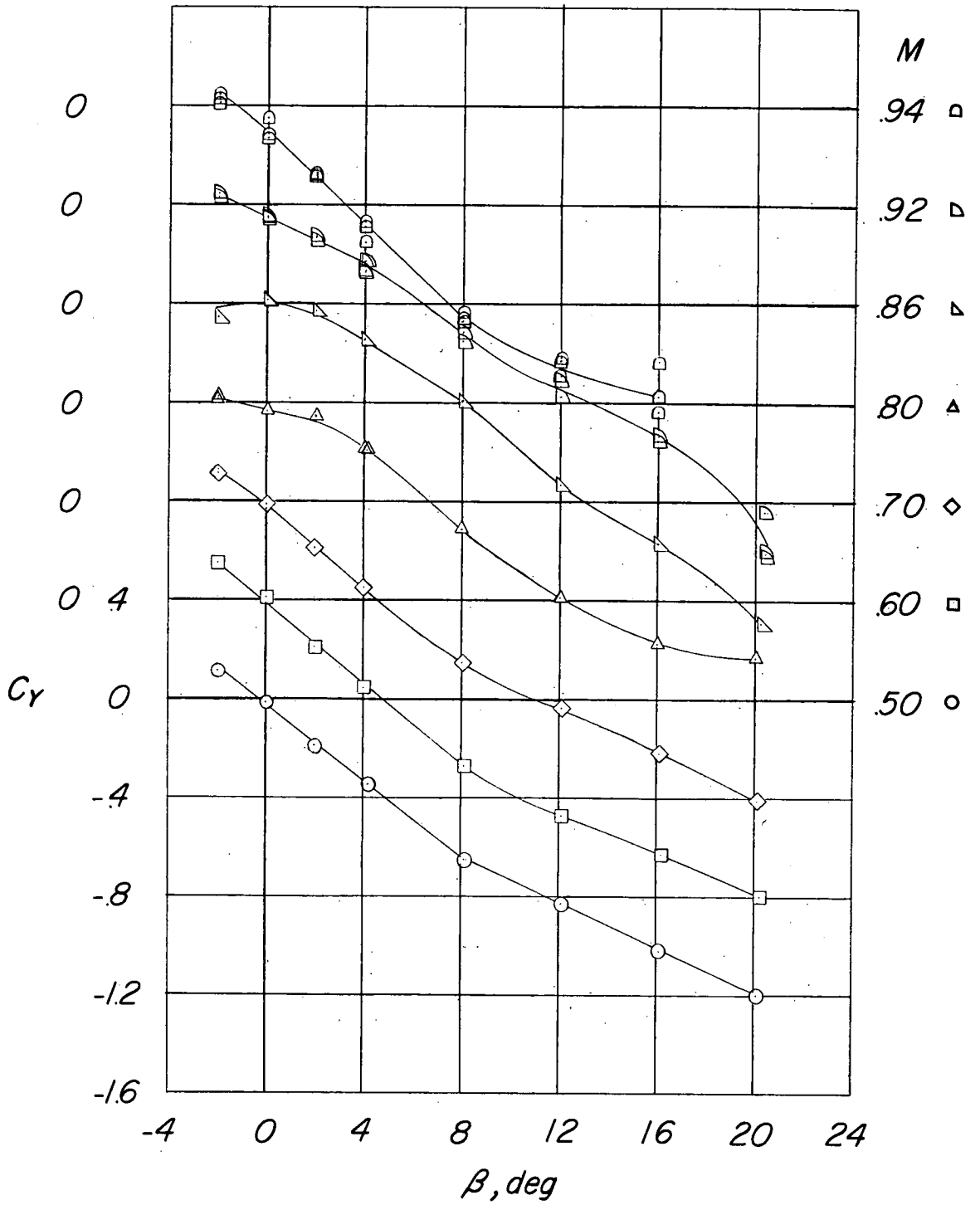


(f) Fuselage plus vertical tail plus horizontal tail. $\frac{h}{b_v} = 0.59$.

Figure 11.- Continued.

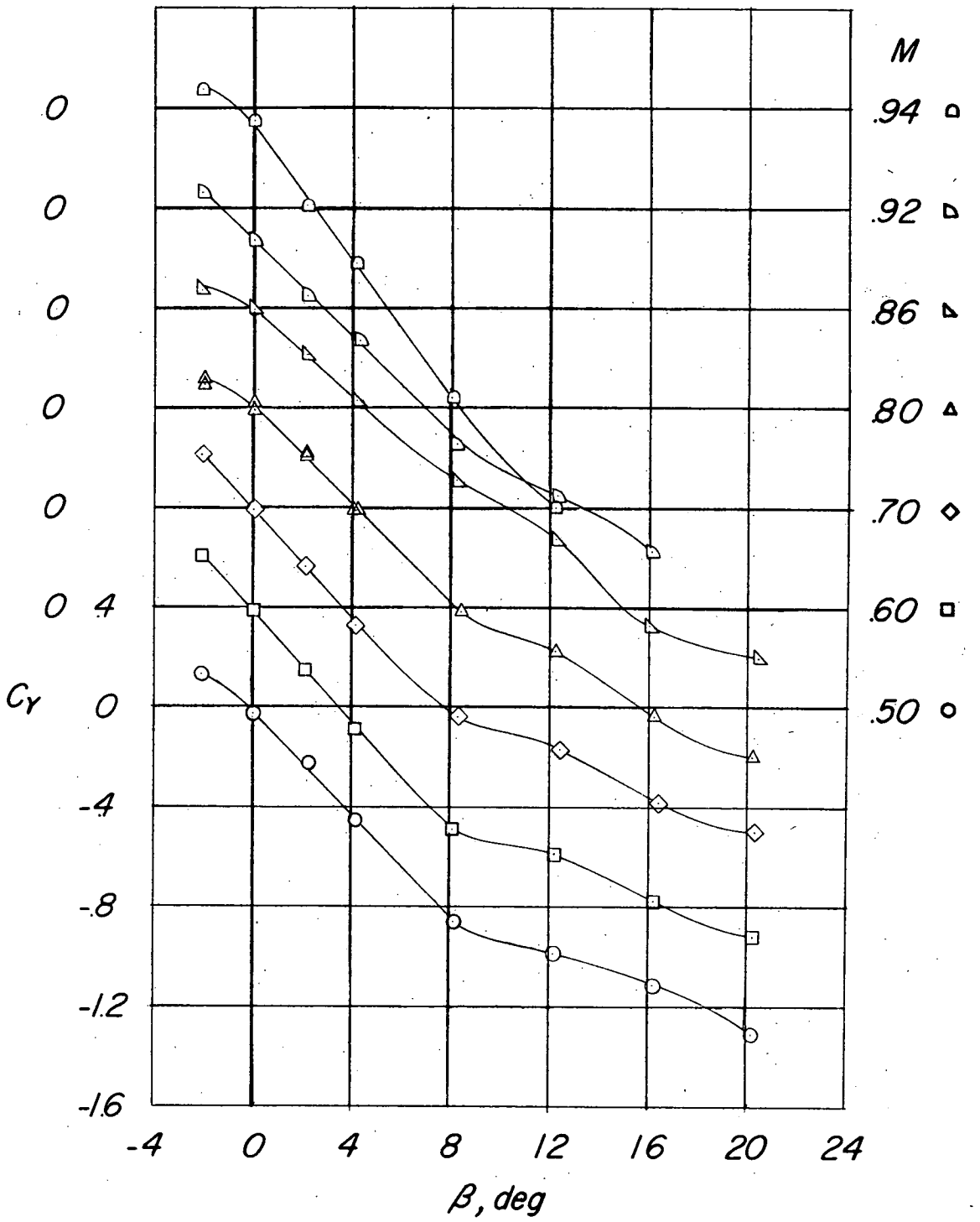


(g) Fuselage plus vertical tail plus horizontal tail. $\frac{h}{b_v} = 1.00$.

Figure 11.- Concluded.

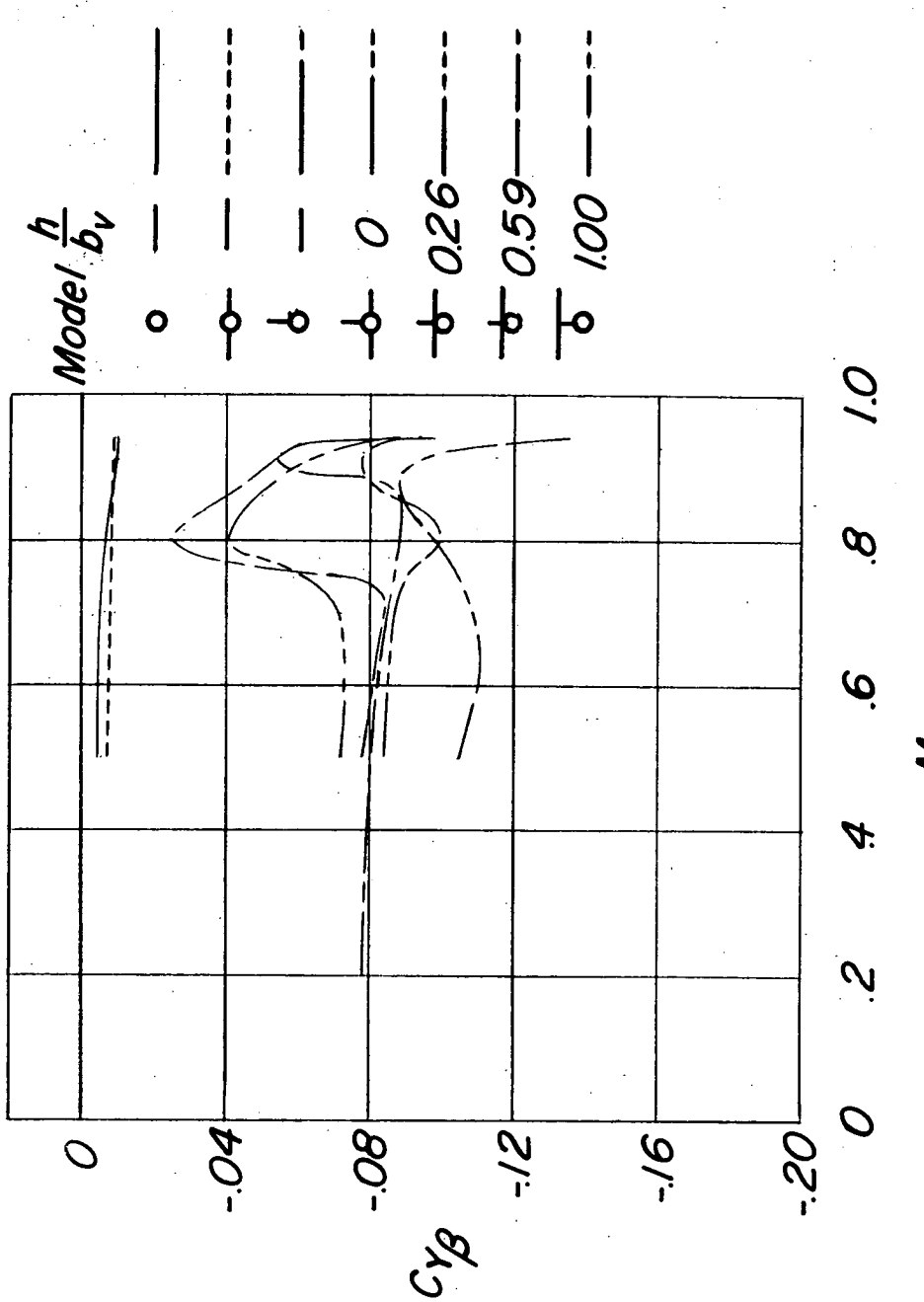


(a) Variation of $C_{Y_\beta}$ with Mach number.

Figure 12.- Summary of experimental variations of $C_{Y_\beta}$ for various horizontal-tail positions. $\alpha = 0^\circ$.

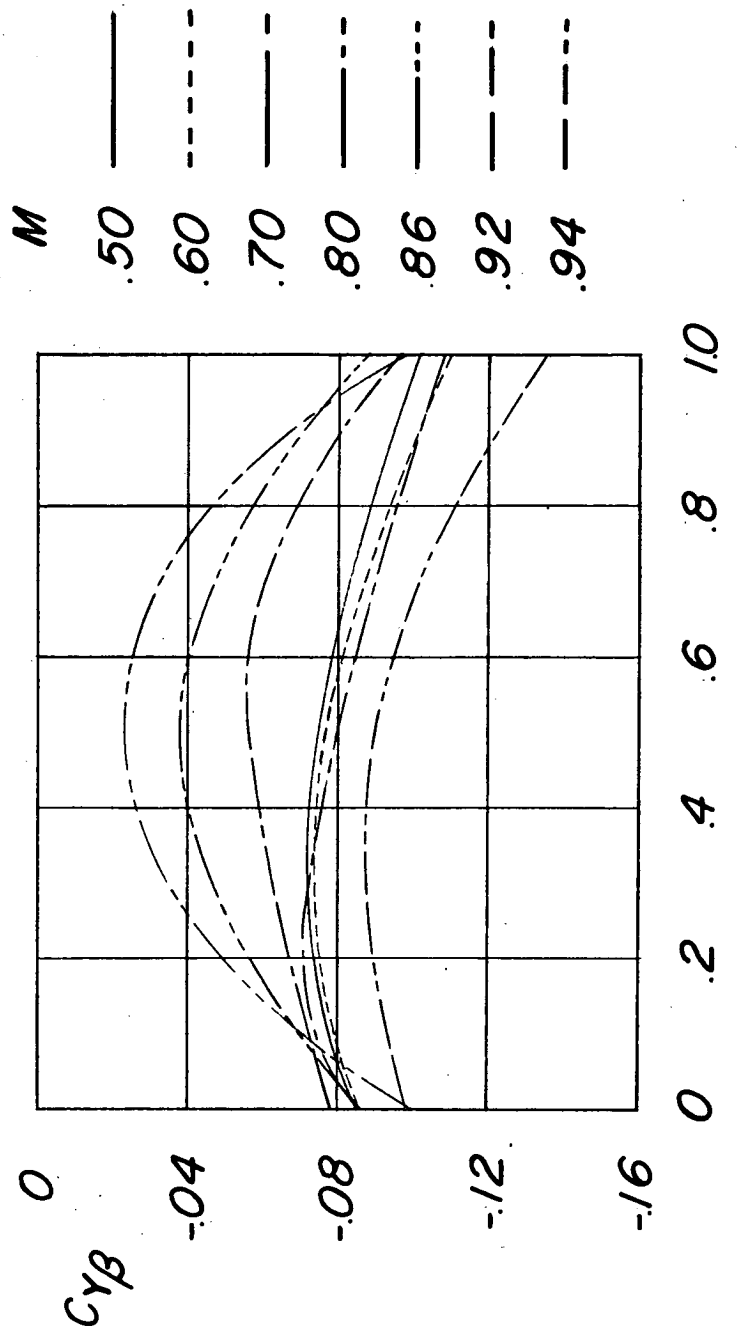


(b) Variation of $C_{Y_\beta}$ with horizontal-tail position.

Figure 12.- Concluded.

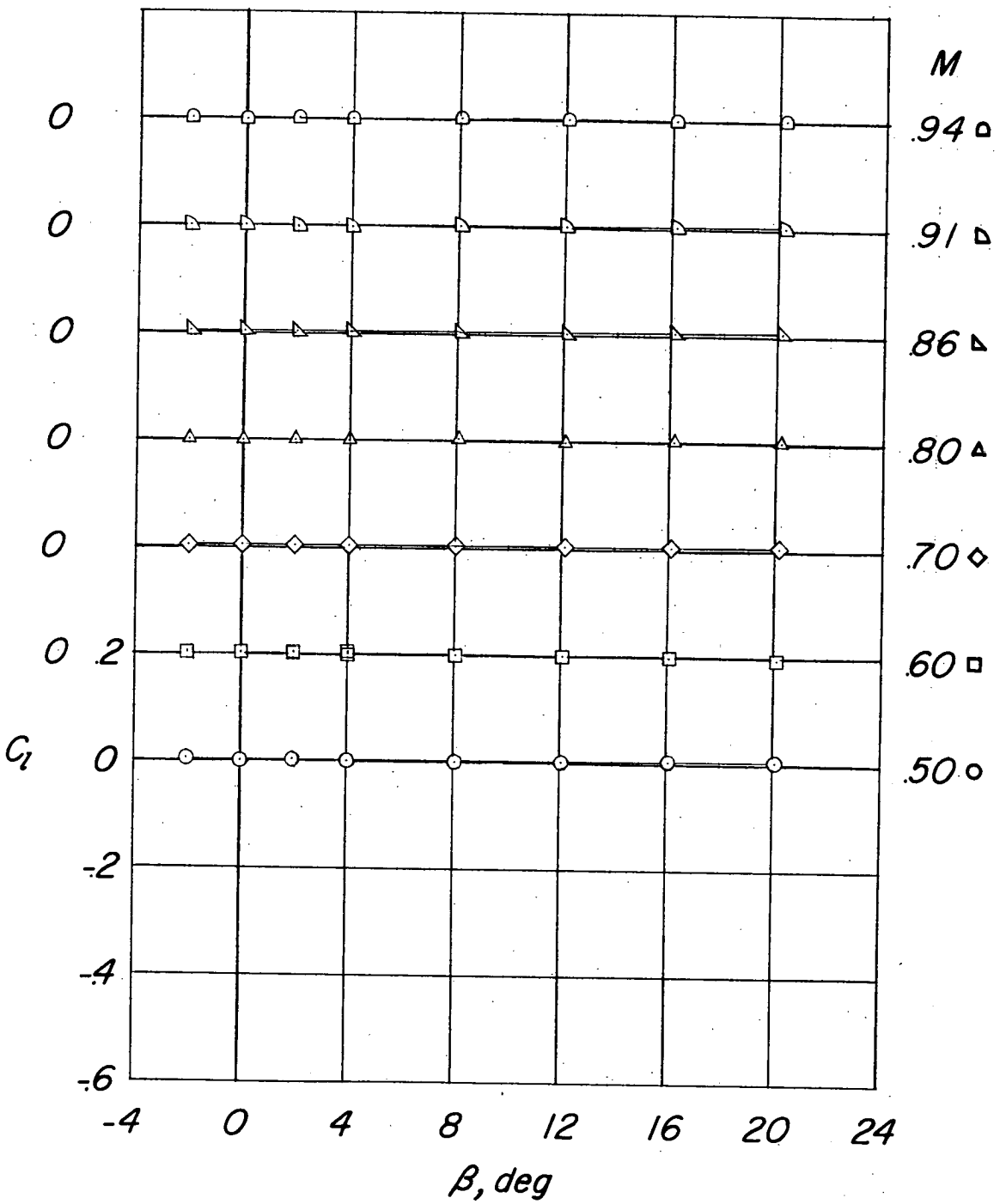


(a) Fuselage alone.

Figure 13.- Variation of $C_l$ with angle of sideslip. $\alpha = 0^\circ$.

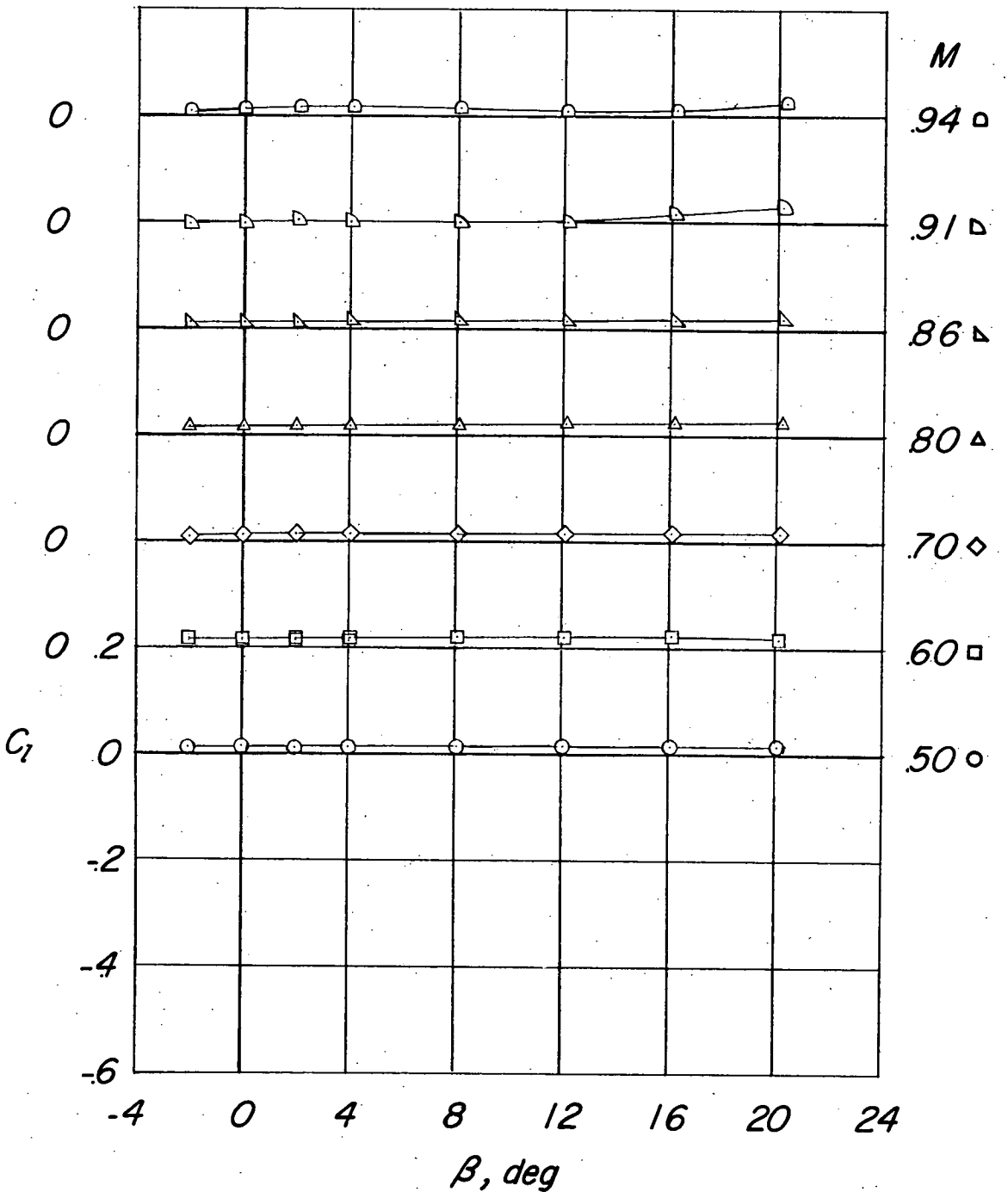


(b) Fuselage plus horizontal tail.

Figure 13.- Continued.

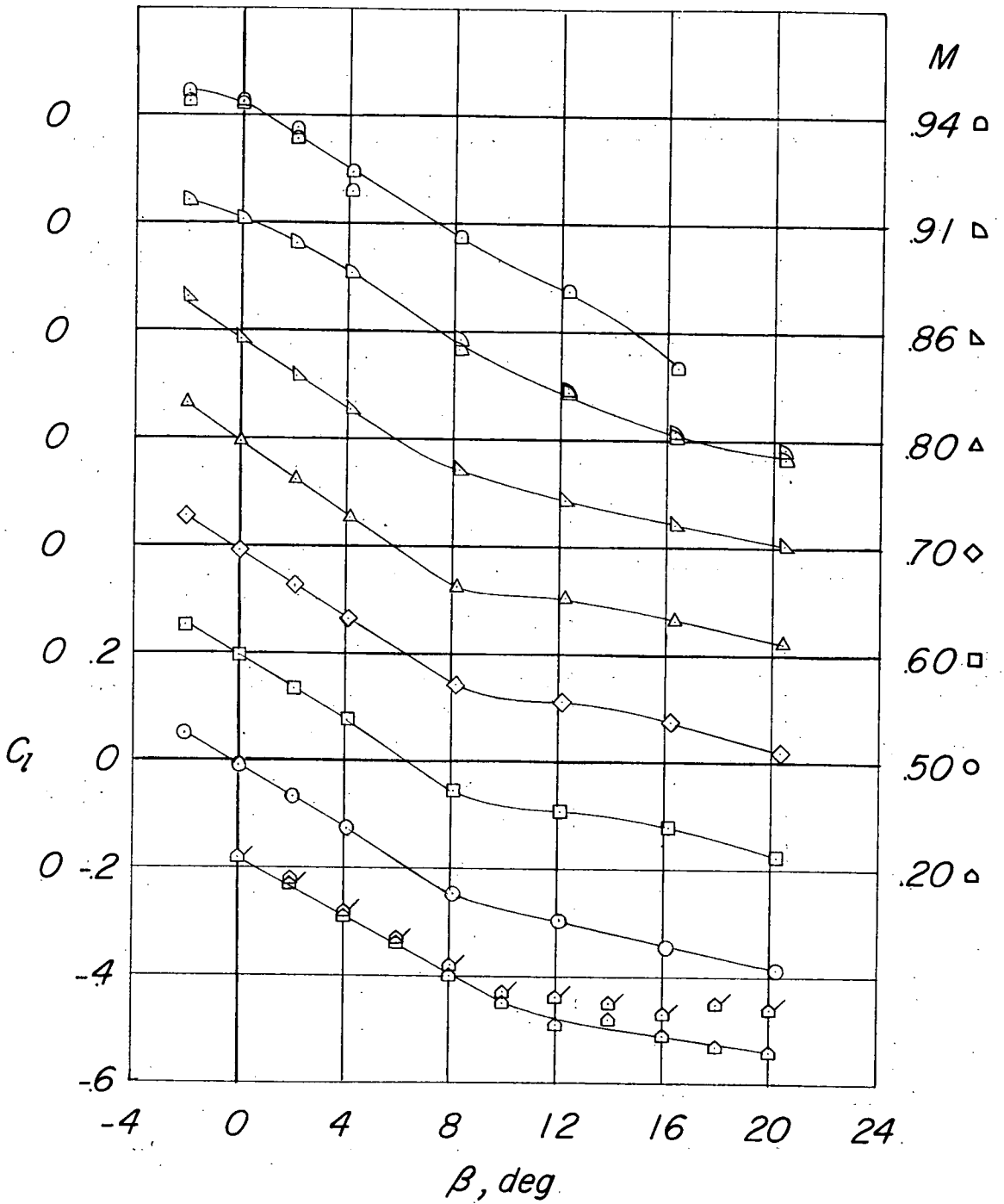


(c) Fuselage plus vertical tail. (Flagged symbols denote tests with modified fuselage nose.)

Figure 13.- Continued.

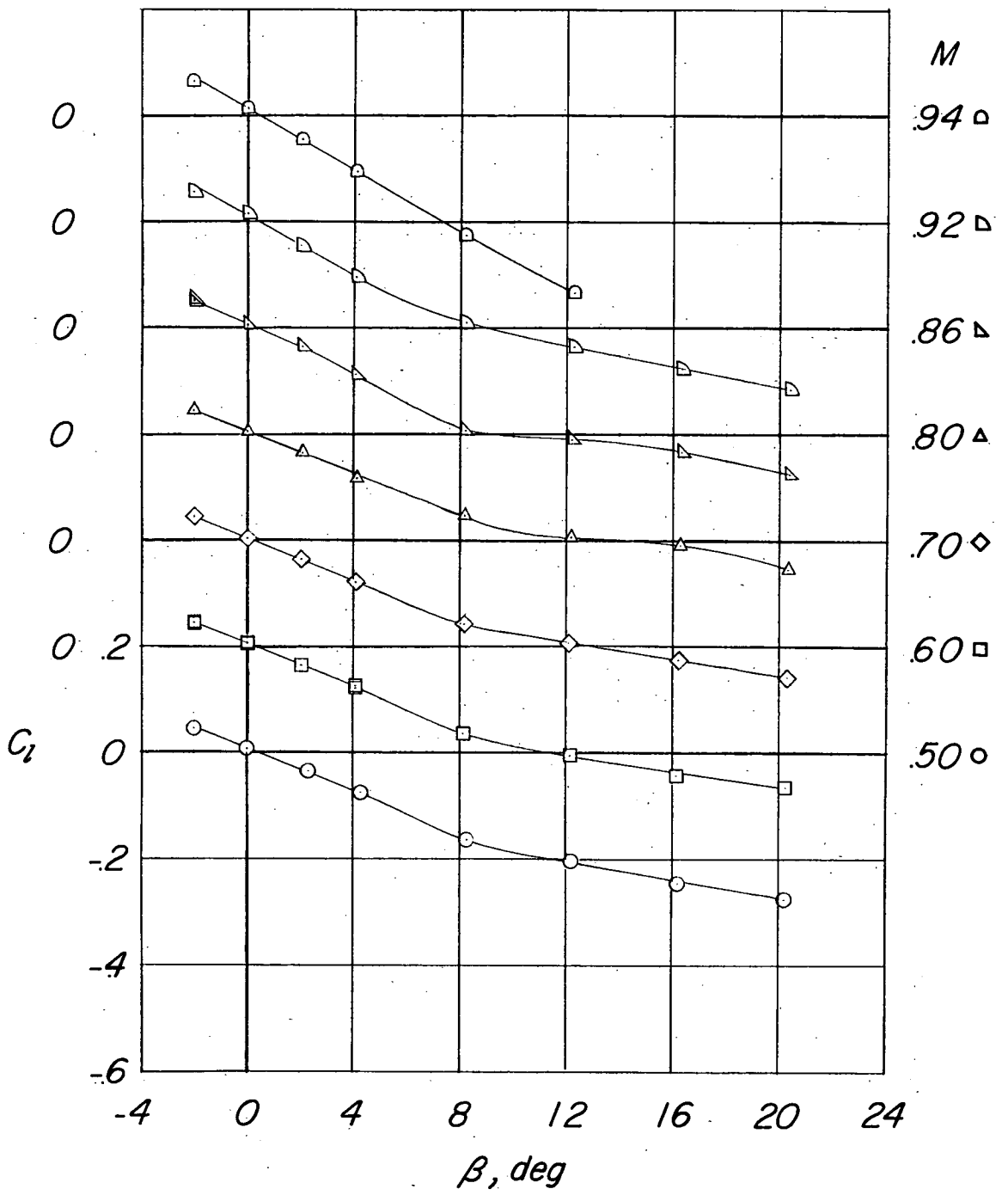


(d) Fuselage plus vertical tail plus horizontal tail. $\frac{h}{b_v} = 0$.

Figure 13.- Continued.

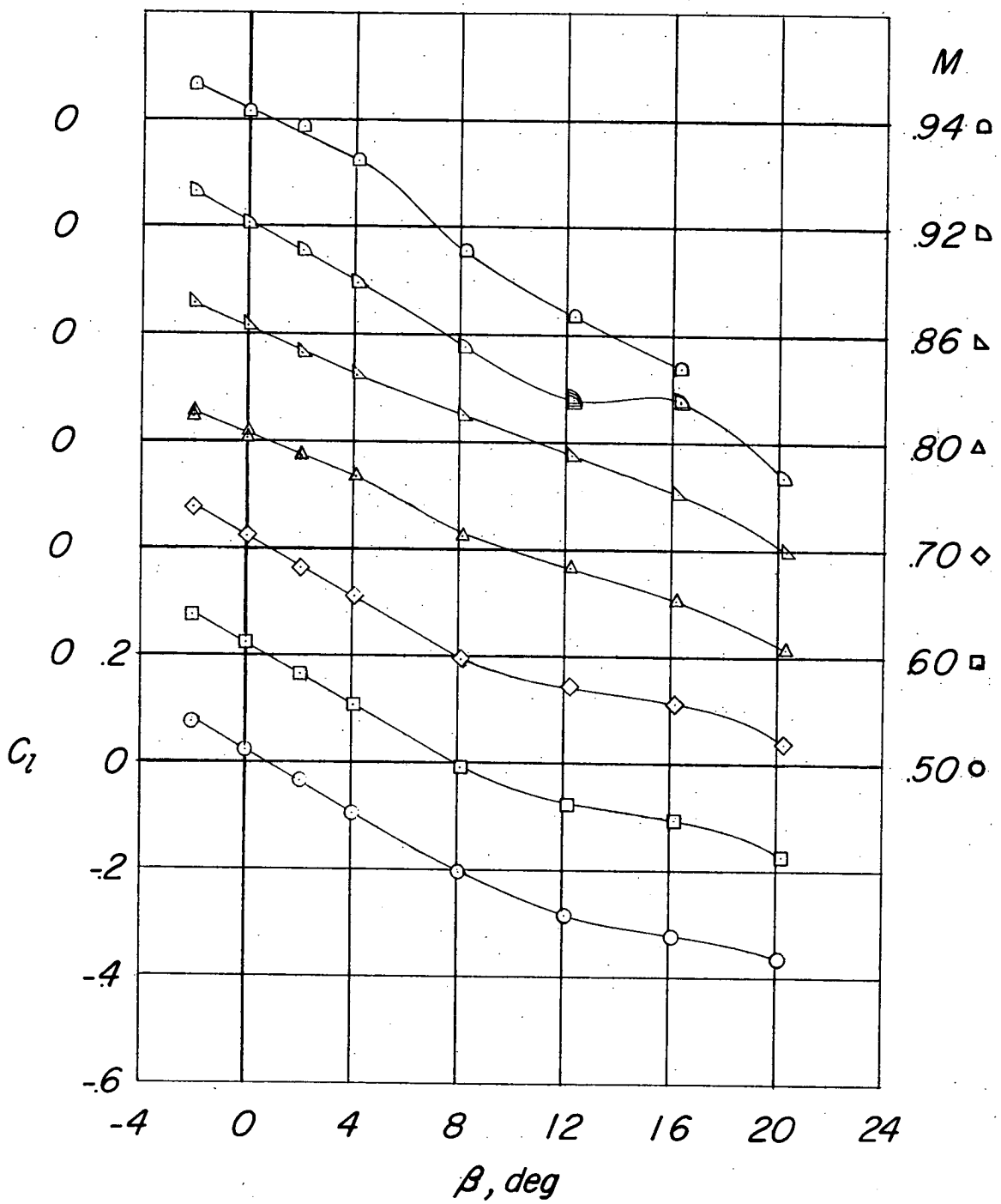


(e) Fuselage plus vertical tail plus horizontal tail. $\frac{h}{b_v} = 0.26$.

Figure 13.- Continued.

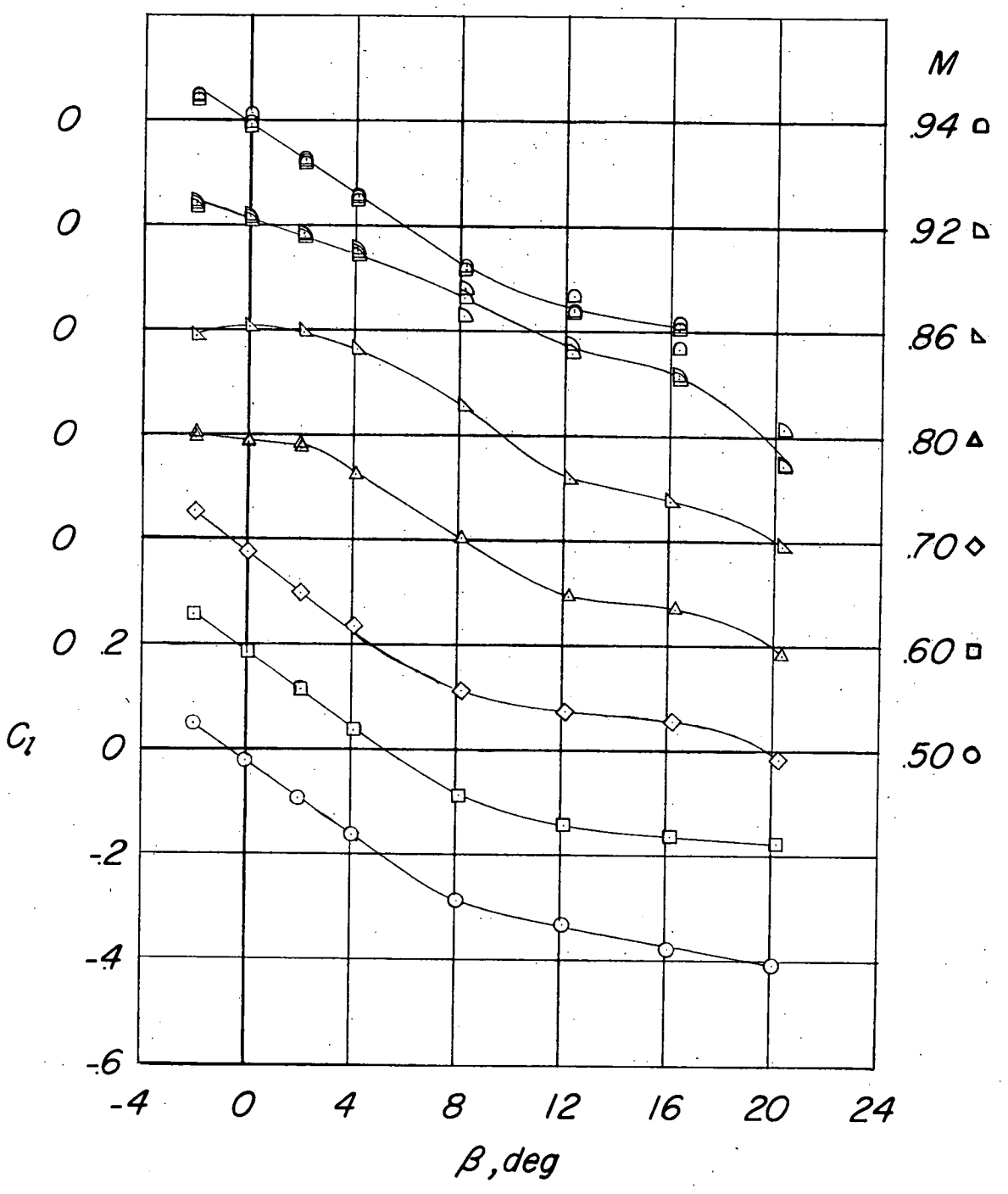


(f) Fuselage plus vertical tail plus horizontal tail. $\frac{h}{b_v} = 0.59$.

Figure 13.- Continued.

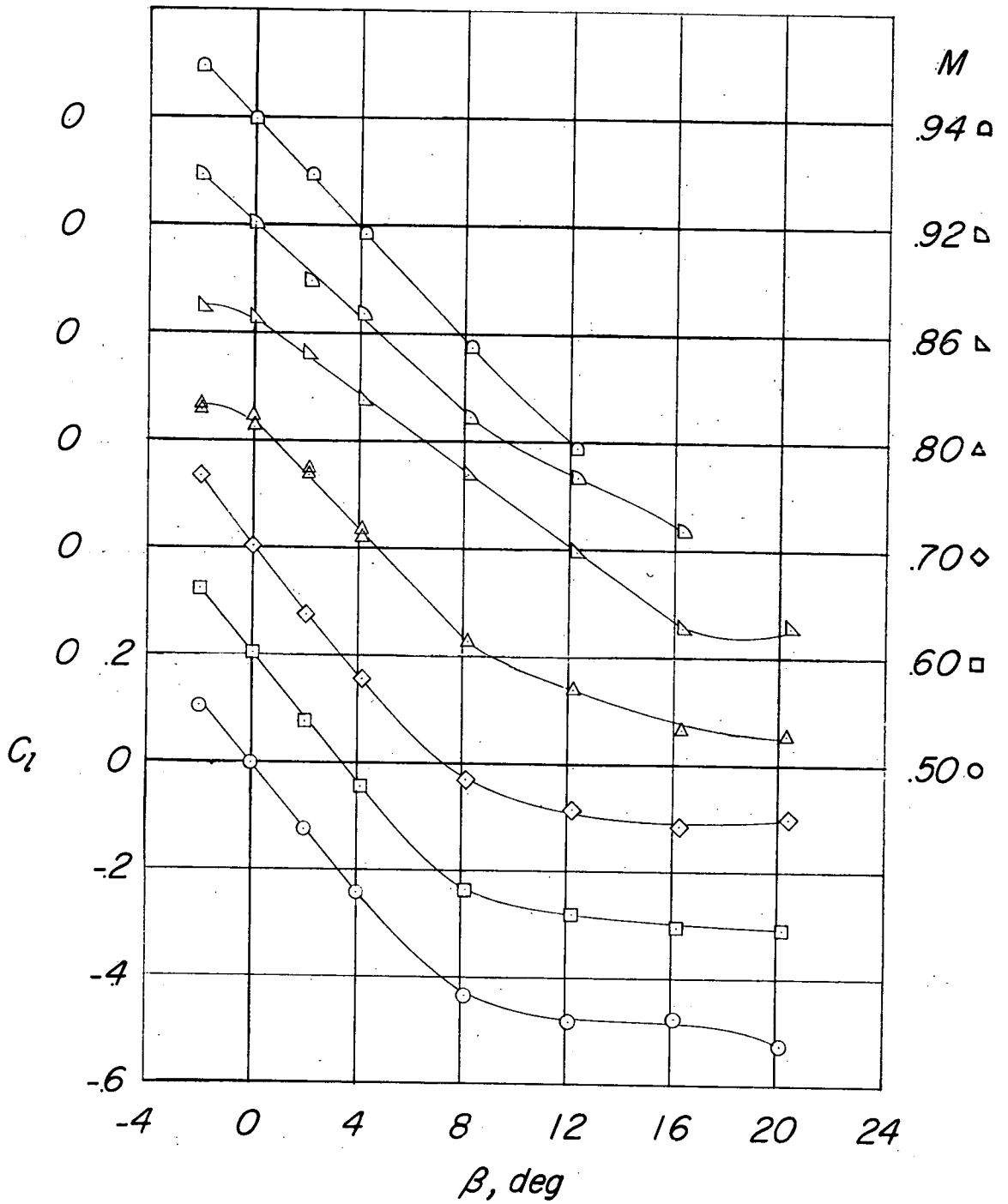


(g) Fuselage plus vertical tail plus horizontal tail. $\frac{h}{b_v} = 1.00$.

Figure 13.- Concluded.

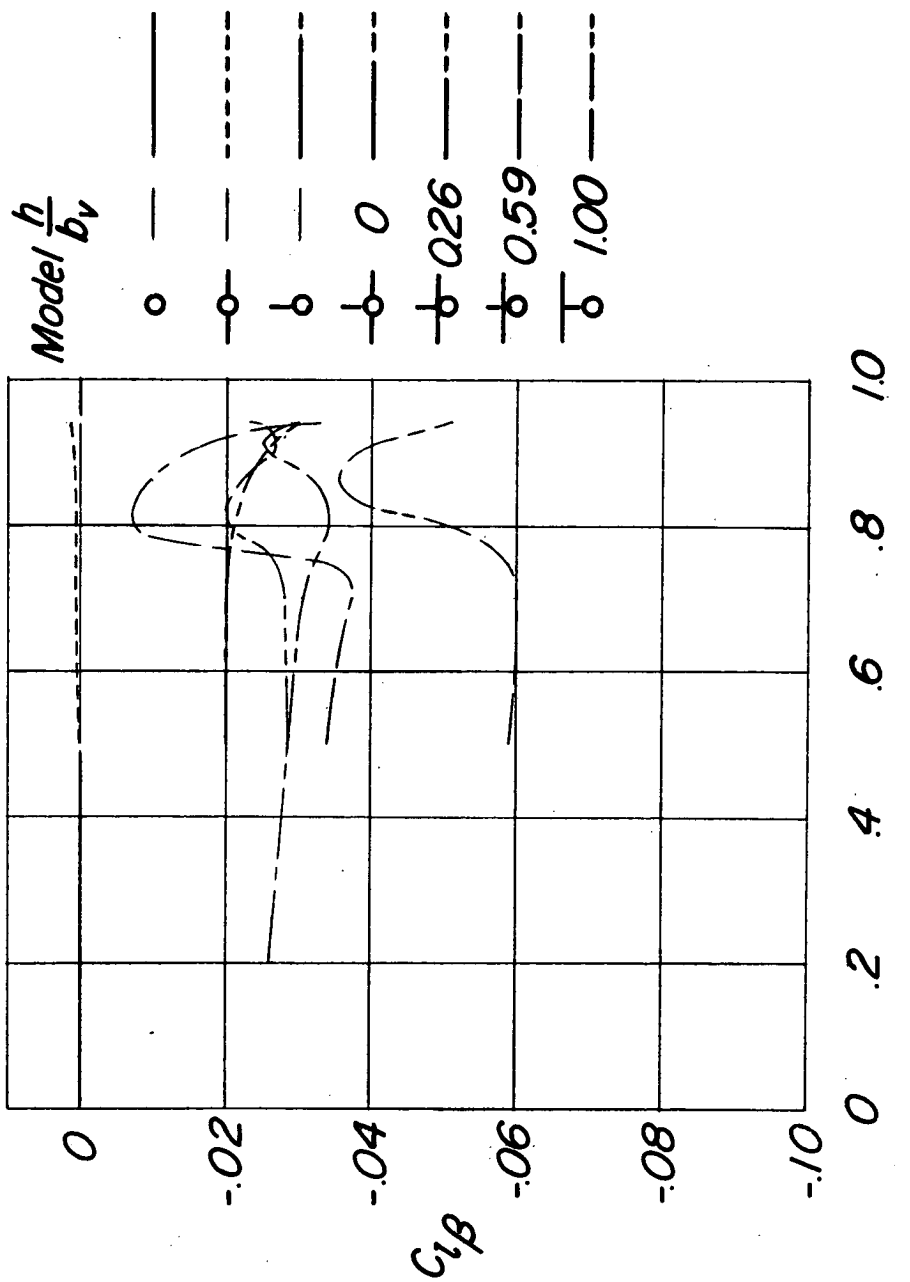


(a) Variation of $C_{l_\beta}$ with Mach number.

Figure 14.- Summary of the experimental variations of $C_{l_\beta}$ for various tail configurations. $\alpha = 0^\circ$.

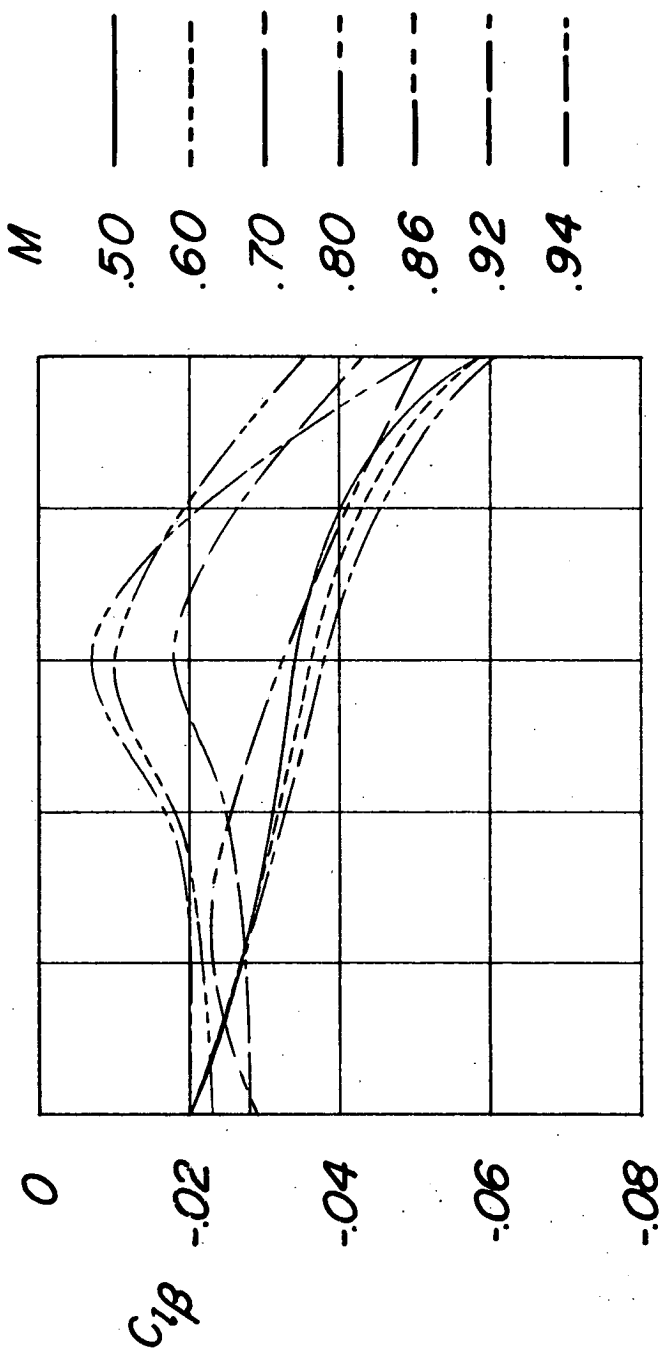


(b) Variation of $C_{l_\beta}$ with horizontal-tail position.

Figure 14.- Concluded.

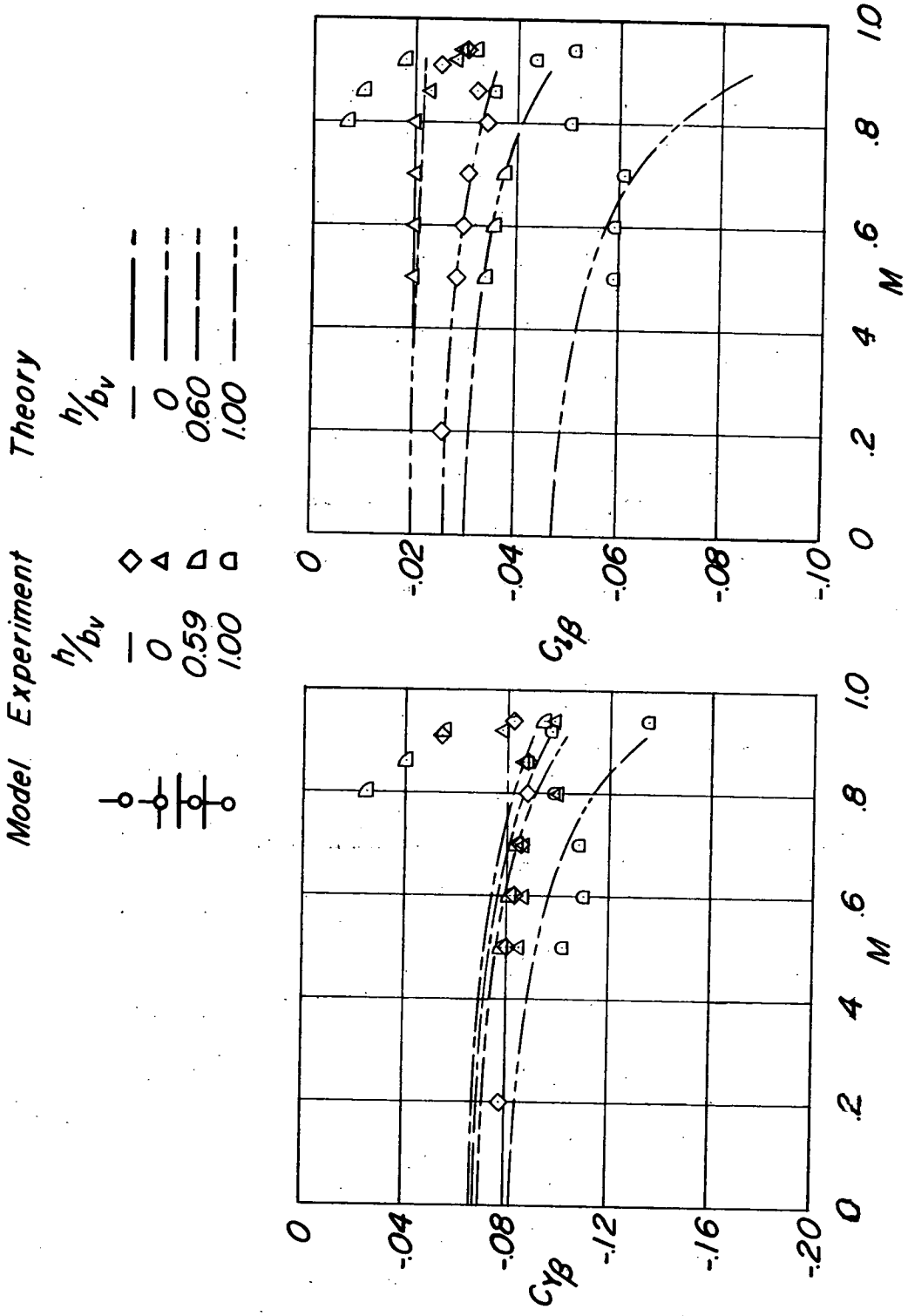


Figure 15.- Comparison of the experimental and theoretical variations of $C_{Y_\beta}$ and $C_{l_\beta}$ with Mach number for various tail configurations.

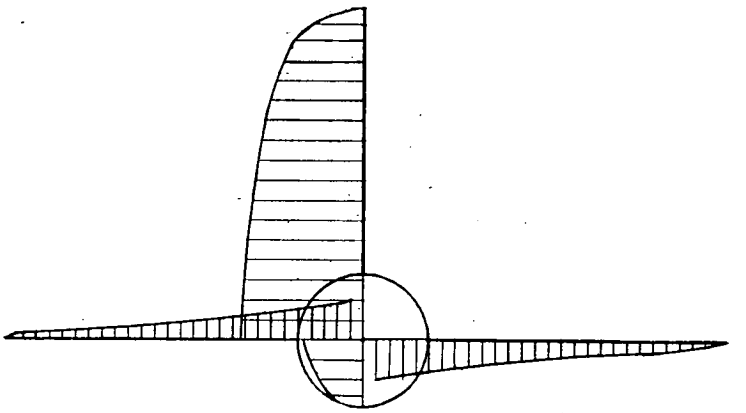

Vertical Tail + Fuselage + Horizontal Tail at $h/b_v = 0$

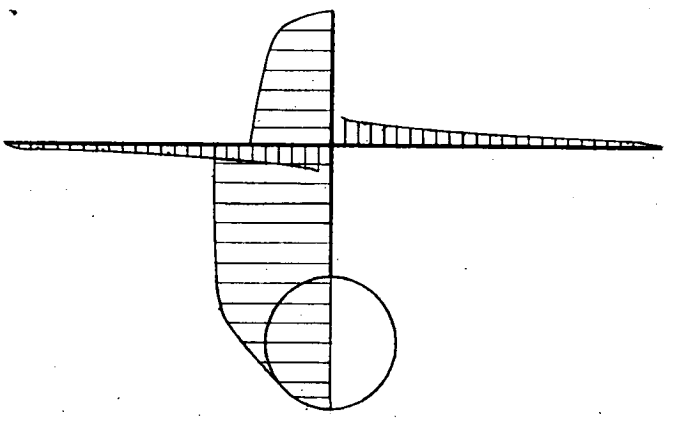

Vertical Tail + Fuselage + Horizontal Tail at $h/b_v = 0.60$

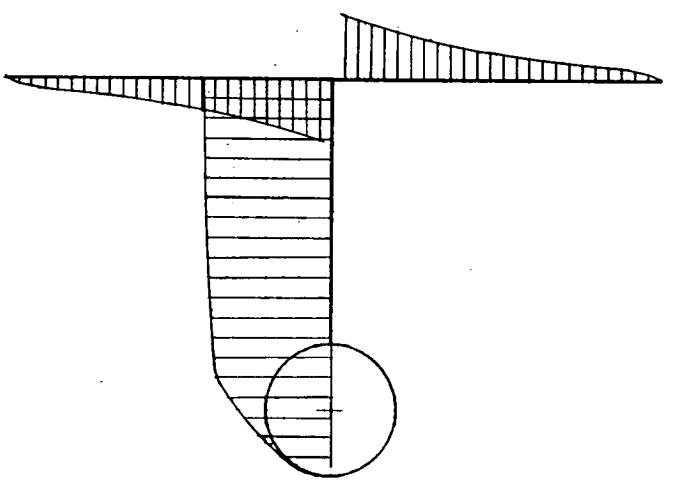

Vertical Tail + Fuselage + Horizontal Tail at $h/b_v = 1.00$

Figure 16.- Sketches of the calculated load distribution on the tail assembly having horizontal tails at $h/b_v$ values of 0, 0.60, and 1.00.

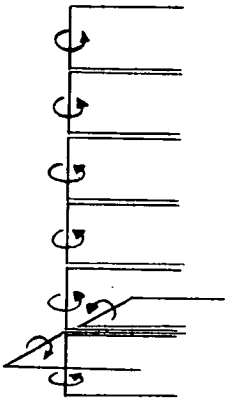

Vertical Tail + Fuselage

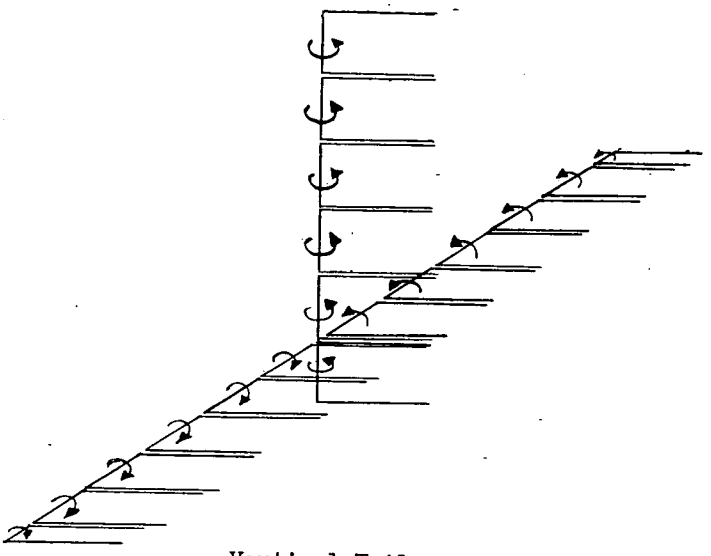

Vertical Tail + Fuselage
+ Horizontal Tail at $h/b_v = 0$

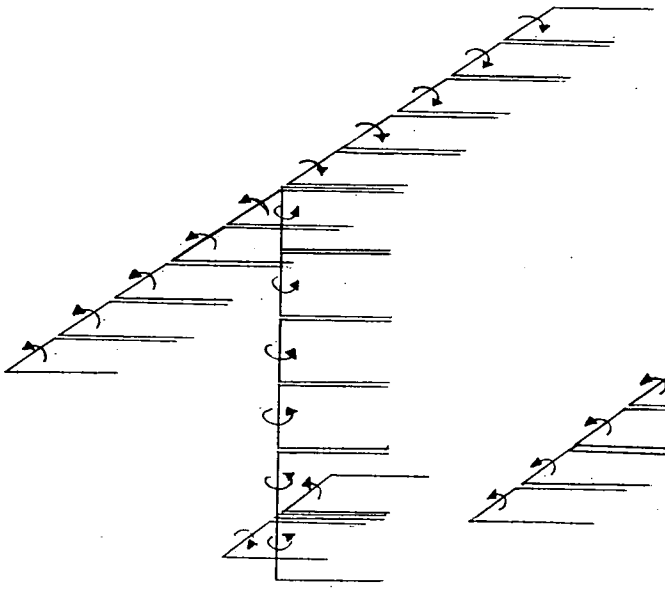

Vertical Tail + Fuselage
+ Horizontal Tail at $h/b_v = 1.00$

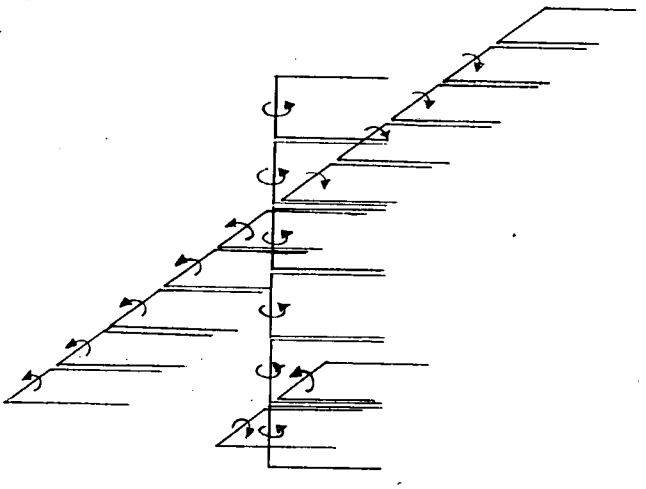

Vertical Tail + Fuselage
+ Horizontal Tail at $h/b_v = 0.60$

Figure 17.- Sketches of the four horseshoe-vortex representations of the tail configurations calculated. Direction of rotation of each horseshoe vortex is indicated for positive circulation. Gaps between adjacent trailing vortices are shown to indicate the number of horseshoe vortices used. All calculations were performed with adjacent trailing vortices coinciding and extending to infinity.



NACA-Langley - 12-2-53 - 325